

CIRCULATING COPY
Sea Grant Depository

ORES-U-T-81-003 C. 2

LOAN COPY ONLY



**WAVE FORCES ON SUBMERGED
ARTIFICIAL REEFS FABRICATED
FROM SCRAP TIRES**

Tae In Kim, Charles K. Sollitt, and
Danil R. Hancock

OREGON STATE UNIVERSITY
SEA GRANT COLLEGE PROGRAM
Publication no. ORESU-T-81-003
(R/CE-7)

FEDERAL SEA GRANT DEPOSITORY
PELL LIBRARY BUILDING
URI, NARRAGANSETT BAY CAMPUS
NARRAGANSETT, RI 02882

WAVE FORCES ON SUBMERGED ARTIFICIAL REEFS
FABRICATED FROM SCRAP TIRES

by

Tae In Kim, Ocean Engineering
Charles K. Sollitt, Ocean Engineering
Danil R. Hancock, Oceanography

Oregon State University
Corvallis, Oregon 97331

A Final Report
to
The Port of Umpqua Commission
and
Sea Grant

Completed July 31, 1981

ORES-U-81-003

(R/CE-7)

ACKNOWLEDGEMENTS

This report was completed by Mr. Tae In Kim as a Master of Ocean Engineering thesis in partial fulfillment of the degree requirements. Dr. Sollitt was the major advisor for this research and co-principal investigator with Mr. Danil Hancock. Financial support for this study was provided by the Port of Umpqua Commission, Douglas County as the initial sponsor and by Sea Grant as co-sponsor under Grant No. NA79AA-D-00106.

TABLE OF CONTENTS

| | | |
|------|--|-----|
| I. | INTRODUCTION | 1 |
| | 1.1 Background | 1 |
| | 1.2 Previous Work | 3 |
| | 1.3 Scope | 4 |
| II. | THEORY | 6 |
| | 2.1 Hydrodynamic Forces on a Submerged Body | 6 |
| | 2.2 Determination of Drag and Inertia Coefficients | 13 |
| | 2.3 Determination of Maximum Force Coefficients | 17 |
| | 2.4 Governing Parameters | 19 |
| | 2.5 Coefficient Dependence on Governing Parameters | 20 |
| III. | EXPERIMENTAL APPARATUS AND PROCEDURES | 30 |
| | 3.1 Tire Configurations | 30 |
| | 3.2 Wave Research Facility | 37 |
| | 3.3 Force and Velocity Measurements | 40 |
| | 3.4 Bottom Resistance Measurements | 47 |
| IV. | RESULTS AND DISCUSSIONS | 48 |
| | 4.1 Observed Wave Profile and Kinematics | 48 |
| | 4.2 Maximum Force Coefficients | 57 |
| | 4.3 Drag and Inertia Coefficients for Tire Units | 68 |
| | 4.4 Validity of Morison Equation | 80 |
| | 4.5 Bottom Resistance Coefficients | 88 |
| | 4.6 Field Application | 90 |
| V. | CONCLUSIONS | 95 |
| | 5.1 Summary | 95 |
| | 5.2 Application of Results | 97 |
| | 5.3 Future Studies | 98 |
| | REFERENCES | 99 |
| | APPENDICES | 102 |

LIST OF FIGURES

| <u>Figure</u> | <u>Page</u> |
|---|-------------|
| 2-1 Drag Coefficient vs. Reynolds Number, Smooth Cylinder in Steady Flow | 8 |
| 2-2 (a) Drag and (b) Inertia Coefficient vs. Reynolds Number, Smooth Cylinder in Periodic Flow | 22 |
| 2-3 (a) Drag and (b) Inertia Coefficient vs. Keulegan-Carpenter Number for Particular Values of R_e and β | 24 |
| 2-4 (a) Maximum Force Coefficient vs. Keulegan-Carpenter Number for Particular Values of β , (b) Mean Lines for Maximum Horizontal Force Coefficient vs. Period Parameter | 27 |
| 3-1 Properties of Tires Used in the Experiment | 31 |
| 3-2 Weight of Tire in Air and in Fresh Water | 32 |
| 3-3 Dimensions of Complex Tire Configurations | 34 |
| 3-4 Drilling and Fabrication of Tire Units | 36 |
| 3-5 Oregon State University Wave Research Facility | 38 |
| 3-6 Details of Test Section | 41 |
| 3-7 Calibration Curves for (a) Near Bottom Water Particle Velocity, (b) Horizontal Force | 43 |
| 3-8 Sample Records of Hydrodynamic Data for the Waves with (a) $T=3.13$ sec. (b) $T=6.25$ sec. | 44 |
| 4-1 Comparisons between Observed Wave Profile and Theoretical Values for the Waves with (a) $T=1.98$ sec. (b) $T=3.61$ sec. (c) $T=6.25$ sec. | 49 |
| 4-2 Comparisons between Observed Near Bottom Water Particle Velocity and Theoretical Values for the Waves with (a) $T=1.98$ sec. (b) $T=3.61$ sec. (c) $T=6.25$ sec. | 52 |
| 4-3 Comparisons between Measured Maximum Water Particle Velocity and Theoretical Values | 54 |
| 4-4 Comparisons Between Measured Maximum Acceleration and Theoretical Values | 56 |

LIST OF FIGURES
(Continued)

| <u>Figure</u> | <u>Page</u> |
|--|-------------|
| 4-5 Maximum Force Coefficients vs. K-C Number for (a) One Tire and (b) Two Tires set Perpendicular to the Waves | 59 |
| 4-6 Maximum Force Coefficients vs. K-C Number for (a) Four Tires Set Perpendicular to the Waves (b) One Tire Set Flat | 60 |
| 4-7 Maximum Force Coefficients vs. K-C Number for (a) Two Tires and (b) Four Tires Set Flat | 61 |
| 4-8 Maximum Force Coefficients vs. K-C Number for (a) One Tire and (b) Two Tires Set Parallel to the Waves | 62 |
| 4-9 Maximum Force Coefficients vs. K-C Number for (a) Four Tires Set Parallel to the Waves (b) Two Tires Stuffed and Four Tires Triangularly Fabricated | 63 |
| 4-10 Maximum Force Coefficients vs. K-C Number for (a) Four Tires with Different Orientations (b) Array with Different Numbers of Tires | 64 |
| 4-11 Maximum Force Coefficients vs. K-C Number for (a) Rosette Shape Configurations (b) Rosette Shape Configurations Compared with Four Tires Set Parallel to the Waves | 65 |
| 4-12 Mean Lines of Maximum Force Coefficients vs. K-C Number | 67 |
| 4-13 Drag and Inertia Coefficients vs. K-C Number for (a) One Tire Set Perpendicular to the Waves (b) Four Tires Set Parallel to the Waves | 70 |
| 4-14 Drag and Inertia Coefficients vs. K-C Number for (a) Two Tires and (b) Four Tires with Different Orientations | 71 |
| 4-15 Drag and Inertia Coefficients vs. K-C Number for Parallel Array with Different Numbers of Tires | 72 |
| 4-16 Drag and Inertia Coefficients vs. K-C Number for (a) Two Tires Stuffed (b) Rosette Shape Configurations | 73 |
| 4-17 Mean Lines of Drag Coefficients vs. K-C Number | 74 |

LIST OF FIGURES
(Continued)

| <u>Figure</u> | | <u>Page</u> |
|---------------|---|-------------|
| 4-18 | Mean Lines of Inertia Coefficients vs. K-C Number | 75 |
| 4-19 | Comparison between the Drag and Inertia Coefficients for Circular Cylinders(Garrison et al., 1977) and Those for Several Tire Unit Configurations | 77 |
| 4-20 | Comparison between the Drag and Inertia Coefficients for Circular Cylinders(Sarpkaya, 1976) and Those for Several Tire Unit Configurations | 78 |
| 4-21 | Comparison between the Measured Force and the Calculated Force for the Waves with (a) T=1.98 sec. (b) T=2.36 sec. | 81 |
| 4-22 | Comparison between the Measured Force and the Calculated Force for the Waves with (a) T=3.61 sec. (b) T=4.42 sec. | 82 |
| 4-23 | Comparison between the Measured Force and the Calculated Force for the Waves with (a) T=6.25 sec. (b) T=9.88 sec. | 83 |
| 4-24 | Phase Lags between the Maximum Horizontal Velocity and the Maximum Horizontal Force vs. K-C Number | 87 |
| 4-25 | Maximum Bottom Velocity by Linear Wave Theory for Specified Wave Height and Water Depth | 91 |

LIST OF TABLES

| <u>Table</u> | | <u>Page</u> |
|--------------|---|-------------|
| 1 | Effective Diameter(D') and Projected Area(A) of Tire Units | 33 |
| 2 | Test Wave Conditions | 39 |
| 3 | Horizontal Wave Forces on the Dynamometer Table with No Tire Array | 46 |
| 4 | Bottom Resistance Coefficients for Tire Units | 89 |
| 5 | Allowable Deep Water Wave Heights(H _o) for Tire Units Ballasted by Concrete to the Level of Tire Bead | 94 |

LIST OF SYMBOLS

| | |
|--------------|--|
| a | Half amplitude of water particle motion over a wave cycle |
| A | Projected area of a submerged body |
| C | Wave celerity equal to L/T |
| C_D | Drag coefficient |
| C_I | Inertia coefficient |
| C_f | Maximum force coefficient |
| $C_{f(cal)}$ | Calculated maximum force coefficient |
| $C_{f(mes)}$ | Measured maximum force coefficient |
| $C_{f(min)}$ | Lowest maximum force coefficient |
| C_m | Added mass coefficient |
| D | Diameter of a cylinder or outer diameter of a tire |
| D' | Effective diameter of the tire units, equal to the length of the tire units along the axis of wave propagation |
| D_i | Inner(wheel) diameter of a tire |
| D_t | Width of a tire |
| $d()$ | Total derivative |
| e | Distance between the wall and the nearest edge of a submerged body |
| E | Voltage |
| F | Horizontal(in-line) force |
| F_C | Calculated horizontal force |
| F_D | Drag force |
| F_H | Horizontal force required to move the tire unit on bottom material |
| F_I | Inertia force |

LIST OF SYMBOLS
(Continued)

| | |
|---------------------------|---|
| F_m, F_{m1}, F_{m2} | Measured horizontal force, measured horizontal forces at time t_1 and t_2 |
| F_{max} | Maximum horizontal force |
| $F_{max(cal)}$ | Calculated maximum horizontal force |
| $F_{max(mes)}$ | Measured maximum horizontal force |
| f | Bottom resistance coefficient |
| $f(\), f_1(\), f_2(\)$ | Arbitrary functions in Section 2.4 |
| G | Dimensionless roughness parameter |
| g | Gravitational acceleration |
| H | Wave height |
| H_o | Deep water wave height |
| H_B | Breaking wave height |
| h | Water depth |
| J | Dimensionless proximity parameter |
| k | The average height of protuberance on the surface of a body |
| $K-C$ | Keulegan-Carpenter period parameter |
| K_s | Shoaling coefficient |
| L | Finite wave length |
| L_o | Wave length in deep water |
| ℓ | Length of circular cylinder |
| NN | The order of representation in Stream-function theory |
| n | Number of tires |
| R_c | Critical Reynolds number |
| R_e | Reynolds number |

LIST OF SYMBOLS
(Continued)

| | |
|---------------------------------|--|
| S | Distance from the ocean bottom |
| T | Wave period |
| t | Time variable |
| U | Horizontal velocity component |
| U_b | Near bottom horizontal velocity component |
| U_{bmax} | Maximum near bottom horizontal velocity |
| U_{max} | Maximum horizontal velocity |
| $\frac{dU}{dt}$ (or \dot{U}) | Horizontal acceleration component |
| \dot{U}_b | Near bottom horizontal acceleration component |
| \dot{U}_{bmax} | Maximum near bottom horizontal acceleration |
| V | Volume of a submerged body, or volume of a tire casing |
| W_{air} | Dry weight of tire |
| $W_{ballast}$ | Required ballast |
| W_{sub} | Submerged weight of tire unit |
| W_{water} | Submerged weight of tire |
| X(n) | Undetermined coefficient in Stream-function theory |
| α | Incident wave angle relative to the axis of a cylinder |
| β | Frequency parameter equal to $D^2 / \nu T$ |
| Δ | Finite increment |
| ϵ | Error term |
| η | Surface wave profile |
| θ | Phase angle equal to $(2 \pi / T) t$ |

LIST OF SYMBOLS
(Continued)

| | |
|-------------|--|
| λ^* | Error(%) between calculated maximum force and measured maximum force |
| π | PI equal to 3.1415926 |
| ν | Kinematic viscosity of water |
| ρ | Mass density of water |
| ϕ | Phase angle between maximum velocity and maximum force |
| ψ | Adopted period parameter |
| Ψ | Stream-function |
| Ψ_η | Stream-function at free surface |
| σ | Wave frequency equal to $2\pi/T$ |

WAVE FORCES ON SUBMERGED ARTIFICIAL REEFS FABRICATED FROM SCRAP TIRES

I. INTRODUCTION

1.1 Background

The value and productivity of marine artificial reefs as fish havens have been recognized by fishermen and scientists for more than 50 years. Increasing demands on fish stocks by recreational and commercial fisheries as well as the degradation of many natural marine habitats has stimulated interest in artificial reefs. Artificial reefs have been constructed in the United States since the 1930's, and over 200 permits for reefs have been issued by the Corps of Engineers. These reefs have been constructed in relatively sheltered locations and have experienced varying degrees of success. Current proposals to construct offshore reefs in exposed locations require a conscientious engineering evaluation of environmental loads and ballast requirements to ensure stable and durable reefs.

A variety of scrap materials have been used to construct reefs. Auto bodies have proved impractical due to the costs of cleaning and transportation and their rapid deterioration rate. Ship hulls provide good stable habitats, but require massive amounts of ballast to resist motion due to currents and waves. Tires, rock, concrete rubble and other scrap materials are effective and durable. Tires are plentiful, cheap and relatively easy to handle and transport to the reef site. At

present, more than 200 million tires are scrapped annually in the United States. Less than 10 percent are reused. The remaining tires may be obtained in bulk at almost no cost.

Rubber tires are essentially inert in salt water, with a deterioration half life of approximately 50 years. Thus, they may be temporarily stored in a marine environment and reclaimed within 50 years if a commercial value should develop. Tires may be configured and ballasted in a variety of ways to provide attractive habitats to many pelagic species. Configurations are selected to provide spaces which are large enough to admit prey fish but small enough to exclude predator fish. They quickly encrust with micro- and macro-organisms, thereby providing an important link in the food-chain.

The Port of Umpqua, Oregon has proposed to construct an artificial reef fabricated from scrap tires at the 27 fathom contour off the coast. The intended purpose of the reef is to restore recreational bottom fishing to this coastal area by enhancing habitats for bottom and reef fishes. This coastal area experiences wave heights which exceed 30 feet annually. The forces associated with these waves are very large compared to those experienced at other reported reef sites. In order to provide a stable yet economical reef design for this site, some basic information relating forces to wave induced water motions is required. This research has been funded by the Port of Umpqua and Sea Grant to investigate fundamental questions required to minimize construction costs and environmental risks while maximizing reef fishery production. Experimental studies were conducted in a large wave channel at the Oregon State University Wave Research Facility to evaluate wave force coefficients and bottom friction coefficients for reef components

fabricated from tires. The results of the study are not site specific. The experimentally determined force coefficients may be applied to any location where design wave conditions are known.

1.2 Previous Work

The scientific study of marine artificial reefs has a relatively short history. Since 1960, considerable efforts have been made by oceanographers and sea-related public organizations to provide descriptive information on the behavior and management of artificial reefs. Biological productivity studies have been made for shallow water sheltered reef sites by several researchers. General considerations for selecting reef sites, construction materials, shape and size of the reef components and its effects on fish ecology have been discussed by many investigators. [Carlisle et al.(1964), Parker et al.(1974), Aska(1978)] Parker et al.(1974) examined the techniques and costs of reef construction with various materials. They proposed a variety of configurations and fabricating procedures for scrap tires to maximize utility as fish habitats.

Regarding engineering aspects of artificial reef designs, little work has been completed beyond general considerations for the stability of reefs on the ocean bottom. Even though the effects of the water depth, sedimentation, currents and waves on the utility and stability of the reefs were recognized, no quantitative studies have been reported which permit a design engineer to select the appropriate ballast to resist loads induced by a specified marine environment at the reef site.

There are three unique features to be mentioned in designing artificial reefs: (1) most artificial reefs have irregular shapes and

can be considered as three-dimensional objects, (2) most artificial reefs are not fixed on the ocean bottom, thus they are vulnerable to lifting, sliding and rolling if appropriate ballast is not provided, and (3) their response to the waves tends to be elastic as opposed to rigid.

Numerous studies have quantified hydrodynamic forces on submerged bodies such as circular cylinders and spheres, following the work of Morison, et al.(1950). Studies on bodies of other shapes are limited and the general applicability of the concept of Morison is still questioned. However, the results of previous investigations for circular cylinders are useful for interpreting the results for artificial reef components.

1.3 Scope

This report summarizes the results of laboratory experiments to establish design criteria for a submerged artificial reef located in offshore regions with severe wave and current conditions. Various rubber tire reef components are tested under wave conditions varying from shallow to deep water. The results of the study are presented so that they may be generally applied to any site where wave, current and sediment conditions are known.

Three major objectives were sought:

1. Determination of maximum force coefficients for tire units in order to provide a rapid reef design procedure.
2. Determination of drag and inertia coefficients for various tire configurations in order to examine the applicability of the Morison equation in predicting horizontal hydrodynamic forces on tire units.

3. Evaluation of frictional resistance of tire units in contact with sea-bed materials in order to determine ballast requirements for reef stability.

In addition, observed wave profiles and kinematics of monochromatic waves in the laboratory were compared to theoretical values predicted by Dean's Stream-function theory and Airy wave theory.

II. THEORY

Introduction

The characteristics of hydrodynamic forces on submerged objects in steady and unsteady flow regimes are briefly discussed in this chapter. This review is intended to provide the necessary background to understand wave forces on tire reef components and will establish force relationships to compare to the behavior of other submerged bodies. The first section introduces established semi-empirical force prediction models. Section 2.2 and 2.3 discuss numerical procedures required to determine force coefficients from measured force and kinematic data. Force coefficient dependence on various parameters is summarized in Section 2.4 and 2.5 for horizontal circular cylinders subjected to periodic flow.

2.1 Hydrodynamic Forces on a Submerged Body

Steady Flow Forces

Steady flow exists when the fluid velocity at any point remains constant over a specified length of time. The flow-induced force on a submerged object is known as the drag force and represented by the symbol F_D :

$$F_D = C_D \frac{\rho}{2} A U^2 \quad (2-1)$$

where ρ is mass density of the fluid, A is the projected area of the body in the direction of flow, U is the steady-state flow velocity, and C_D is the drag coefficient. [Ippen(1966)] This formula may be derived

from dimensional analysis and is consistent with known relationships for turbulent shear stresses on flat plates and pipe walls.

The drag force on an object consists of two parts: the frictional drag and the pressure(or form) drag. The friction existing between the flow and the surface of the body produces a shear stress and resulting force which has a component in the direction of the incident flow. The pressure drag is due to the differences in pressure over the front and back halves of the body. The percentage partitioning of the total drag force between these two components varies as a function of Reynolds Number. For the circular cylinder, the contribution of the skin friction drag to total drag varies from 6 percent(at $Re = 5 \times 10^3$) to 1 percent(at $Re = 2 \times 10^6$). [Achenbach(1968)]

A number of experiments have been conducted to evaluate drag coefficients for objects of familiar shape such as circular cylinders and spheres. It has been determined that the choice of C_D for a circular cylinder in a particular steady flow design situation must take into account the following factors: the scale and intensity of turbulence in the approaching flow; the roughness of the cylinder surface, the proximity of a wall to the cylinder, vibration of the cylinder, and the nature of the flow. The last factor is represented in parametric form by the Reynolds number written

$$Re = \frac{U \cdot D}{\nu} \quad (2-2)$$

where ν is the kinematic viscosity of the flowing water, D is the diameter of the object. The drag coefficient variation as a function of Reynolds number is well established for the case of a smooth cylinder in

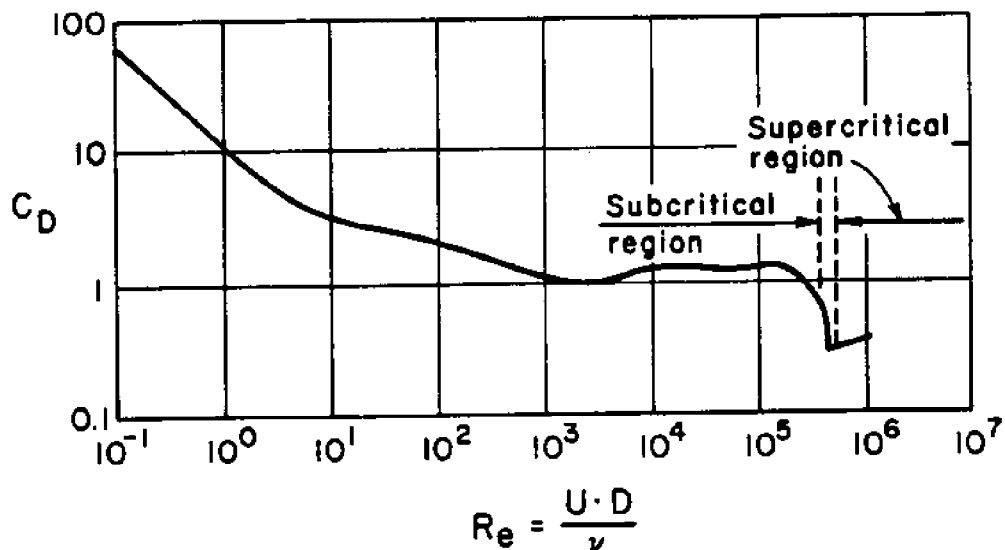


Fig. 2-1 Drag Coefficient vs. Reynolds Number, Smooth Cylinder in Steady Flow [Schlichting(1955)]

steady flow as shown in Fig. 2-1. An abrupt drop in the drag coefficient observed at Reynolds number between 10^5 and 10^6 is called "the critical point". This is due to the considerable decrease of the pressure drag resulting from the alteration in the flow pattern. In general, flow around a body separates from the object at a location termed the separation point, part of a separation line. A wake region is formed within the separation line on the down stream side of the object. In this zone there exists low pressure which accounts for much of the pressure drag on the object. Near the critical Reynolds number, the separation points move further towards the rear of the object and the zone of low pressure is greatly reduced, in turn reducing the pressure drag. Although the skin friction drag increases during the process, its increase is far less than the accompanying decrease in the pressure drag,

and the combined effect results a sudden drop in the total drag force. There are limited data available on drag coefficients for Reynolds numbers exceeding 10^6 .

Because of symmetry, there exists no lateral, or lift force to the flow direction unless the body is so close to another body that the flow around it becomes asymmetrical.

Unsteady or Accelerating Potential Flow Forces

The concept of potential flow is based on the assumption of an ideal liquid which has no viscosity, described as being inviscid. Although such a fluid does not exist in nature, there are circumstances in the flow of real liquids wherein the effects of viscosity are of secondary importance and thus predictions based on potential flow are very close to actual hydrodynamic conditions.

In the absence of viscosity no shear stress is developed by the motion of fluid past a submerged body. Only pressure forces can contribute to the drag force on a body submerged in an ideal fluid. In the case of steady potential flow, however, the fluid particles flowing near the surface of the object do not separate to form a wake, and thus the pressure distribution would be symmetrical fore and aft.

Theoretically, a body submerged in a steady-state potential flow can experience no net force on it by the motion of the ambient fluid.

But in an accelerating potential flow, there can be a force. This consists of two parts, the first of which is the buoyancy-like force due to the pressure gradient between upstream and downstream sides of the body. This force is equal to the product of the displaced mass and the fluid acceleration. The second part of the force accounts for the

added mass effect and is due to the distortion of the flow field around the body. Any body held in the accelerating fluid is subjected to this force which can be expressed in terms of the mass of fluid displaced by the body. The combined effects yield an expression of inertia force, denoted by F_I , exerted on a body submerged in a accelerating potential flow. This force is simply an expression of Newton's Second Law,

$$F_I = C_I \rho V \frac{dU}{dt} \quad (2-3)$$

where ρ is mass density of the fluid, V is the volume displaced by the body, $\frac{dU}{dt}$ is the acceleration of the fluid, and C_I is the inertia or mass coefficient. The contribution of the added mass to the total inertia force can be thought of as a fraction of the displaced mass and called the added mass coefficient. The inertia coefficient can be defined as $C_I = 1 + C_m$, in which C_m denotes the added mass coefficient. If a massless body is accelerated in still fluid, the first part of the inertia force is absent and inertia coefficient should be identical to the added mass coefficient. With potential flow theory, added mass coefficients can be analytically determined by integrating the pressure distribution over the surface of the body. The resulting values are 1.0 for an infinitely long cylinder and 0.5 for a sphere. Because of symmetry, there is no inertia force perpendicular to the flow direction unless the body is placed close to another body or solid surface.

Recent studies show that cylinders placed on or near a boundary experience considerable lift forces.[Jones(1978)] However, lift forces may not be significant for reef stability due to the permeable nature of most reef components. For this reason, the analysis of lift forces

on submerged reefs is excluded in this study.

Wave Forces

The flow under waves is unsteady and oscillatory. A submerged body experiences time-varying velocity and acceleration of the flow over a wave cycle. If the fluid around a fixed body starts to move, initially the flow pattern about the body closely resembles potential flow. The fluid travels along the surface of the body and no separation occurs. If the flow continues to move in one direction for a period of time, a boundary layer develops along the surface of the body, and the friction force becomes a significant part of the total force on the body. Then flow separation occurs, and the pressure drag becomes a major part of the total force. Because the flow is oscillatory, the process described above is interrupted when the direction of flow reverses. After the flow reverses, the entire process begins on the opposite side of the body until the next flow reversal and so forth.

The basic nature of the flow pattern depends on the period of time for which the flow continues in one direction before it reverses. If the period is very short, the flow about the body will be very close to inviscid, potential flow and inertia forces will govern the total force on the body. If the period of flow is very long, the flow will be quasi-steady and drag forces will dominate the total force. For flow periods between these extremes, both the inertia and drag force will contribute to the total force on the body. The widely used semi-empirical formulations used for estimating the wave force on a fixed body is the so-called Morison equation: [Morison et al. (1950)]

$$F = C_D \frac{\rho}{2} A U|U| + C_I \rho V \dot{U} \quad (2-4)$$

where $F = F_D + F_I$ is the total force on the body, and $\dot{U} = \frac{dU}{dt}$ is instantaneous acceleration of the fluid. $U|U|$ has been introduced in place of U^2 in order to ensure that the drag force is applied in the same direction as the instantaneous fluid velocity U . Other terms are as previously defined. The work of Morison et al.(1950), which led to Eq.(2-4), is based on the assumption that the total force can be obtained by adding the two components of force linearly, a drag force analogous to drag in steady flow and an inertia force as in potential flow. Their work was for cylindrical, vertical piles. They found that for any specific experiment with specific wave parameters, values of C_D and C_I could be chosen such that Eq.(2-4) gave good agreement with the time history of the measured force. The maximum forces occur at the instant when the vector sum of the drag and inertia forces reaches its maximum. In most cases, the maximum force experienced by an object is considerably higher than either the drag force or the inertia force alone. Morison and his co-workers did not give any information on how C_D and C_I varied with experimental parameters.

Near-bottom water motion under the waves is parallel to the bottom and oscillatory. Theoretical studies have shown that a double amplitude distance of water movement, $2a$, is necessary before flow separation from an object occurs. Yamamoto and Nath(1976), for example, have estimated the no-separation condition for pipes as $2a/D < 1.5$, D being the diameter of the pipe. Until the instant of flow separation, the real fluid effects are minimal and the flow-induced force on the cylinder can

be predicted based on potential flow concepts, and the first term of Eq.(2-4) can be neglected.

A designer may be more interested in the maximum value rather than in the time history of wave forces on an object under the selected design wave conditions. For design purposes, the maximum force coefficient, denoted by C_f , has been successfully introduced by several investigators.[Sarpkaya(1976), Grace(1977)] The maximum design force is defined as

$$F_{\max} = C_f \frac{\rho}{2} A U_{\max}^2 \quad (2-5)$$

Eq.(2-5) is the form of the drag force in a steady flow expressed by Eq.(2-1), even though coefficients in both equations are quite different. However, under the longer waves where separation occurs and flow is quasi-steady, the inertia force is negligible in Eq.(2-4) and the maximum force coefficient C_f may be identical with the drag coefficient C_D in Eq. (2-4). Under intermediate wave length conditions, the maximum force may not be achieved at the same instant as the maximum velocity. Nevertheless, Eq. (2-5) may be used to determine the magnitude of the maximum force.

2.2 Determination of Drag and Inertia Coefficients

Based on Morison's formula, many experimental works have been performed to determine the drag and inertia coefficients for submerged bodies of familiar shape such as circular cylinders and spheres. The results have been presented as a function of any parameter of significance, e.g., the Reynolds number or the Keulegan-Carpenter number.

For the circular cylindrical pipe, the general form of the Morison equation, Eq. (2-4), becomes

$$F = C_D \frac{\rho}{2} (D \ell) U |U| + C_I \rho \left(\frac{\pi D^2}{4} \right) \ell \dot{U} \quad (2-6)$$

where D , ℓ is the outer diameter and length of the cylinder, respectively, and U being the instantaneous velocity of the ambient flow. It was recognized that the drag and inertia coefficients in Eq. (2-6) are not constant throughout the wave cycle. [Sarpkaya(1976)] At the initial instants of flow, C_D is equal to its steady state value and $C_I = 2$ as obtained from potential flow conditions. As time progresses neither C_D nor C_I remains the same and changes with the changes in the flow, reflecting the past history and affected by the gross features of the current state. However, the coefficients C_D and C_I are assumed constant over a wave cycle for the convenience of application. To determine the coefficients C_D and C_I , the measured forces are related with either measured or theoretical kinematics of the ambient flow. Various theories can be used to predict the required kinematics from a given wave height H , wave period T , water depth h , and distance up from the sea floor to the point in question, S . If the theoretical kinematics are used, the resulting values of C_D and C_I are associated uniquely with the particular wave theory and attempts to use these values with other wave theories may result in large errors.

Three methods are available to determine C_D and C_I for a submerged body under unsteady flow: 1) least square, 2) maximum value, and 3) Fourier [Sarpkaya(1974)] decomposition methods. The two most common methods are described in the following paragraphs.

Least Square Method

The method of least-squares consists of the minimization of the error between the measured and calculated forces. The coefficients C_D and C_I are chosen so that there is a minimum mean square error between predicted and actual force traces over a wave cycle. Letting F_m represent the instantaneous measured force and F_c the force calculated through the use of Eq. (2-6), and writing

$$\epsilon^2 = (F_m - F_c)^2 \quad (2-7)$$

A total squared error can be obtained by integrating Eq. (2-7) with respect to time over one complete cycle of the wave motion. The equation becomes

$$\int_0^T \epsilon^2 dt = \int_0^T (F_m^2 + F_c^2 - 2 F_m F_c) dt \quad (2-8)$$

T being the period of wave motion. Taking the derivatives of Eq. (2-8) with respect to C_D and C_I , and setting the result to zero, one will minimize the square of the total error between the predicted and the measured forces:

$$\frac{d}{dC_D} \int_0^T \epsilon^2 dt = 0 \quad (2-9a)$$

$$\frac{d}{dC_I} \int_0^T \epsilon^2 dt = 0 \quad (2-9b)$$

Since Eq. (2-9) is a function of C_D and C_I , one can finally solve the

equation to obtain C_D and C_I :

$$C_D = \frac{\int_0^T F_m U |U| dt \int_0^T \dot{U}^2 dt - \int_0^T U |U| \dot{U} dt \int_0^T F_m \dot{U} dt}{\frac{\rho}{2} D \ell \left[\int_0^T \dot{U}^2 dt \int_0^T U^4 dt - \left(\int_0^T U |U| \dot{U} dt \right)^2 \right]} \quad (2-10a)$$

$$C_I = \frac{\int_0^T F_m \dot{U} dt \int_0^T U^4 dt - \int_0^T F_m U |U| dt \int_0^T U |U| \dot{U} dt}{\frac{\rho}{4} \pi D^2 \ell \left[\int_0^T \dot{U}^2 dt \int_0^T U^4 dt - \left(\int_0^T U |U| \dot{U} dt \right)^2 \right]} \quad (2-10b)$$

Maximum Value Method

Another approach to the drag and inertia coefficients is based on the following fact: the acceleration of the ambient flow is maximum when the velocity is zero, and it is zero when the velocity is maximum. For harmonic motion, it follows that the inertia force is maximum when the drag force is zero and it is zero when the drag force is maximum. The maximum value method is simple to use. The coefficients C_D and C_I can be determined by relating the maximum peak values of the velocity and acceleration of the ambient flow with the corresponding forces at each instant. The coefficients are given as:

$$C_D = \frac{F_m(t_1)}{\frac{\rho}{2} D \ell U_{\max}^2} \quad (2-11a)$$

$$C_I = \frac{F_m(t_2)}{\frac{\rho}{4} \pi D^2 \ell \dot{U}_{\max}} \quad (2-11b)$$

where t_1 , t_2 are the time at which the velocity and the acceleration are at their maxima, U_{\max} , \dot{U}_{\max} respectively and $F_m(t_1)$, $F_m(t_2)$ are the measured forces at the point of time t_1 and t_2 , respectively. The inertia force is always in phase with the acceleration of the flow. The inertia force is zero when the acceleration becomes zero. Therefore, the drag coefficients calculated by Eq. (2-11a) would exclude the effect of inertial forces. However, there is a phase-lag between the drag force and the velocity of the flow because the formation of a wake at the rear side of the object does not coincide with the wave cycle. Consequently, when the inertia force is maximum, the drag force still has some value, instead of zero as the theory predicts.

Though it is possible utilizing Fourier analysis procedures, there is no easy way to separate the drag component from the inertia component. [Nath, Yamamoto(1976)] The observed phase-lag may introduce errors in the evaluation of the inertia coefficients.

2.3 Determination of Maximum Force Coefficients

As previously mentioned, the peak value of the measured force can be simply related to the maximum velocity of the ambient flow obtained either from direct measurement or from a suitable wave theory. Then, the measured maximum force coefficient, denoted by $C_{f(\text{mes})}$, is calculated as

$$C_{f(\text{mes})} = \frac{\text{Maximum of the measured force in a cycle}}{\frac{\rho}{2} A U_{\max}^2} \quad (2-12)$$

Another approach is possible for the simple-harmonic wave condition predicted by Airy wave theory. For a sinusoidally oscillating flow represented by $U = -U_{\max} \cos \theta$, with $\theta = 2\pi t/T$, T being the period of oscillation, the least squares values of C_D and C_I for circular cylinders, Eq.(2-10), become [Sarpkaya(1976)]

$$C_D = -\frac{8}{3\pi} \int_0^{2\pi} \frac{F_m \cos \theta |\cos \theta|}{D U_{\max}} d\theta \quad (2-13a)$$

and

$$C_I = \frac{2U_{\max} T}{\pi^3 D} \int_0^{2\pi} \frac{F_m \sin \theta}{\rho D \ell U_{\max}^2} d\theta \quad (2-13b)$$

in which F_m represents the measured force. Since $\dot{U} = \frac{2\pi}{T} U_{\max} \sin \theta$, it can be shown that the Morison Equation, Eq. (2-4) yields

$$F_{\max} = [C_D + \frac{\pi^4 C_I^2}{4C_D} \left(\frac{1}{U_{\max} T/D} \right)^2] \frac{\rho}{2} (D \ell) U_{\max}^2 \quad (2-14)$$

Comparing Eq. (2-14) with Eq. (2-5), the calculated maximum force coefficient, denoted by $C_{f(\text{cal})}$ can be written as

$$C_{f(\text{cal})} = C_D + \frac{\pi^4 C_I^2}{4 C_D (K-C)^2} \quad (2-15)$$

in which $K-C = U_{\max} \cdot T/D = 2a/D$, a being the half amplitude of water particle motion. The period parameter $K-C$ is known as Keulegan-

Carpenter number which will be discussed further in the following section. For this particular case of sinusoidal oscillation, $C_{f(mes)}$ is not necessarily equal to either $C_{f(cal)}$ or to a similar coefficient obtained through the use of the semi-peak-to-peak value of the measured force. [Sarpkaya(1976)]

2.4 Governing Parameters

Past studies indicate that wave forces on submerged objects such as circular cylinders, spheres and discs are in general dependent on the following parameters

$$F = f(t, T, U_{max}, D, \rho, \nu) \quad (2-16)$$

where ρ , ν are the mass density and kinematic viscosity of the fluid, respectively and T is the period of oscillation. Grouping the variables on the basis of dimensional analysis [Sarpkaya(1976)]

$$\frac{F}{\frac{\rho}{2} D \ell U_{max}^2} = f\left(\frac{t}{T}, \frac{U_{max} T}{D}, \frac{U_{max} D}{\nu}\right) \quad (2-17)$$

or introducing the phase angle $\theta = 2\pi t/T$,

$$\frac{F}{\frac{\rho}{2} D \ell U_{max}^2} = f(\theta, K-C, Re) \quad (2-18)$$

where $Re = \frac{U_{max} D}{\nu}$ is the Reynolds number and $K-C$ is Keulegan-Carpenter

number or period parameter defined by

$$K-C = \frac{U_{\max} \cdot T}{D} \quad (2-19)$$

For the objects of other shapes such as tire reef components, D may be defined as the length of the objects along the direction of ambient fluid velocity U . (See Section 3.1)

Equation(2-18), combined with Eq. (2-4), yields

$$C_D = f_1(\theta, K-C, R_e) \quad (2-20a)$$

$$C_I = f_2(\theta, K-C, R_e) \quad (2-20b)$$

The phase parameter can be eliminated by considering time-invariant averages of the force coefficients. Thus, Eq. 2-20 gives

$$\begin{Bmatrix} C_D \\ C_I \end{Bmatrix} = f_1(K-C, R_e) \quad (2-21)$$

2.5 Coefficient Dependence on Governing Parameters

Several researchers have made extensive studies to clarify the variation of C_D and C_I as functions of the Reynolds number and/or period parameter based on the Morison equation. Keulegan and Carpenter (1958) studied the force on a horizontally placed circular cylinder in two-dimensional flow oscillating with simple sinusoidal motion. They placed a cylinder at the node point of a standing wave so that the fluid motion at the location of the test cylinder was sinusoidal and in the horizontal direction only. The drag and inertia coefficients obtained

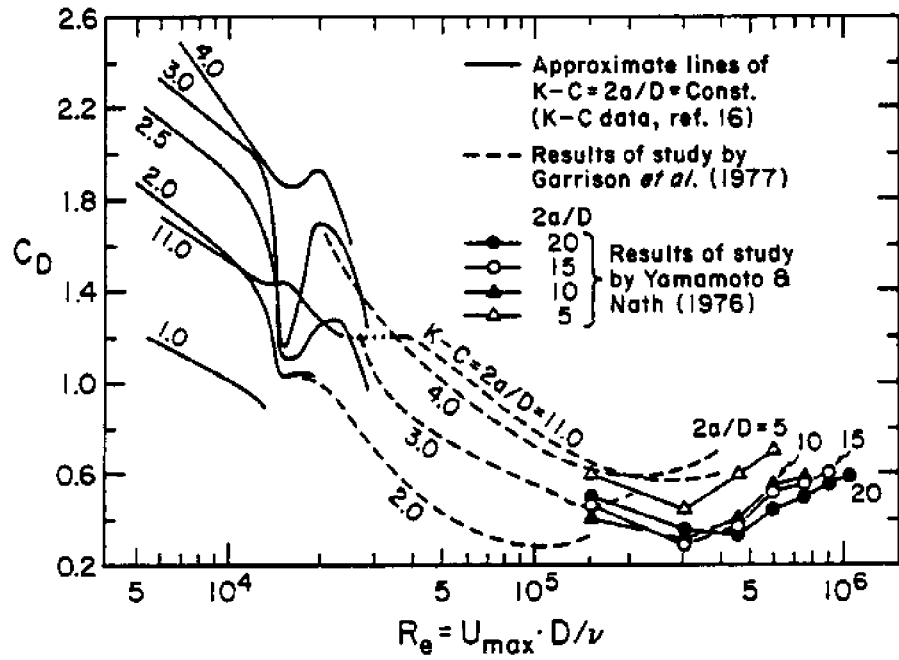
from the experiments were presented as smoothly varying functions of the period parameter, $K-C=U_{\max} \cdot T/D$. They found that for small values of the period parameter ($K-C < 3$) the force was accurately given by the potential flow solution, namely, by the second term of Eq. (2-4) with C_I equal to 2 for a cylinder and 1 for a plate.

Sarpkaya(1975) carried out tests similar to Keulegan and Carpenter using a U-tube oscillator instead of a standing wave oscillator. The drag and inertia coefficients, plotted as functions of the period parameter, were generally similar to those of the previous investigation.

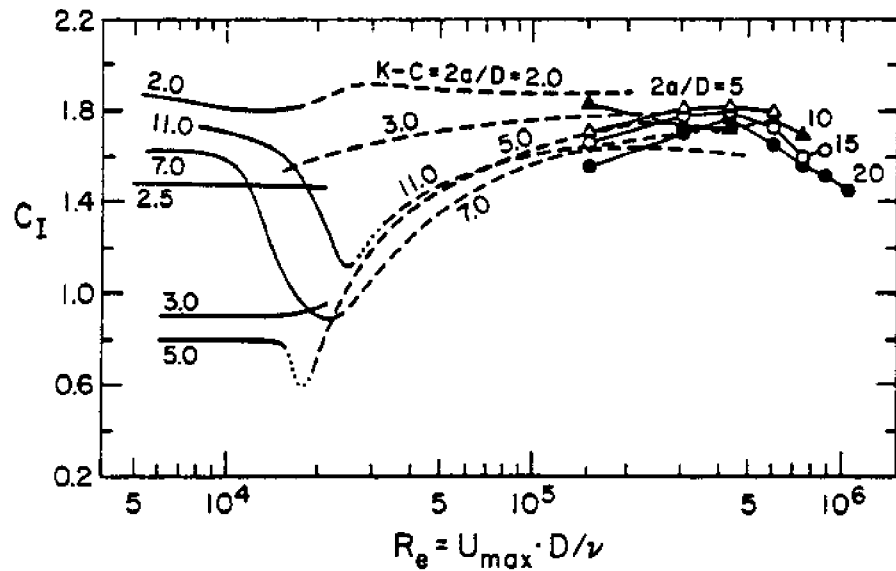
Garrison et al.(1977) used a different type of test apparatus to investigate the effect of both Reynolds number and the period parameter in sinusoidally oscillating flow. The test cylinder was suspended from a carriage by struts into a water channel and the carriage was driven in sinusoidal motion by a linkage connected eccentrically to a flywheel. With this device they were able to obtain data over a range of high Reynolds numbers and their results are presented in Fig. 2-2 with those obtained by reploting the data of Keulegan and Carpenter. The period parameter $K-C$ is equal to $2a/D$, a being the half amplitude of the fluid motion, or in this case, the half amplitude of the cylinder oscillation.

Yamamoto and Nath(1976) also performed a similar test to that of Garrison et al. The test cylinder was connected to a carriage which was driven at speeds sufficient to yeild Reynolds number up to 10^6 . Their results are shown in Fig. 2-2 along with the results of other investigators.

The drag coefficient shown in Fig. 2-2a appears to vary slowly with Reynolds number for $R_e < 10^4$ but in the range $10^4 < R_e < 2.5 \times 10^4$ some dramatic variations take place. At values of $R_e > 2.5 \times 10^4$ the



(a)



(b)

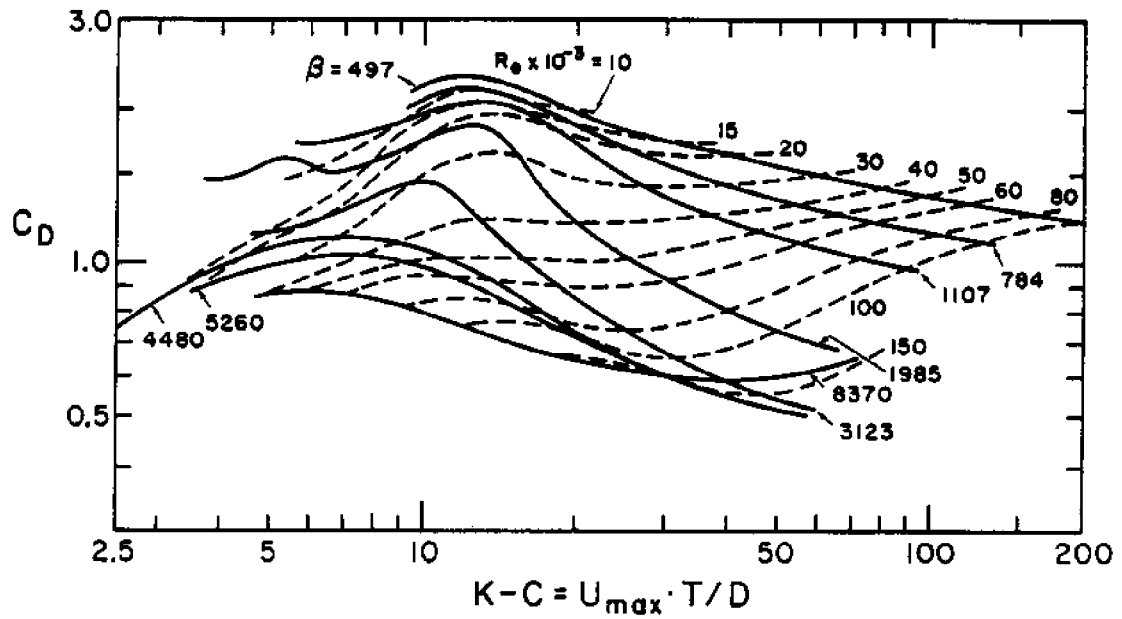
Fig. 2-2 (a) Drag and (b) Inertia Coefficients vs. Reynolds Number, Smooth Cylinder in Periodic Flow

variation is again gradual and appears to approach a constant value at high Reynolds number. At low values of Reynolds number C_I tends to be independent of the Reynolds number but highly dependent upon $2a/D$. The results pass through a region of extreme variations in the $10^4 - 3 \times 10^4$ Reynolds number range and tend to increase to constant values at high Reynolds number. As the Keulegan-Carpenter number decreases, C_D and C_I tend to their potential flow value of zero and 2.0, respectively. However, at Reynolds number greater than 5×10^5 , drag coefficients tend to increase while inertia coefficients tend to decrease.

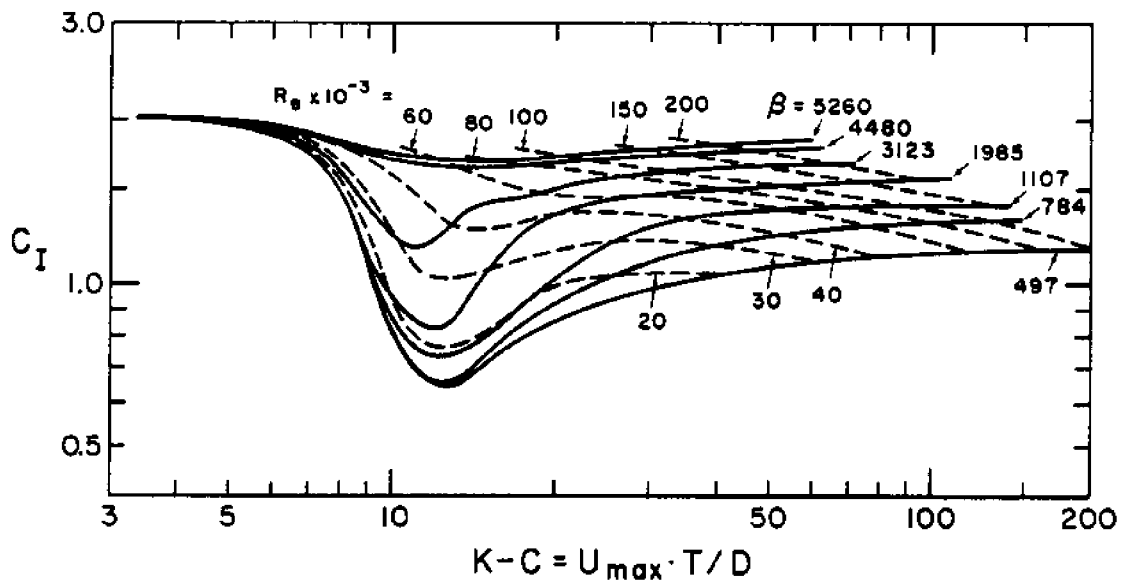
Sarpkaya(1976) presented the results of a comprehensive and detailed series of tests of two-dimensional oscillatory flow forces on circular cylinders. He used a large U-shaped water tunnel, 16 ft high and 30 ft wide. The in-line force data was sufficiently comprehensive to determine C_D and C_I as functions of both the period parameter and a viscosity parameter. Instead of using the usual Reynolds number as a viscosity parameter, Sarpkaya used a dimensionless parameter termed "frequency parameter", which is the Reynolds number divided by the period parameter, and is denoted by

$$\beta = \frac{R_e}{K-C} = \frac{D^2}{\nu T} \quad (2-22)$$

Since T was fixed at the natural period of the water tunnel, measurements were obtained as a function of $K-C$ for fixed β for each cylinder. Fig. 2-3 shows the variation of C_D and C_I as functions of $K-C$ taking Reynolds number and β as independent variables. For small $K-C$ (less than 3), values of C_I measured by Sarpkaya lie close to the potential flow value of 2, as was determined by Keulegan and Carpenter.



(a)



(b)

Fig. 2-3 (a) Drag and (b) Inertia Coefficients vs. Keulegan-Carpenter Number for Particular Values of R_e and β [Sarpkaya (1976)]

For large β , C_I lies close to 2 for all $K-C$. The drag coefficient passes through a maximum and then decreases with increasing $K-C$. For R_e smaller than 3500, the maximum values of C_D and the minimum values of C_I appear in the range $10 < K-C < 15$.

Other important factors that influence drag and inertia coefficients are roughness on the surface of the body and proximity of a plane wall to the body. The cylinder surface roughness is represented by k , the average height of protuberances on the surface, and the dimensionless parameter describing relative roughness for a cylinder is

$$G = \frac{k}{D} \quad (2-23)$$

The proximity effect of a cylinder can be expressed in dimensionless parametric form as

$$J = \frac{e}{D} \quad (2-24)$$

where e is the distance between the wall and the nearest edge of the circular cylinder. The roughness effect on circular cylinder under the steady flow has two distinct features. First, the critical Reynolds number, R_c , decreases as the roughness on an object surface of specified size and shape is increased. Second, C_D progressively increases with increasing relative roughness.

For oscillating flows about rough cylinders, the drag and inertia coefficients may be assumed to be functions of three parameters, namely

$$\left\{ \begin{array}{c} C_D \\ C_I \end{array} \right\} = f(R_e, K-C, k/D) \quad (2-25)$$

Sarpkaya(1976) studied the effect of the varying roughness of a cylinder on C_D and C_I as the functions of Reynolds number by maintaining $K-C$ constant under the flow of simple harmonic oscillation. The volume of his data enabled him to obtain the following conclusions: for large values of $K-C$, the drag coefficient for a rough cylinder is larger than that for a smooth cylinder and does not vary appreciable with $K-C$. The inertia coefficient is considerably lower than that for a smooth cylinder and it too does not appreciably vary with $K-C$ for sufficiently large values of $K-C > 25$.

The proximity effect in a steady flow has been investigated in some detail by Jones(1971). He found that variations in e/D (from 0.0 to 0.16) had no discernible effect on C_D . Nath and Yamamoto and others(1974, 1976) carried out a series of theoretical and experimental studies on the proximity effect for the case of oscillatory flow. For the range of small values of period parameter($K-C \leq 2$) in which drag force is negligible and wave forces can be predicted by potential theory, the inertia coefficient rapidly reduces from 3.5(at $e/D=0$) to 2.0($e/D=0.5$) as e/D increases. The value of C_D increases as the cylinder approaches the boundary. It is noticable that the value of C_D for the near boundary flow($e/D=0.083$) is about two times as large as that for the free stream flow. This is probably due to the flow blockage effect of the plane boundary.

The maximum force coefficient defined by Eq. (2-12) was shown to be strongly period parameter dependent by Sarpkaya(1976) and Grace(1979). From the measured force data in the laboratory U-tube, Sarpkaya obtained a unique relationship between the measured maximum force coefficient, $C_{f(mes)}$, and Keulegan-Carpenter period parameter as shown in Fig. 2-4a.

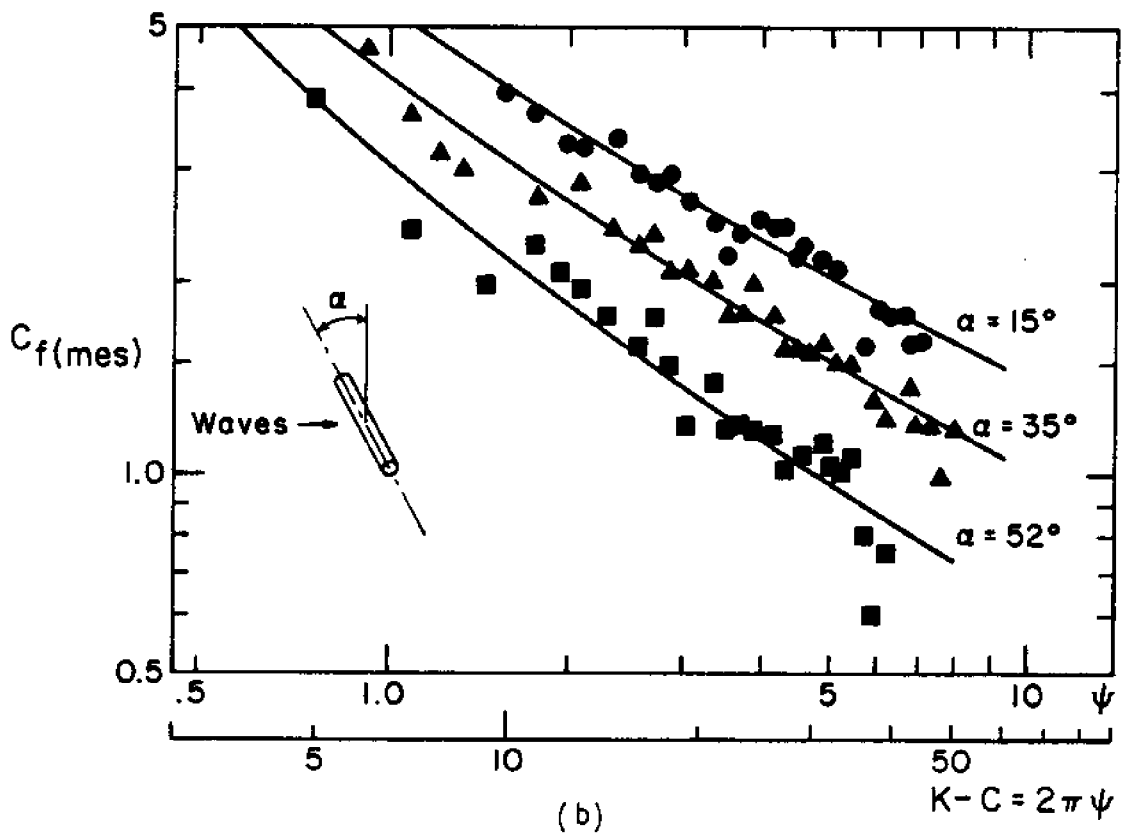
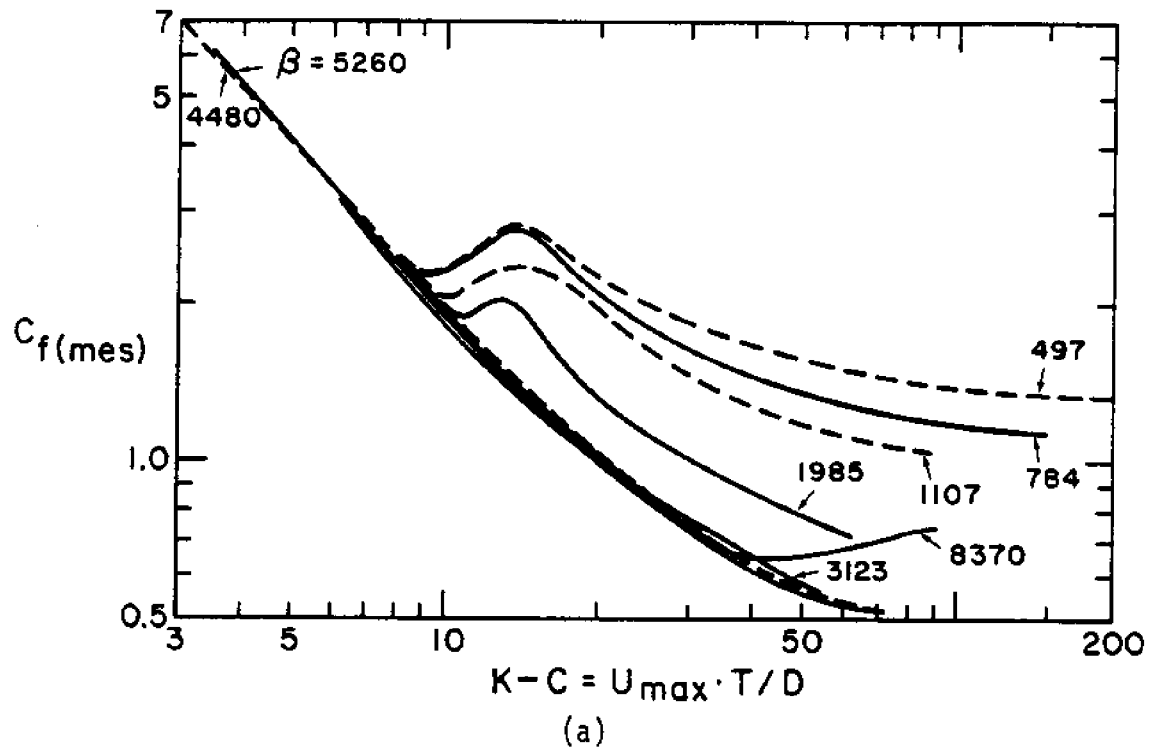


Fig. 2-4 (a) C_f (mes) vs. $K-C$ for Particular Values of β [Sarpkaya(1976)] (b) Mean Lines of C_f (mes) vs. ψ [Grace(1979)]

It shows that in the drag dominated region of the flow ($k-C < 10$) the constant lines are very similar to those shown in Fig. 2-3a for the drag coefficient. In the inertia dominated region, the maximum force coefficient is nearly independent of R_e and increases with decreasing $K-C$.

Grace carried out a field study of ocean wave forces on a cylinder placed on the ocean bottom and subjected to swell with several different incident angles relative to the axis of the pipe. The measured peak horizontal forces were directly correlated with measured maximum horizontal velocity to yield maximum force coefficients by Eq. 2-12. He used a measured period parameter, ψ , as defined by

$$\psi = \frac{U_{bmax}^2}{\dot{U}_{bmax} \cdot D} \quad (2-26)$$

where U_{bmax} and \dot{U}_{bmax} represent the maximum velocity and the maximum acceleration, respectively, at a point very near the ocean bottom. For simple harmonic oscillation, ψ is the Keulegan-Carpenter number divided by 2π so that for simple harmonic motion,

$$K-C = 2 \pi \psi \quad (2-27)$$

His results are shown in Fig. 2-4b. The measured maximum force coefficient exponentially decays as the Keulegan-Carpenter number (or the measured period parameter) increases. The magnitude increases significantly as the cylinder orientation becomes perpendicular to the incident waves. The results of Sarpkaya and Grace show that the measured maximum force coefficients for circular cylinders are strongly dependent on the Keulegan-Carpenter number, varying as an inverse exponential

function.

The maximum force coefficient dependence on the Keulegan-Carpenter period parameter for other submerged object shapes has not been clarified in the literature. However, one may expect a similar trend for the case of three dimensional bodies such as rubber tire configurations. While three dimensional bodies bear little geometric similarity to cylinders, the dependence of wave forces on the length of the fluid path trajectory relative to the body dimension is still expected to be important. Furthermore, surface roughness and proximity effects are expected to produce proportional changes in three dimensional bodies.

III. EXPERIMENTAL APPARATUS AND PROCEDURES

Introduction

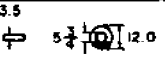
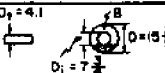
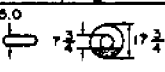
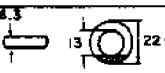
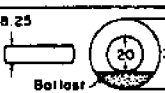

Laboratory tests were conducted in a wave channel to obtain force data on tire configurations of various sizes and shapes. The force data were collected concurrently with surface wave profiles and water particle kinematics so that force coefficients and their dependence on the governing parameters could be determined. A test for determination of resistance coefficients of tire configurations in contact with marine sediments was completed so that ballast requirements could be calculated to resist wave forces on the various tire configurations. This chapter describes test materials and laboratory equipment as well as discusses methodology utilized in the experiments.

3.1 Tire Configurations

A variety of scrap rubber tires can be utilized as reef material. Passenger car tires are the most plentiful resource and are available in a range of sizes. The outer diameter of most passenger car tires varies between 19 inches and 27 inches and inner(wheel) diameter varies between 10 inches and 15 inches. Truck tires are also available in great quantities with outer diameters varying from 24 to 60 inches and wheel diameters from 14 to 36.5 inches.



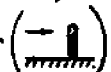
The experiments conducted in this study utilized six different tire diameters, specifically, 12", $15\frac{3}{8}$ ", $17\frac{3}{4}$ ", $22\frac{3}{4}$ ", 37" and $42\frac{3}{8}$ ". Their dimensions are shown in Fig. 3-1. The first four tire sizes were used in laboratory experiments and the remaining two sizes were used for field experiments. The smaller tires were used in the laboratory experiments

Fig. 3-1 Properties of Tires Used in the Experiment

| Nominal D (ft) | Dimensions (inch) | Projected Area (ft ²) | | $\frac{D_i}{D}$ | $\frac{D_t}{D}$ | $\frac{B}{D_t}$ | Ballast (concrete) | |
|-------------------|---|-----------------------------------|-------|-----------------|-----------------|-----------------|----------------------|-----------------------|
| | | — or | ⊙ | | | | V (ft ³) | W _{sub} (lb) |
| 1.0 |  | .273 | .605 | .479 | .292 | .89 | .033 | 2.9 |
| 1.3 |  | .415 | .966 | .503 | .266 | .93 | .061 | 5.3 |
| 1.5 |  | .579 | 1.391 | .437 | .282 | 1.00 | .112 | 9.6 |
| 1.9 |  | .936 | 1.901 | .571 | .277 | .77 | .158 | 13.6 |
| 3.1 |  | 2.120 | 5.285 | .541 | .223 | 1.03 | .588 | 50.6 |
| 3.5 |  | 3.053 | 6.750 | .558 | .249 | .90 | .890 | 76.5 |

to avoid blockage effects across the two dimensional cross section.

Each individual tire has three major orientations as reef components:

(1) flat  on the ocean bottom, (2) parallel  or (3) perpendicular  to the direction of wave propagation. The projected area of each case is given for tires of all sizes. In Fig. 3-1, the outer diameter is identified as D, the inner diameter as D_i, the tread width as D_t, and the casing depth as B. Mean values of the ratios D_i/D, D_t/D, B/D_t of six sample tires were found to be 0.515, 0.265 and 0.92, respectively.

The weight of tire is a function of D, D_i/D, B/D_t, thickness and density of the rubber casing. The weight in air is compared with that in water in Fig. 3-2 for sample tires of six different outer diameter. The submerged weight is only 13.5 to 16 percent of the dry weight. The unit weight of the rubber tire material was evaluated to be 73 to 74 lbs/ft

yielding a specific gravity of 1.14 to 1.16. This indicates that rubber tires require additional ballast to significantly increase the submerged weight. The weight of concrete ballast available in the cylindrical segment between the tire bead and tread is identified in the last column of Fig. 3-1.

Using the sample tires, seven different unit configurations were selected according to the recommendations of marine biologists. [Ref. 4 and 22] The selection criteria were: 1) to provide a variety of habitat sizes to attract a variety of bottom fish, 2) to maximize surface area for marine growth, 3) to minimize frontal area to reduce wave and current loads, 4) to maximize bottom surface area to increase bottom friction resistance and 5) to utilize combinations which are

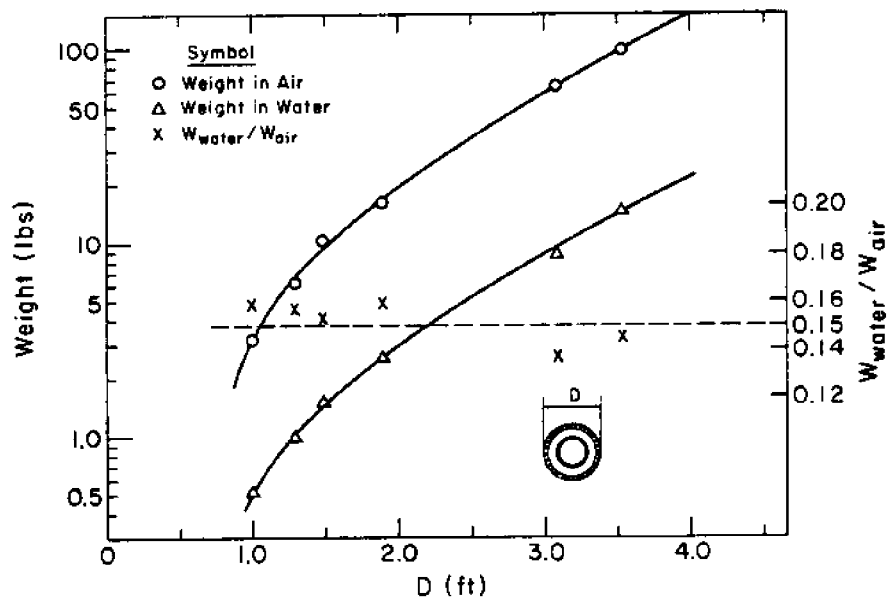
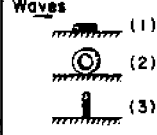
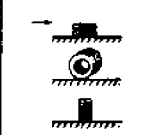
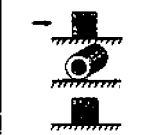
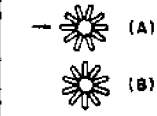

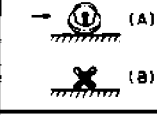
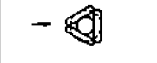


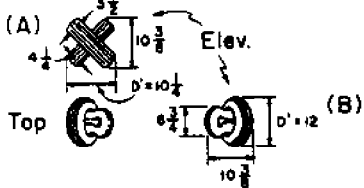
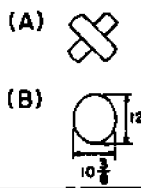
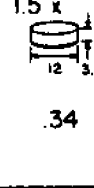
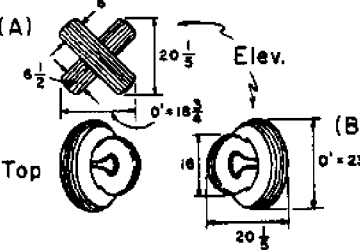
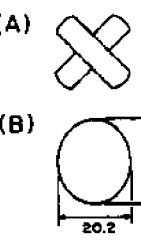
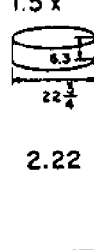
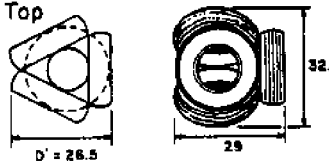
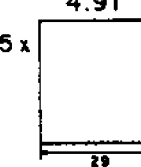
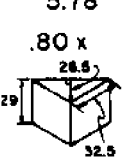
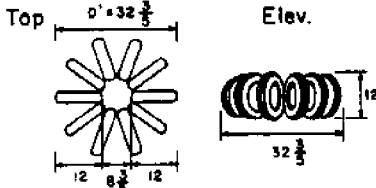
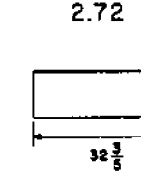
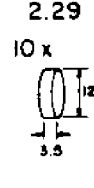
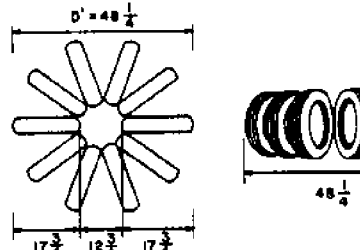
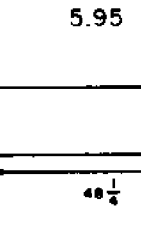
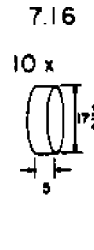
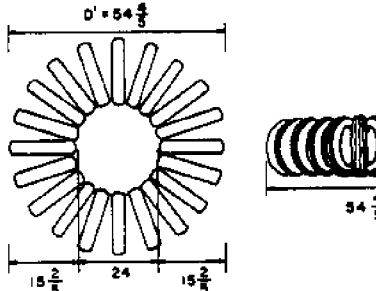

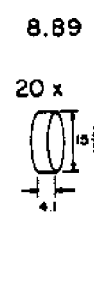
Fig. 3-2 Weight of Tire in Air and in Fresh Water

Table 1. Effective Diameter(D') and Projected Area(A) of Tire Units

| Configuration | D=1.0 ft | | D=1.283 ft | | D=1.479 ft | | D=1.896 ft | | Average | |
|--|----------|----------------------|------------|----------------------|------------|----------------------|------------|----------------------|---------|----------------------|
| | D'/D | $A/\frac{\pi}{4}D^2$ | D'/D | $A/\frac{\pi}{4}D^2$ | D'/D | $A/\frac{\pi}{4}D^2$ | D'/D | $A/\frac{\pi}{4}D^2$ | D'/D | $A/\frac{\pi}{4}D^2$ |
|  (1) (2) (3) | 1.0 | 0.348 | 1.0 | 0.321 | 1.0 | 0.337 | 1.0 | 0.332 | 1.0 | 0.335 |
| | 1.0 | 0.348 | 1.0 | 0.321 | 1.0 | 0.337 | 1.0 | 0.332 | 1.0 | 0.335 |
| | 0.292 | 0.760 | 0.267 | 0.747 | 0.282 | 0.810 | 0.277 | 0.673 | 0.280 | 0.748 |
|  | 1.0 | 0.695 | 1.0 | 0.642 | 1.0 | 0.674 | 1.0 | 0.663 | 1.0 | 0.669 |
| | 1.0 | 0.695 | 1.0 | 0.642 | 1.0 | 0.674 | 1.0 | 0.663 | 1.0 | 0.669 |
| | 0.584 | 0.760 | 0.535 | 0.747 | 0.564 | 0.810 | 0.554 | 0.673 | 0.559 | 0.748 |
|  | 1.0 | 1.390 | 1.0 | 1.283 | 1.0 | 1.348 | 1.0 | 1.326 | 1.0 | 1.337 |
| | 1.0 | 1.390 | 1.0 | 1.283 | 1.0 | 1.348 | 1.0 | 1.326 | 1.0 | 1.337 |
| | 1.168 | 0.760 | 1.070 | 0.747 | 1.128 | 0.810 | 1.108 | 0.673 | 1.118 | 0.748 |
|  (A) (B) | 2.72 | 3.463 | - | - | 2.72 | 3.463 | - | - | 2.72 | 3.463 |
| | 2.72 | 3.463 | - | - | 2.72 | 3.463 | - | - | 2.72 | 3.463 |
|  | - | - | 3.56 | 4.53 | - | - | - | - | 3.56 | 4.53 |
|  (A) (B) | 1.0 | 0.709 | - | - | - | - | 1.0 | 0.595 | 1.0 | 0.648 |
| | 0.854 | 0.866 | - | - | - | - | 0.824 | 0.896 | 0.839 | 0.881 |
|  | - | - | - | - | - | - | 1.165 | 1.739 | 1.165 | 1.739 |

relatively simple and economical to construct. The stability of each unit configuration was tested for tires of varying sizes and different orientations. Table 1 shows projected areas of each tire unit configuration according to its orientation. An effective diameter of the tire units, D' , in Table 1 is defined as the length of the tire units in the direction of wave propagation and D is the outer diameter of the component tires. D' is identical to D for the first three configurations with orientations(1) and (2) in Table 1. The effective diameter of each tire unit was used for calculation of Keulegan-Carpenter period

Fig. 3-3 Dimensions of Complex Tire Configurations

| Configuration | Dimensions (inch) | A (ft ²) | V (ft ³) |
|------------------------------|---|---|---|
| 2 Tires stuffed (D=1.0') |  |  |  |
| 2 Tires stuffed (D=1.9') |  |  |  |
| 4 Tires triangle (D=1.9') |  |  |  |
| 10 Tires rosette (D=1.0') |  |  |  |
| 10 Tires rosette (D=1.5') |  |  |  |
| 20 Tires rosette (D=1.3') |  |  |  |

parameter and Reynolds number represented by $K-C=U_{bmax} \cdot T/D'$ and $Re=U_{bmax} \cdot D'/\nu$, respectively.

The tire casing volume is defined so that inertia coefficients may be calculated for each tire unit configuration. For the first three configurations in Table 1, the volumes are defined by

$$V = \left(\frac{\pi}{4} D^2 \right) (D_t) \cdot n \quad \text{for orientation(1) and (2)} \quad (3-1a)$$

$$V = \frac{\pi}{4} (D^2 - D_j^2) (D_t) \cdot n \quad \text{for orientation(3)} \quad (3-1b)$$

where n is the number of tires used.

The projected area and the volume of tire casings for the other four configurations are calculated from the geometries of the tire units as shown in Fig. 3-3. The projected areas of two stuffed tires are calculated as the area of a cross(Orientation A) and ellipse(OrientationB). The volume of tire casing is calculated as 1.5 times that of a single tire. The projected area for rosette configurations is calculated as the outer diameter of the tires multiplied by the outer diameter of the resulting rosette. The volume of a rosette configuration is calculated as the volume of one tire casing multiplied by the total number of tires in the rosette. The triangle configuration is made of four tires of $D = 22\frac{3}{4}$ " and takes its projected area as approximately 75 percent of the rectangle formed by its width and height. Its volume is defined as approximately 85 percent of a triangular column formed by its width, height and length along the direction of wave propagation. Previously defined projected area(A) and volume of tire casing(V) and effective diameter(D') of each tire unit are maintained throughout all

calculations of C_D , C_I , C_f , K-C and R_e .

Holes were drilled in each tire to facilitate fabrication and submersion of reef components. Six holes are drilled in each tire: One at the bottom, one on top and other four at quarter points on both side walls. The top hole is for escape of entrapped air inside the tire casing when submerged. A steel pipe of $\frac{3}{4}$ " diameter is fixed through the center of the concrete ballast to fix the tire on the dynamometer test table. Each tire was ballasted by filling with concrete up to the bottom level of the bead as shown in Fig. 3-4. For connection with other tires, bolts of $\frac{1}{2}$ " diameter with 2" washers and nuts were used as shown in Fig. 3-4.

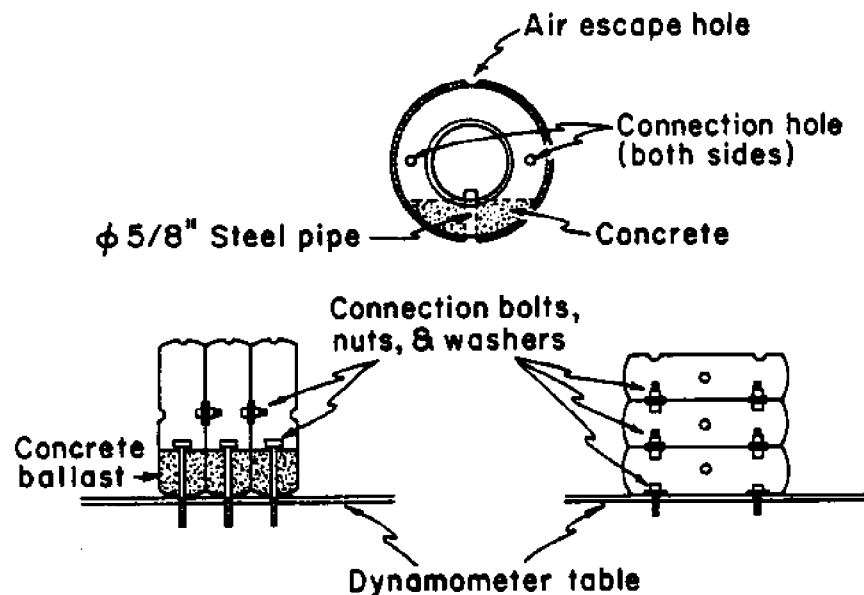


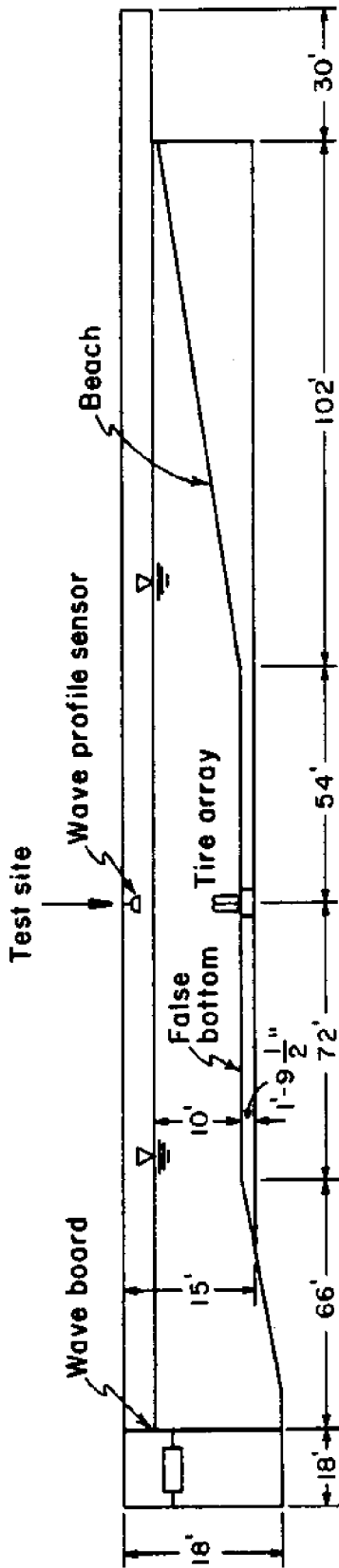
Fig. 3-4 Drilling and Fabrication of Tire Units

3.2 Wave Research Facility

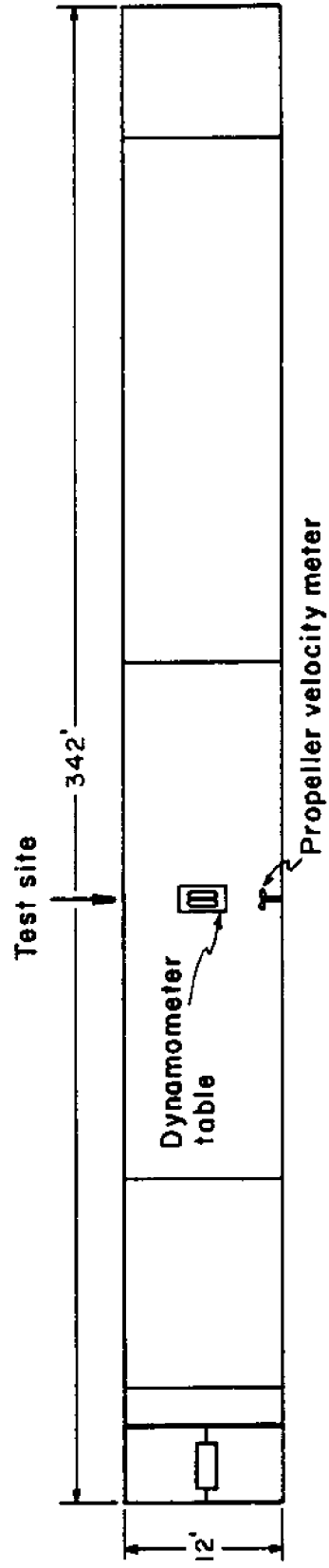
The experiments were conducted at the Oregon State University Wave Research Facility. Fig. 3-5 shows the dimensions and physical layout of the wave channel. The hydraulic wave generator is a flap-type board which is hinged at the bottom. It is activated by a 150 horsepower, 76 gallon per minute pump and is controlled by a hydraulic servo-mechanism which is coupled to an electronic function generator. This facility is capable of producing solitary, periodic, and random waves with breaking wave heights up to 5 feet.

A dynamometer table was placed at the test site to measure the horizontal force exerted on the various tire units attached to the table surface. The false bottom of the channel was located flush with the dynamometer table by placing concrete slabs on steel angles attached to either side of the channel. A water depth of 10 feet above the false bottom was maintained during the test.

Monochromatic waves with amplitudes up to 75 percent of the theoretical breaking height were utilized in the test. Seven different wave periods (1.98 to 9.88 seconds) were chosen to match specified cases (Case 4 to Case 8) in Dean's Stream-function wave theory. Table 2 shows the test wave conditions and associated wave kinematics at the channel bottom as predicted by Airy theory. The selected wave conditions span a range of relative depths from deep to shallow water. Sixteen waves with various wave periods and wave heights form a test set for each tire configuration. A total of 656 runs were made to complete the stability study of 41 cases made from seven different configurations, four different tire sizes and three different orientations.



Sectional Elevation



Plan

Fig. 3-5 Oregon State University Wave Research Facility

Table 2. Test Wave Conditions (h= 10.0ft)

| T (sec) | h/L ₀ | H (ft) | L (ft) | H/L | Airy's Theory | | Case (γ-Theory) |
|------------|------------------|-----------|-----------|------|---------------|--------------------------|--------------------|
| | | | | | 2a(ft) | U _{bmax} (ft/s) | |
| 1.98 | 0.50 | 0.84 | 20.3 | 0.04 | 0.07 | 0.11 | 8-A |
| | | 1.68 | 21.2 | 0.08 | 0.16 | 0.23 | 8-B |
| | | 2.52 | 22.5 | 0.11 | 0.26 | 0.34 | 8-C |
| 2.36 | 0.35 | 1.13 | 28.3 | 0.04 | 0.24 | 0.32 | 7.5-A |
| | | 2.26 | 28.3 | 0.08 | 0.48 | 0.64 | 7.5-B |
| | | 3.38 | 28.8 | 0.12 | 0.72 | 0.96 | 7.5-C |
| 3.13 | 0.20 | 1.56 | 45.0 | 0.04 | 0.82 | 0.81 | 7-A |
| | | 3.12 | 46.6 | 0.07 | 1.63 | 1.62 | 7-B |
| | | 4.69 | 49.1 | 0.10 | 2.36 | 2.43 | 7-C |
| 3.61 | 0.15 | 1.73 | 55.4 | 0.03 | 1.22 | 1.06 | 6.5-A |
| | | 3.47 | 57.7 | 0.06 | 2.44 | 2.12 | 6.5-B |
| 4.42 | 0.10 | 1.83 | 71.8 | 0.03 | 1.76 | 1.29 | 6-A |
| | | 3.66 | 74.4 | 0.05 | 3.16 | 2.59 | 6-B |
| 6.25 | 0.05 | 1.95 | 108.2 | 0.02 | 3.11 | 1.56 | 5-A |
| | | 2.67 | 110.1 | 0.02 | 4.36 | 2.14 | 5-* |
| 9.88 | 0.02 | 1.95 | 179.3 | 0.01 | 5.27 | 1.68 | 4-A |

* Mid point of Case 5-B and 5-C

$$L_0 = (g/2\pi)T^2 \quad L = L_0 \tanh(2\pi/L)h$$

$$U_b = \frac{\pi H}{T} \frac{\sin(2\pi/T) \cdot t}{\sinh(2\pi/L)h}$$

$$a = \frac{1}{2} \int_0^T U_b dt = \frac{T}{2\pi} U_{bmax}$$

3.3 Measurement Techniques

The wave surface profile was sensed by a Sonic Systems Model 86 acoustic profiler. This instrument senses distance by measuring the delay time for a pulsed acoustic signal to propagate to the water surface and reflect back to the transducer head. The product of delay time with the speed of sound is equal to twice the distance to the water surface. Signal conditioning within the instrument provides a calibrated voltage output which is proportional to the distance to the water surface. The output is recorded on a visicorder oscillograph simultaneously with wave force and velocity measurements. The instrument samples the distance at 60 cycles per second, yielding a nearly continuous wave record.

The horizontal wave forces on the various tire configurations were sensed by the strain gages attached to four legs of the dynamometer table. The detailed structure of the dynamometer table is shown in Fig. 3-6. The table is made of $3' - 10\frac{1}{4}'' \times 3' - 8\frac{1}{2}'' \times \frac{1}{2}''$ aluminum plate and is connected to four legs of 1" aluminum rod through pinned rod ends. Thus the top of the support legs experience no resisting moment when displaced horizontally by any force acting upon the table. The aluminum rods are rigidly welded $5'' \times 2'' \times \frac{1}{4}''$ steel channel. Strain gages are attached to each leg three inches off bottom and are referred to as Gage A, B(wave board side) and Gage C, D(beach side). The dynamometer table was isolated on four sides by a sealed wooden enclosure to minimize extraneous forces caused by the movement of water between the bottom of wave channel and the false bottom. The table plate has holes of one inch diameter drilled at three inch centers to relieve the vertical forces on the table caused by wave induced bottom

wave profile and horizontal forces. The distance between the meter and the false bottom was adjusted to be between three and eleven inches according to the size of the tire units being tested. The elevation of the velocity measurement was adjusted to coincide with the geometric center of the tire units. This type of velocity indicator is limited to speed measurements; direction cannot be inferred from the records.

The calibration curves for horizontal force and near bottom water particle velocity are given in Fig. 3-7. Force calibrations were accomplished by displacing the dynamometer table with a cable and weight system, and recording the magnitude of resulting voltage at each strain gage pair. Calibration for water particle velocity was performed by pulling the velocity meter in a still water at five different speeds and recording the magnitude of resulting voltage in each step. The relationship obtained from the calibration can be written as

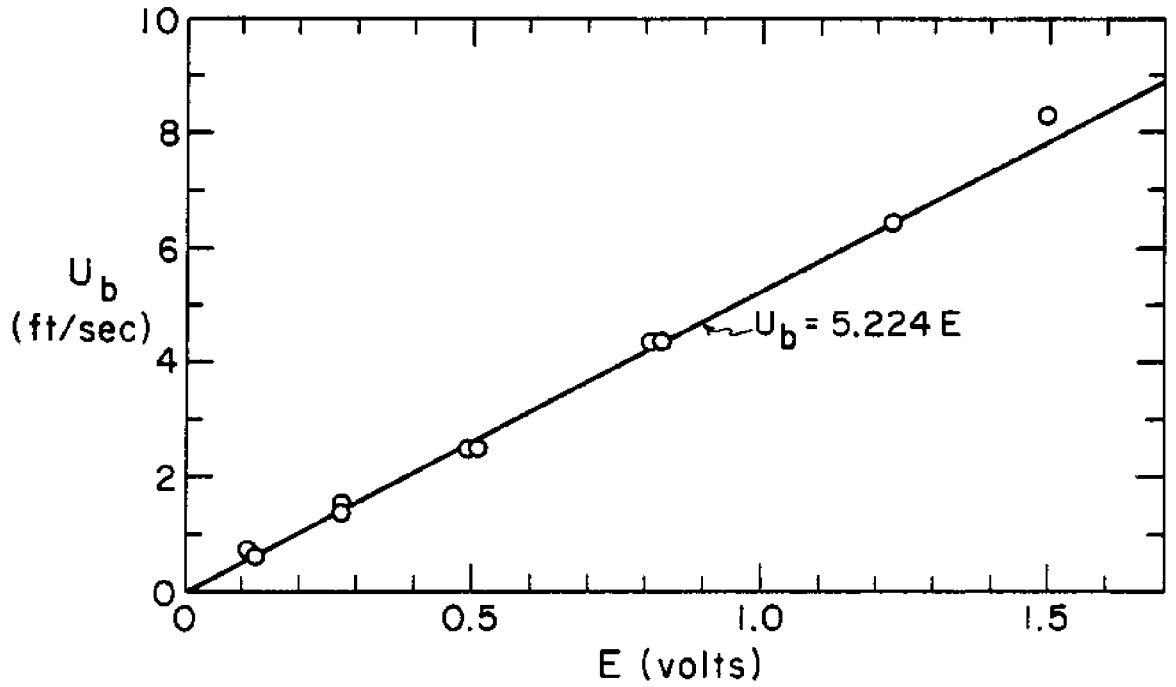
$$U(\text{ft/sec}) = 5.224 E(\text{volts}) \quad (3-2a)$$

and

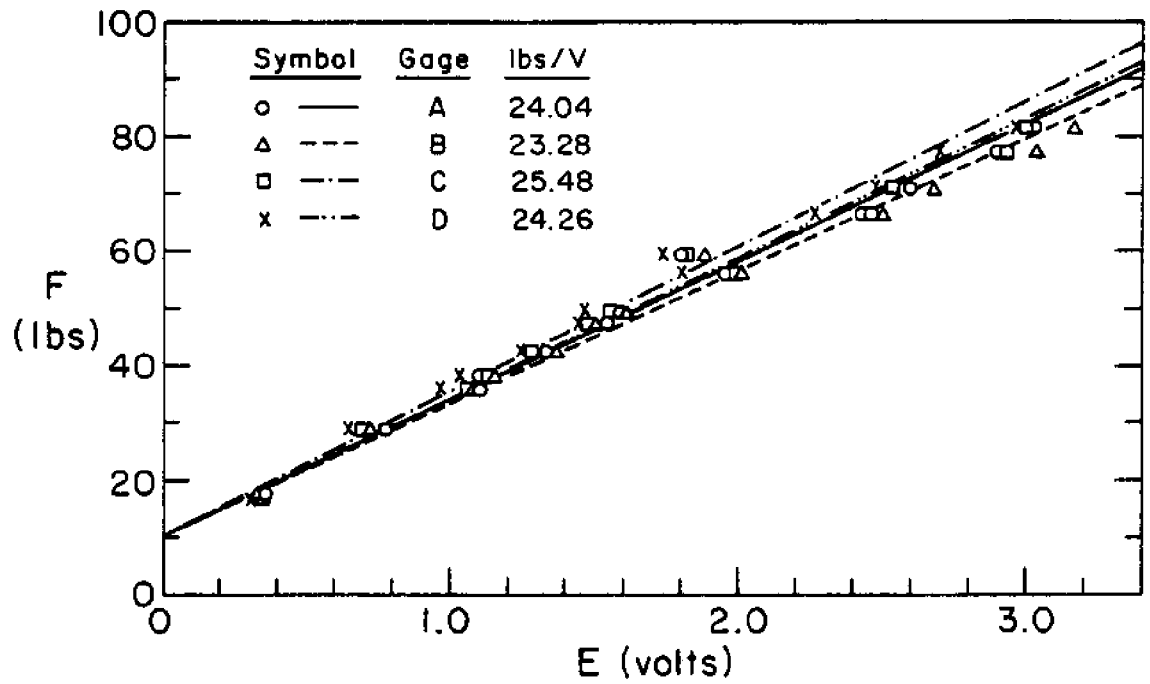
$$\begin{Bmatrix} F_A \\ F_B \\ F_C \\ F_D \end{Bmatrix} = \begin{Bmatrix} 24.04 \\ 23.28 \\ 25.48 \\ 24.26 \end{Bmatrix} \begin{Bmatrix} E_A \\ E_B \\ E_C \\ E_D \end{Bmatrix} \quad (3-2b)$$

where F is the horizontal force on tire units in pounds, E is the measured voltage in volts. A, B, C, D designate the identity of each gage attached to each leg of the dynamometer table.

A sample record of surface wave profile(η), near bottom water particle velocity(U_b) and horizontal forces on tire unit(F) is shown in



(a)



(b)

Fig. 3-7 Calibration Curves for (a) Near Bottom Water Particle Velocity (b) Horizontal Force

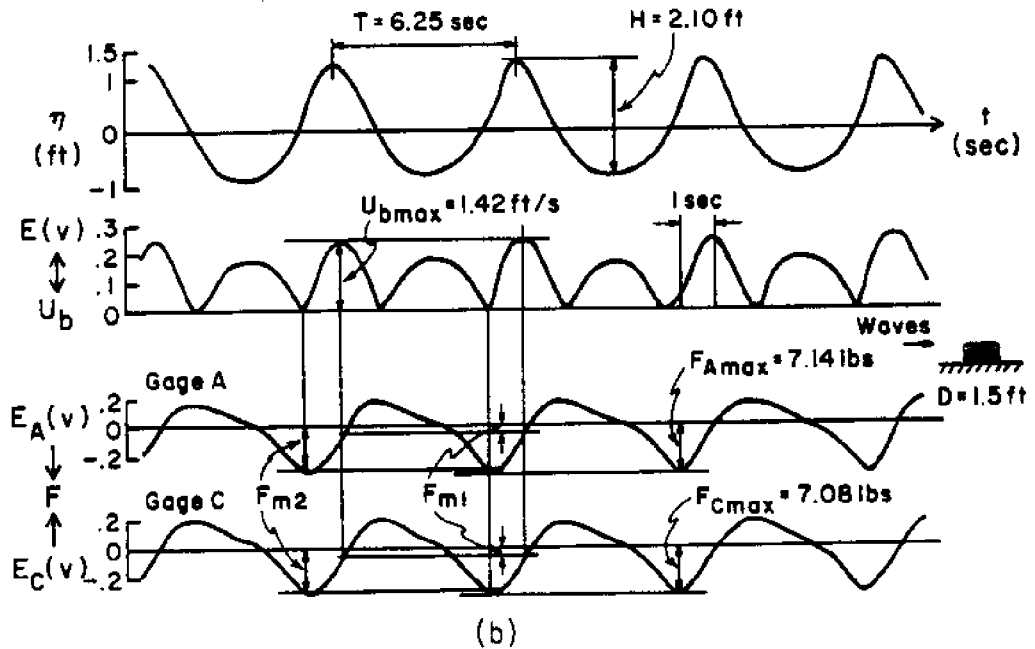
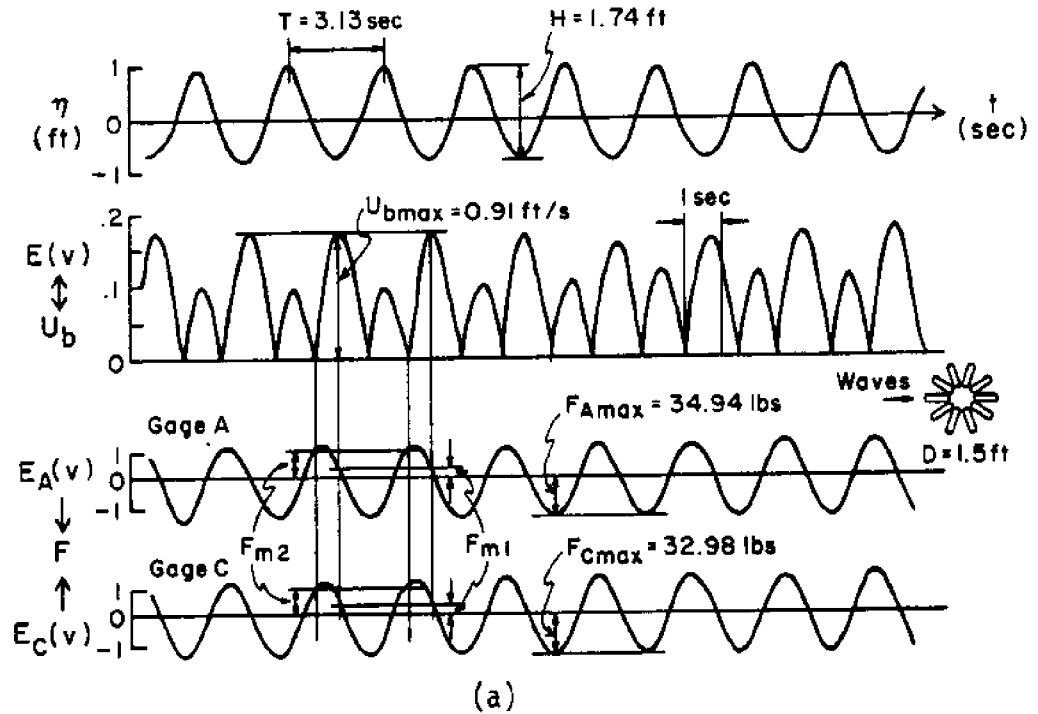


Fig. 3-8 Sample Records of Hydrodynamic Data for
 (a) $T=3.13$ sec. (b) $T=6.25$ sec.

Fig. 3-8 for the wave periods of 3.13 seconds and 6.25 seconds. All hydrodynamic data signals were recorded on a Honeywell Model 1508 Visicorder oscillograph. This system is capable of recording up to six channels at one time, utilizing light sensitive graph paper. The chart speeds range from 0.1 to 80 inches per second. Zero output responses are recorded for all channels prior to the initiation of each test run. This is to establish a datum from which maximum positive and negative displacements are determined. Horizontal forces of most test runs were sensed by the strain gage A and C. F_{m1} and F_{m2} are the horizontal forces at the point of maximum velocity and maximum acceleration (zero velocity) respectively. They are used in determining drag and inertia coefficients as represented by Eq. 2-11.

A test without tires on the dynamometer table revealed that the table experiences measurable horizontal wave forces in the absence of tires. This may be due to pressure gradients and shear stresses on the table plate by the surrounding fluid motion. The wave forces without tires on the table are given in Table 3. The net horizontal force on tire units should be the F in Eq. 3-2b less the corresponding force in Table 3.

Table 3. Horizontal Wave Forces on the Dynamometer
Table with No Tire Array

| T (sec) | H (ft) | Measured U_{bmax} (ft/s) | Maximum Force(Lbs) | | Force at $U_b=U_{bmax}$ (Lbs) | |
|------------|-----------|-------------------------------|--------------------|--------|-------------------------------|--------|
| | | | Gage A | Gage C | Gage A | Gage C |
| 1.98 | 0.93 | 0.15 | 0.37 | 0.38 | 0.24 | 0.26 |
| | 1.77 | 0.27 | 0.53 | 0.49 | 0.32 | 0.38 |
| | 2.53 | 0.49 | 0.77 | 0.56 | 0.29 | 0.33 |
| 2.36 | 1.70 | 0.48 | 0.88 | 0.82 | 0.40 | 0.38 |
| | 2.57 | 0.86 | 1.25 | 1.40 | 0.66 | 0.89 |
| | 3.33 | 1.16 | 2.04 | 1.91 | 1.01 | 1.15 |
| 3.31 | 1.63 | 0.82 | 0.98 | 1.02 | 0.66 | 0.77 |
| | 3.03 | 1.88 | 2.97 | 2.20 | 1.54 | 1.79 |
| | 4.77 | 2.54 | 3.80 | 3.19 | 2.66 | 2.88 |
| 3.61 | 2.05 | 1.24 | 1.73 | 1.51 | 1.06 | 1.02 |
| | 3.02 | 1.91 | 2.52 | 2.20 | 1.86 | 1.53 |
| | 4.57 | 2.67 | 3.69 | 3.19 | 3.00 | 2.88 |
| 4.42 | 1.93 | 1.23 | 1.33 | 1.23 | 1.00 | 0.84 |
| | 3.93 | 2.67 | 3.21 | 2.88 | 2.16 | 2.50 |
| 6.25 | 2.11 | 1.75 | 1.49 | 0.97 | 1.33 | 0.79 |
| | 2.90 | 2.15 | 1.86 | 1.61 | 1.66 | 1.43 |
| 9.88 | 1.87 | 1.56 | 0.66 | 0.49 | 0.56 | 0.41 |

3.4 Bottom Resistance Measurements

The horizontal force on tire reefs should be ultimately resisted by bottom friction on tire surfaces in contact with marine sediments so that

$$F \leq f \cdot W_{\text{sub}} \quad (3-3)$$

where F is the net horizontal force on a tire unit, W_{sub} is the submerged weight of a tire unit including ballast and f is the bottom resistance coefficient. The value of f depends mainly upon the area of contact, roughness of the tire surface and grain size distribution of bottom sediments. Fine sand is the most common material on the near shore ocean bottom. The bottom resistance coefficients f are evaluated for two bottom conditions, namely, fine sands and a concrete surface.

An artificial ocean bottom was formed by spreading fine sands on the bottom of wave channel to a depth of six inches. In water, each tire unit was placed on the sand and pulled horizontally until it began to move. The force necessary to move the tire unit divided by the submerged weight of the tire unit yields the bottom resistance coefficients. In a similar manner, bottom resistance coefficients for a finished concrete surface were also determined.

The sands used in the experiment were taken from Warrenton Sand Pit, Warrenton, Oregon which was shown to have similar sand properties to the sea-bed materials sampled at 27 fathom contour off the Umpqua coast. The grain size distributions of test materials is shown in Appendix B along with that of sea-bed sediment off the Umpqua coast.

IV. RESULTS AND DISCUSSION

Introduction

In this chapter, the measured surface wave profiles, near bottom water particle velocities and maximum accelerations are compared with theoretical values utilizing linear wave theory and Dean's Stream-function theory to evaluate the validity of experimental data for wave kinematics. The maximum force coefficients are presented and correlated with the Keulegan-Carpenter period parameter. The drag and inertia coefficients based on the Morison equation were evaluated using the maximum value method. The measured force history for several tire unit configurations are compared with the values calculated by using the drag and inertia coefficients to evaluate the validity of the Morison equation for tire reef components. A general procedure for tire reef design which utilizes the results of this study is summarized at the end of this chapter.

4.1 Observed Wave Profile and Kinematics

Surface Wave Profile

A sample comparison of observed and theoretical values of the surface wave profile, η , during one wave cycle is given in Fig. 4-1 for waves of four different periods and heights. According to linear wave theory [Airy(1845)] the surface profile of a wave at a given location is a sinusoid represented as

$$\eta(t) = \frac{H}{2} \sin \frac{2\pi}{T} t \quad (4-1)$$

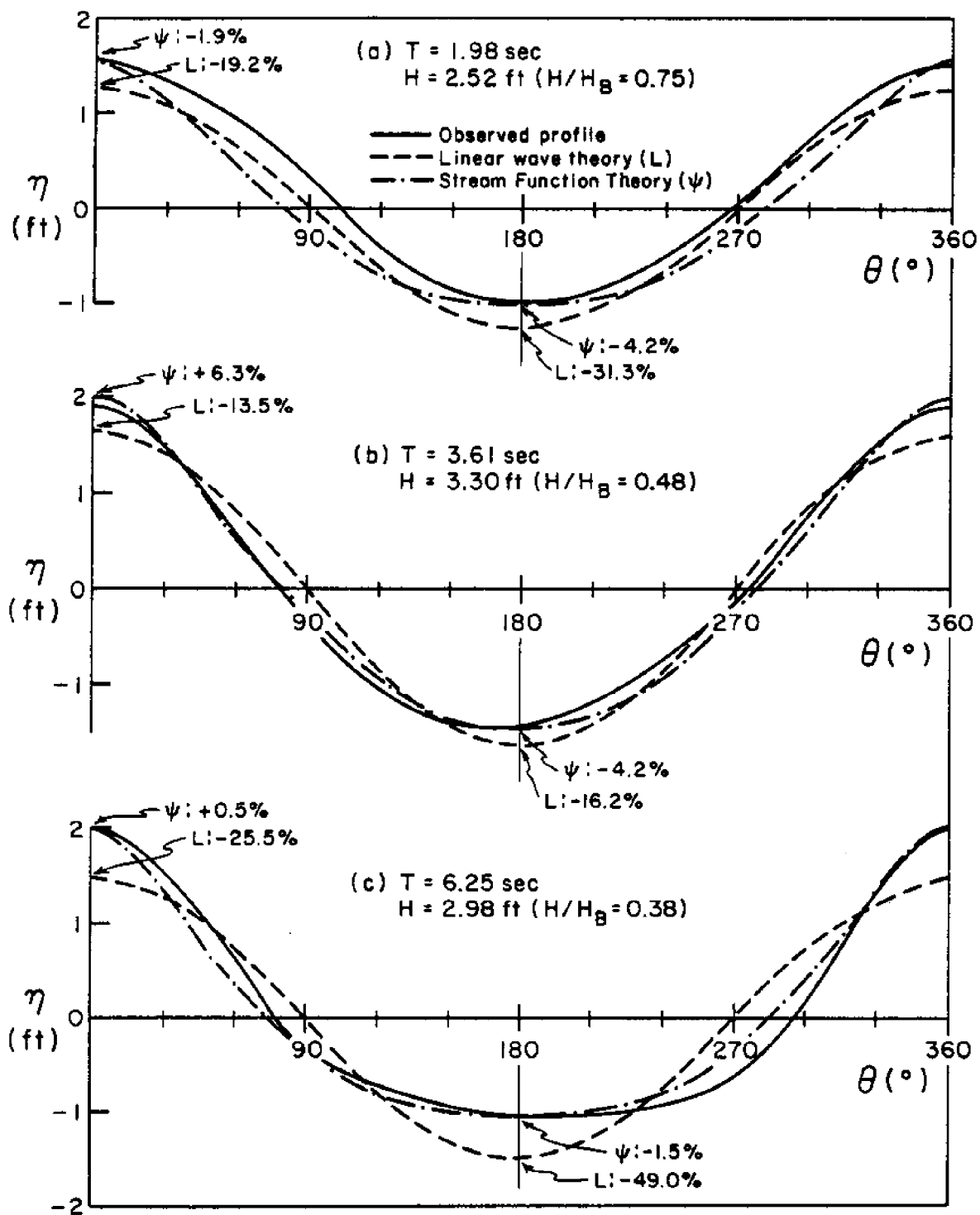


Fig. 4-1 Comparisons between Observed Wave Profile and Theoretical Values for (a) $T=1.98$ sec. (b) $T=3.61$ sec. (c) $T=6.25$ sec.

where H , T represent the wave amplitude and period, respectively.

Dean's Stream-function theory [Dean(1965)] has provided a more rigorous description of water wave properties. Accordingly, the surface wave profile as a function of time is given as

$$\eta(t) = \frac{T}{L} \psi_0 - \frac{T}{L} \sum_{n=1}^{NN} X(n) \sinh \frac{2\pi}{L} n(h + \eta) \cos n \frac{2\pi}{T} t \quad (4-2)$$

where NN is the order of the representation, and h is water depth, ψ_0 represents the constant value of the Stream-function on the free surface and L , $X(n)$ represent the undetermined wave length and coefficients respectively. For a specified wave height, period and water depth, the parameters L and $X(n)$'s are chosen to minimize the error in the dynamic free surface boundary condition. Dean(1974) presented his theoretical dynamic and kinematic computations in dimensionless form for 40 cases of wave conditions consisting of different h/L_0 and H/H_B , [Ref. 6] where $L_0 = gT^2/2\pi$, the linear wave theory deep water wave length, and H_B represents the breaking wave height. The value of h/L_0 ranges from .002(Case 1) to 2(Case 10) while $H/H_B = 0.25, 0.50, 0.75, 1.00$ corresponding to Case A, B, C, D respectively.

As shown in Fig. 4-1, linear wave theory underpredicts at the crest and overpredicts at the trough and the error becomes greater as wave period increases (-49% at $T=6.25$ sec.). Dean's stream function theory slightly underpredicts at the crest of short waves (-1.9% at $T=1.98$ sec.), however, it overpredicts at the crest of longer waves. Nevertheless, the error is below 10%. Stream-function theory generally concurs with measured values under the trough for all the waves.

Near Bottom Water Particle Velocity

Water particles oscillate back and forth close to the bottom of a wave channel or on the sea floor as waves propagate over the water surface. The near bottom velocity of water particle motion is given by linear wave theory as

$$U_b(t) = \frac{\pi H/T}{\sinh \frac{2\pi}{L}h} \cdot \sin \frac{2\pi}{T}t \quad (4-3)$$

The maximum value, U_{bmax} , occurs under both the wave crest and trough where $\sin \frac{2\pi}{T}t = 1.0$, then

$$U_{bmax} = \frac{\pi H/T}{\sinh \frac{2\pi}{L}h} \quad (4-4)$$

where $L = \frac{gT^2}{2\pi} \tanh \frac{2\pi}{L}h$ is the wave length at depth h .

Dean's Stream-function theory evaluates the bottom velocity as

$$U_b(t) = - \sum_{n=1}^{NN} X(n) \frac{2\pi}{L}n \cdot \cos \frac{2\pi}{T}t \quad (4-5)$$

and the maximum value occurs under the crest with a magnitude of

$$U_{bmax} = - \sum_{n=1}^{NN} X(n) \left[\frac{2\pi}{L}n \right] \quad (4-6)$$

The measured U_b 's for four selected waves are shown in Fig. 4-2 along with the theoretical values computed from Eq. 4-3 and Eq. 4-5 for

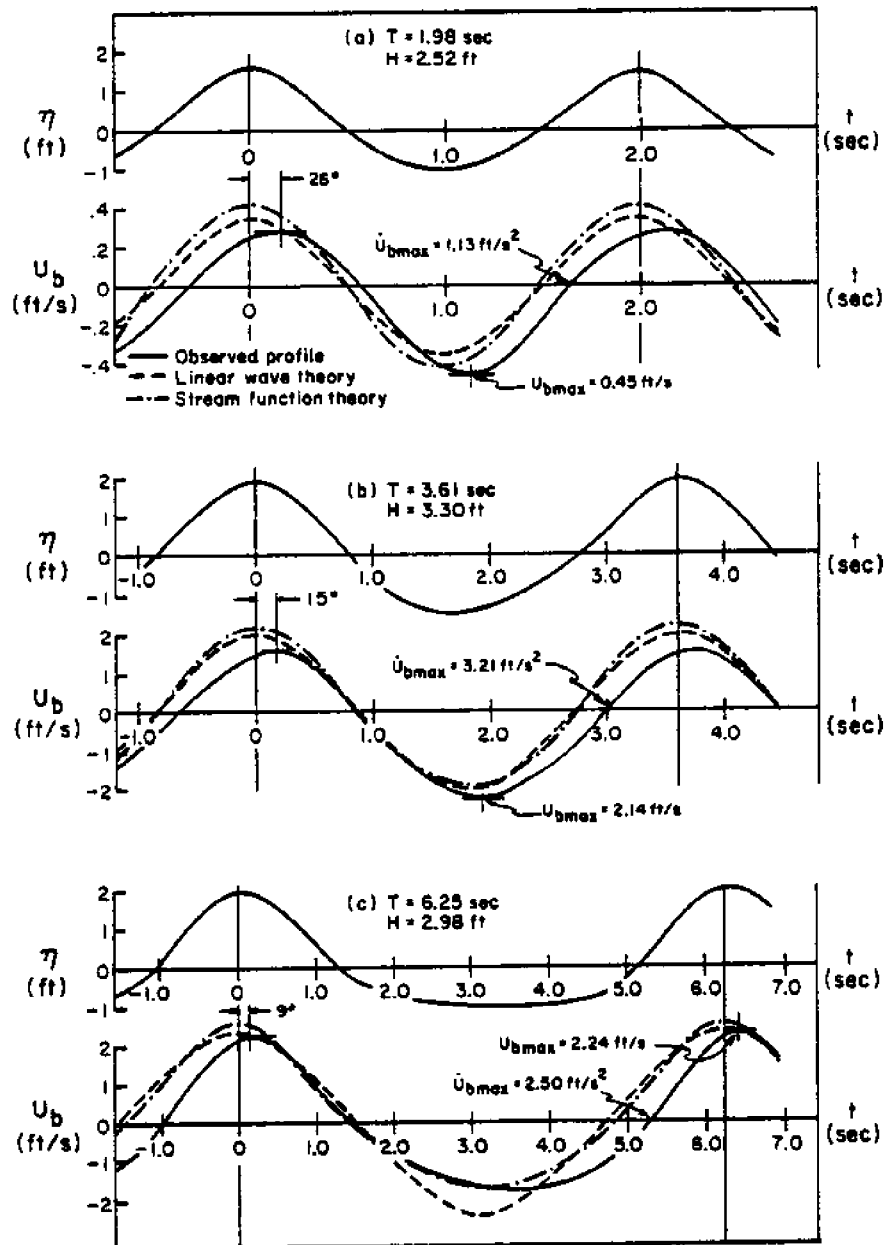


Fig. 4-2 Comparisons between Observed near Bottom Water Particle Velocity and Theoretical Values for (a) $T=1.98$ sec. (b) $T=3.61$ sec. (c) $T=6.25$ sec.

specific values of H , T and h . As shown in Fig. 4-2, linear wave theory correlates better with bottom velocities under shorter waves ($T \leq 4.42$ sec.). However, Stream-function theory correlates better with bottom velocities under longer waves ($T \geq 6.25$ sec.).

A phase lag is observed between the surface profile and the measured bottom velocity. The reason for this apparent phase lag is not certain, however, it is probable due to a slow frequency response in the current meter. The magnitude of phase lag decreases from an ensemble average of 26° (at $T=1.98$ sec.) to 9° (at $T=9.88$ sec.). This phase lag, if it is due to the response of the velocity measurement system, may considerably alter the magnitudes of the drag and inertia coefficients calculated by the maximum value method, as discussed in Section 2.2. The frequency response characteristics of the Novar Model 403 Streamflo propeller current meter has been reported. Kobune(1978) has determined that this meter experiences no phase lag or amplitude attenuation for periods in excess of three seconds: shorter periods were not examined. The measured velocity and force profiles were used without any modification in calculating the drag and inertia coefficients and the results are discussed in Section 4.3.

Another striking feature is that the measured maximum velocities do not occur under the wave crest for shorter waves ($T=1.98-4.42$ sec.). Instead, they occur under the trough. This observation is contrary to theory but reported in some other experiments. [Jensen(1978), Goda(1964)]

To understand this unusual phenomenon more clearly, the ratios of theoretical U_{bmax} and averaged values of measured U_{bmax} for particular wave periods are plotted in Fig. 4-3 for the observed range of wave frequency represented by $\sigma^2 h/g$, where $\sigma = \frac{2\pi}{T}$ being wave frequency. For

short wave periods ($T \leq 3.61$ sec. or $\sigma^2 h/g \geq 0.94$), the measured values of U_{bmax} are greater than the theoretical values and the difference increases as T decreases. For longer wave periods ($T \geq 4.42$ sec. or $\sigma^2 h/g \leq 0.63$), the measured values are smaller than the theoretical values and the difference increases as T increases.

Judging from these observations, one might hypothesize the existence of a near bottom current which flows in opposition to the wave, i.e., toward the wave generator. Because the wave flume is a closed system, waves breaking on the beach may cause a return flow down the beach and towards the wave generator. This near bottom return current, if present, would reduce the actual velocity under the crest

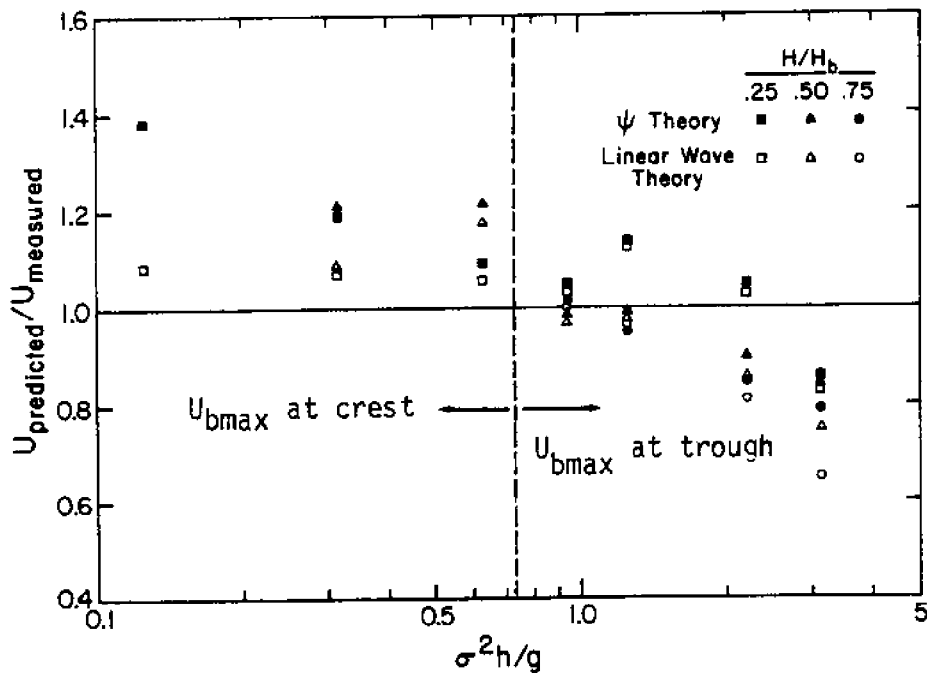


Fig. 4-3 Comparisons between Measured Maximum Water Particle Velocity and Theoretical Values at Elevation near Channel Bottom

and enhance that under the trough for all waves.

According to finite amplitude wave theories, the difference between the maximum velocity under the crest and trough is small for short waves (large h/L_0) and increases as the wave period increases at a given depth. Thus, a return current may have a more pronounced effect on short waves. For longer waves, e.g. $T \geq 6.25$ sec., U_{bmax} still occurs under the crest because the difference between the crest and trough velocities exceeds the magnitude of the return current.

In spite of the anomalous behavior at high wave frequencies, the results of Fig. 4-3 indicate that linear wave theory provides a useful prediction for maximum bottom velocities at intermediate and low wave frequencies. This result has been confirmed by several investigators. [Le Mehaute et al. (1968), Grace (1976)]

Near Bottom Water Particle Acceleration

According to linear wave theory, water particle acceleration at the bottom of the wave channel or sea floor is given by

$$\dot{U}_b(t) = \frac{2\pi^2 H/T^2}{\sinh \frac{2\pi h}{L}} \cos \frac{2\pi t}{T} \quad (4-7)$$

and its maximum value, \dot{U}_{bmax} , occurs under both the down-crossing and the up-crossing point of surface wave profile where the horizontal velocity is zero. Its magnitude is

$$\dot{U}_{bmax} = \frac{2\pi^2 H/T^2}{\sinh \frac{2\pi h}{L}} = \frac{2\pi U_{bmax}}{T} \quad (4-8)$$

Dean's Stream-function theory evaluates the bottom water particle acceleration as

$$\dot{U}_b(t) = \sum_{n=1}^{NN} X(n) \left(\frac{2\pi}{T} n\right) \left(\frac{2\pi}{L} n\right) \sin n\frac{2\pi}{T}t \quad (4-9)$$

where NN , $X(n)$, T and L are as previously defined in Eq. 4-2.

For the present study, near bottom water particle accelerations were not measured directly in the laboratory. Instead, maximum values (\dot{U}_{bmax}) were determined graphically by evaluating the maximum slope of the velocity records so that

$$\dot{U}_{bmax} = \left. \frac{d U_b}{dt} \right|_{max} \approx \left. \frac{\Delta U_b}{\Delta t} \right|_{max} \quad (4-10)$$

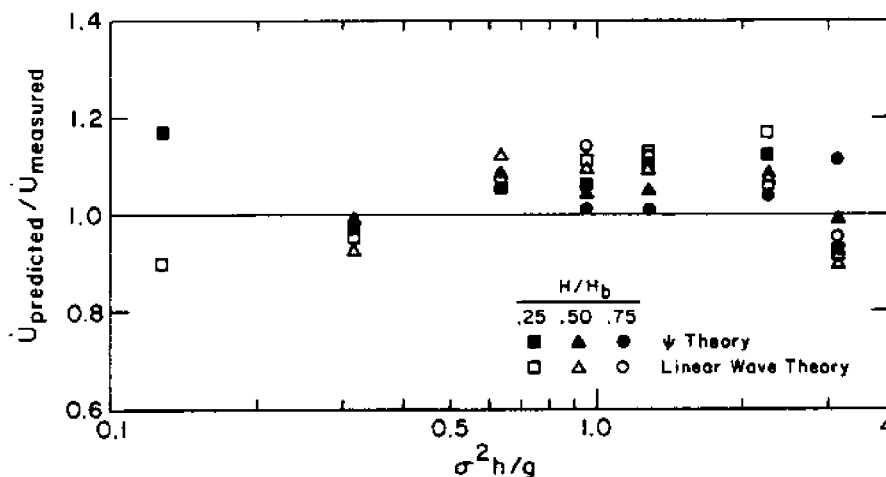


Fig. 4-4 Comparison between Measured Maximum Acceleration and Theoretical Values

It was found that the maximum slope does occur at the instant when $U_b=0$. As shown in Fig. 4-2, however, \dot{U}_{bmax} occurs at the up-crossing point of the velocity curve for all of the waves examined.

Fig. 4-4 shows a comparison between the mean values of measured \dot{U}_{bmax} and two theoretical values. Stream-function theory provides a better predicted value for bottom water particle acceleration than linear wave theory for all wave conditions considered. The errors are, however, below 20 percent for both theories.

4.2 Maximum Force Coefficients

Measured maximum forces are correlated with measured maximum near bottom water particle velocities to yield maximum force coefficients as

$$C_{F(mes)} = \frac{F_{max(mes)}}{\frac{\rho}{2} A U_{bmax}^2} \quad (4-11)$$

where $F_{max(mes)}$ is taken as the average of the horizontal net forces experienced simultaneously by four strain gages which were attached to each leg of the dynamometer table. Most force records were obtained by using both Gage A and C at the same time. The water temperature was maintained about 20° C during the test yielding the density of water, ρ , and kinematic viscosity, ν , to be 1.937 slugs/ft³ and 1.06 x 10⁻⁵ ft²/sec, respectively. The projected areas(A) are as defined in Table 1.

The resulting maximum force coefficients show dependence both on Reynolds number and Keulegan-Carpenter period parameter, however, a more

definitive relationship was observed with respect to the period parameter. The Reynolds number ranged from 1.1×10^4 to 1.2×10^6 and the period parameter from 0.2 to 20. (Refer Section 3.1 concerning the definitions of parameters) The maximum force coefficients for various tire configurations and different orientations are given in Fig. 4-5 to Fig. 4-11 as functions of Keulegan-Carpenter period parameter. Instead of $C_{f(mes)}$, a simplified notation C_f is used hereafter to represent the measured maximum force coefficients in this section. The plots of the measured maximum force coefficients vs. Reynolds number are not given in this report.

The maximum force coefficients display an exponential decay (maximum 40 to minimum 1.1) as the value of the period parameter increases over the observed range. Fig. 4-5 to Fig. 4-9a illustrate the maximum force coefficients of all tire sizes together for the first three tire configurations shown in Table 1. There exist minor increases in C_f as tire size increases, however, the size effects on C_f are insignificant for all cases considered. The case with one tire set perpendicular to the direction of wave propagation (Fig. 4-5a) is of particular interest. This case yields the largest K-C number (up to 50) because D' is the smallest of all cases tested. The tail of the maximum force coefficients curve shows an apparent leveling off trend as K-C number increases. This is similar to reported results for circular cylinders. [Sarpkaya(1976), Grace(1979)] This behavior may help one to extrapolate C_f values at slightly larger K-C numbers than that observed in the model tests.

Two stuffed tires with $D=1.9$ ft have almost the same magnitude of C_f as those of four tires fabricated in a triangular form as shown in Fig. 4-9b. However, the values of C_f are lower than those of any

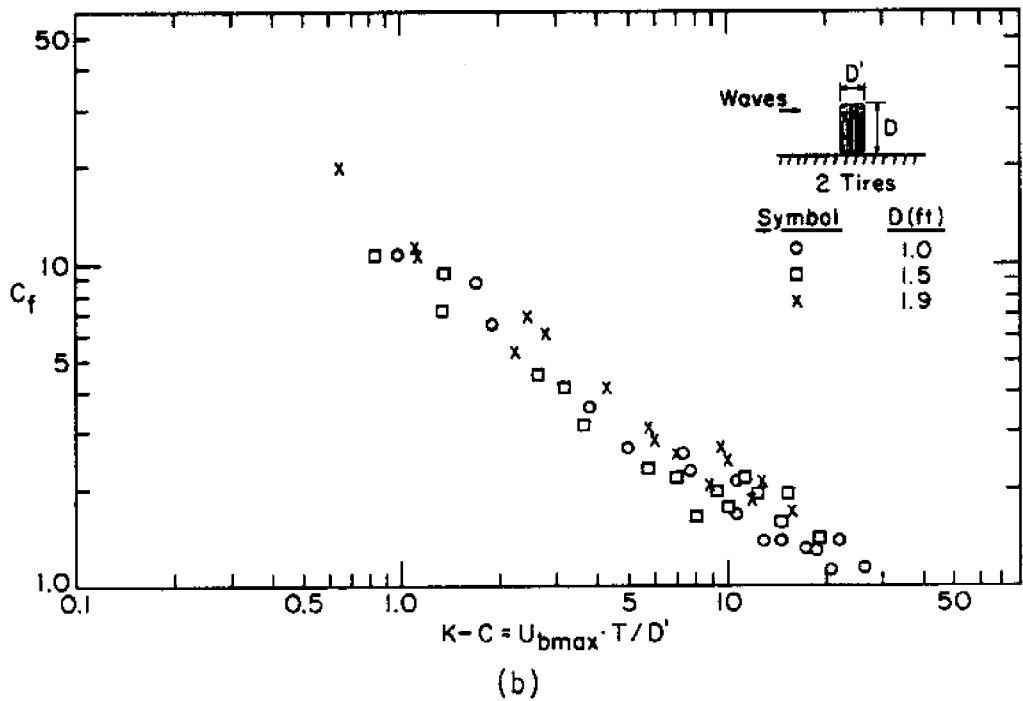
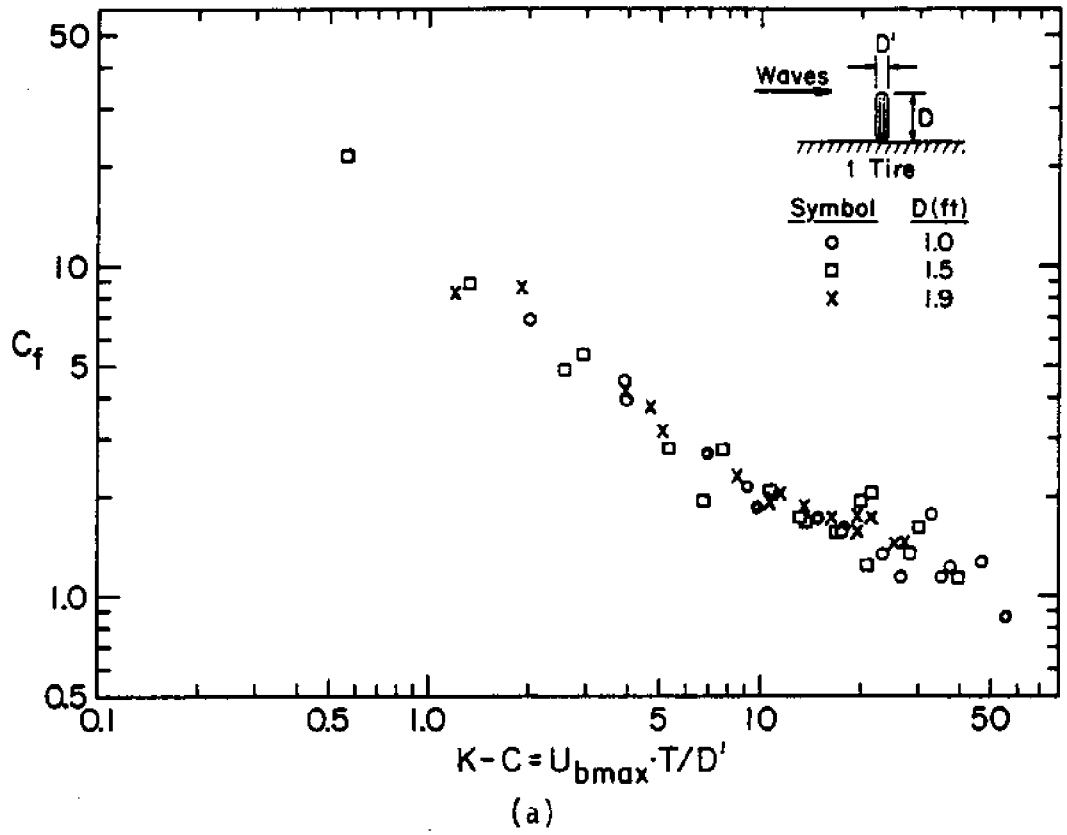
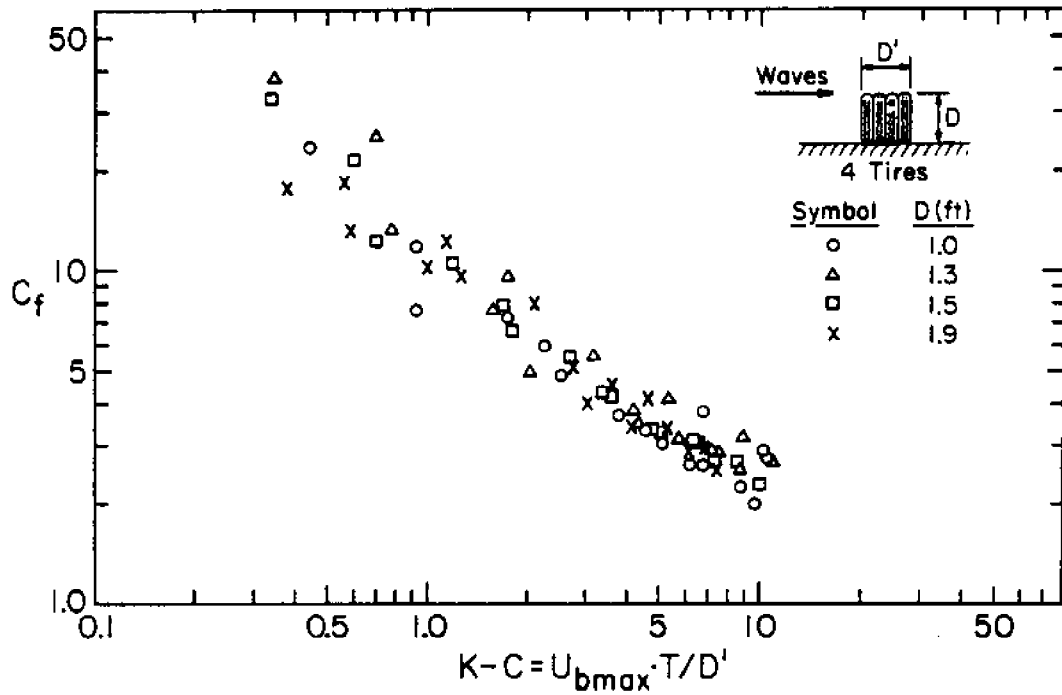
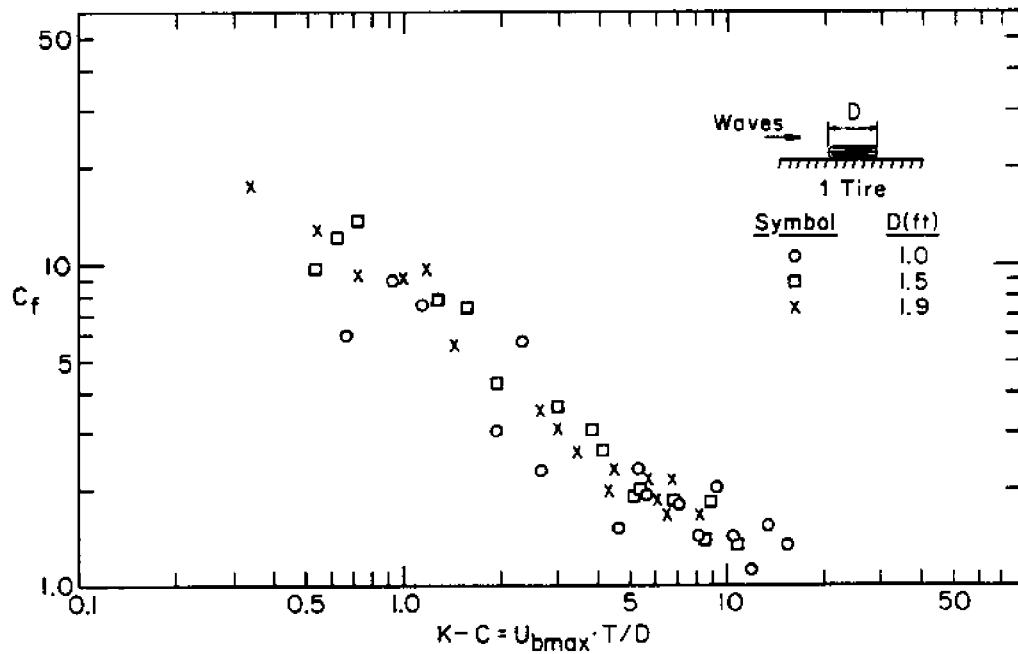


Fig. 4-5 Maximum Force Coefficients vs. K-C Number for (a) One Tire and (b) Two Tires Set Perpendicular to the Waves



(a)



(b)

Fig. 4-6 Maximum Force Coefficients vs. K-C Number for (a) Four Tires Set Perpendicular to the Waves (b) One Tire Set Flat

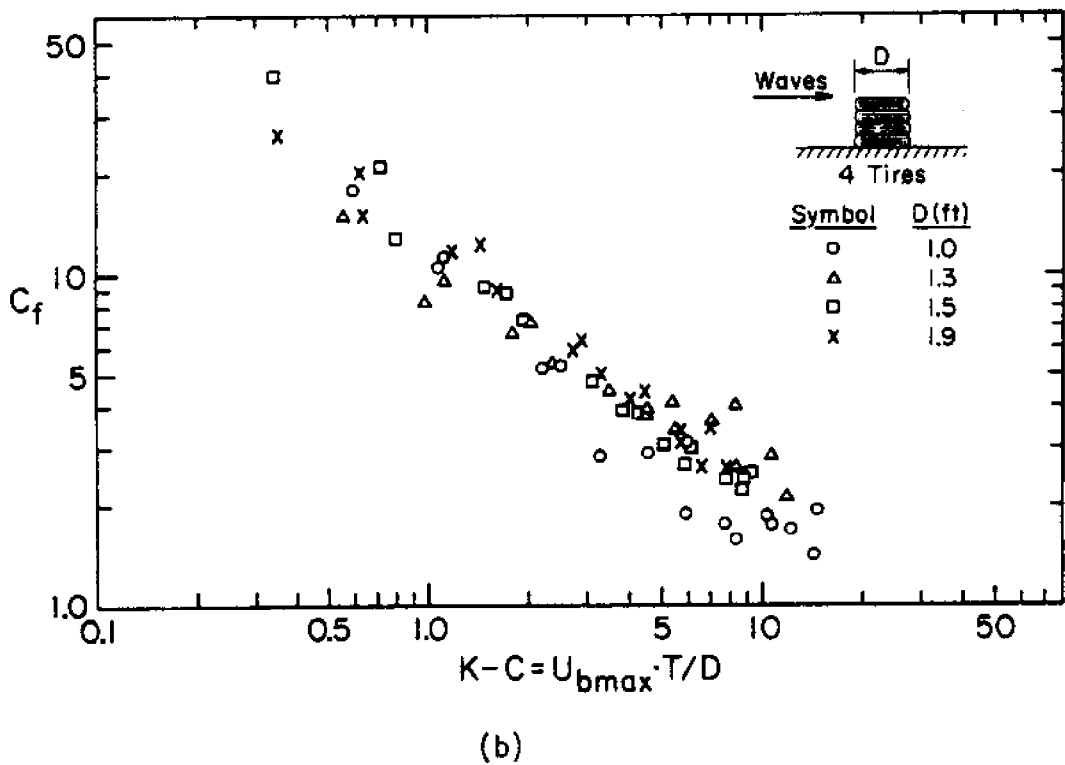
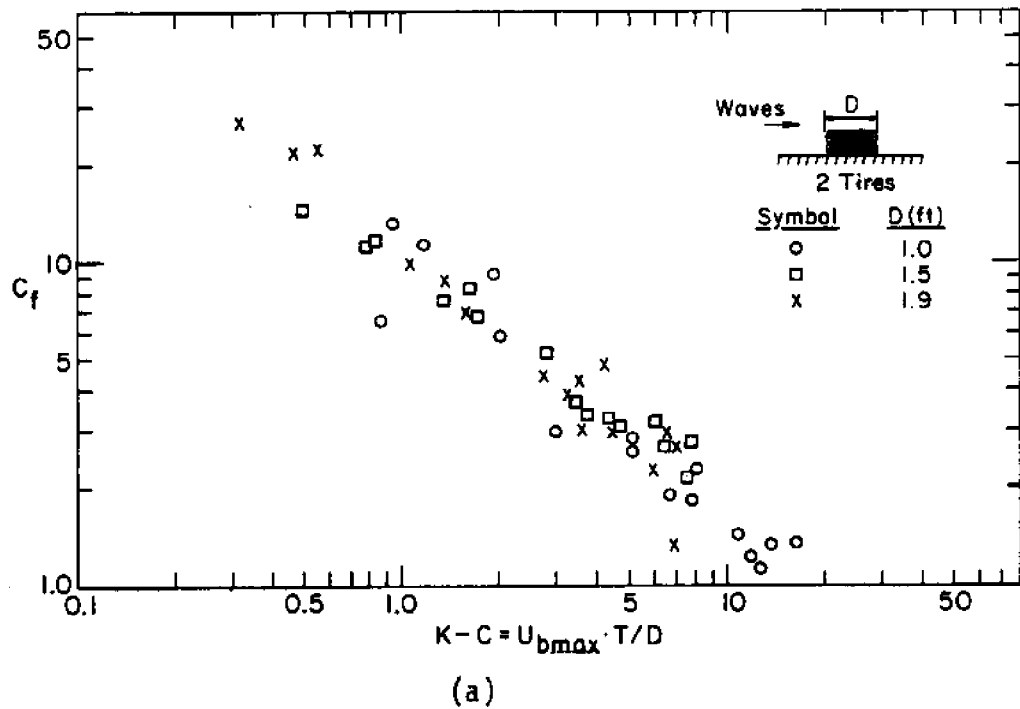
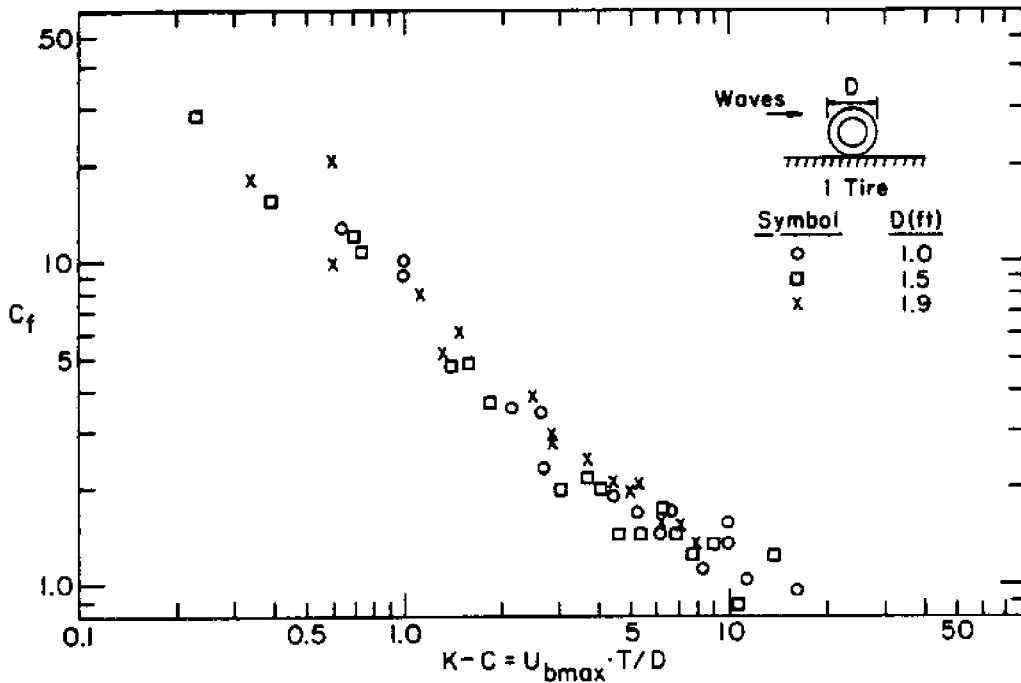
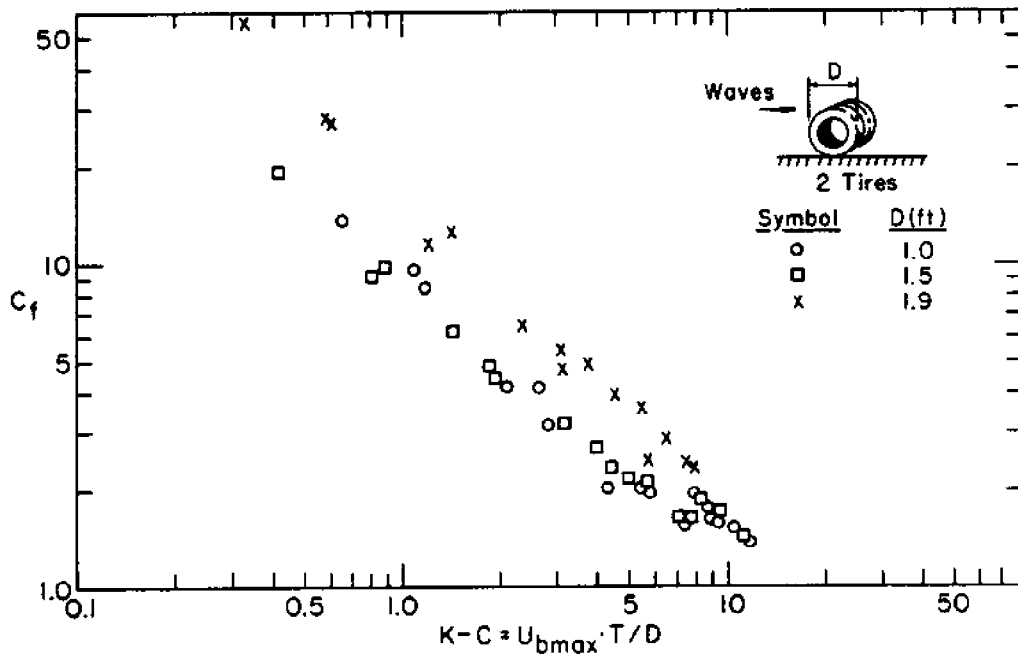


Fig. 4-7 Maximum Force Coefficients vs. K-C Number for (a) Two Tires and (b) Four Tires Set Flat



(a)



(b)

Fig. 4-8 Maximum Force Coefficients vs. K-C Number for (a) One Tire and (b) Two Tires Set Parallel to the Waves

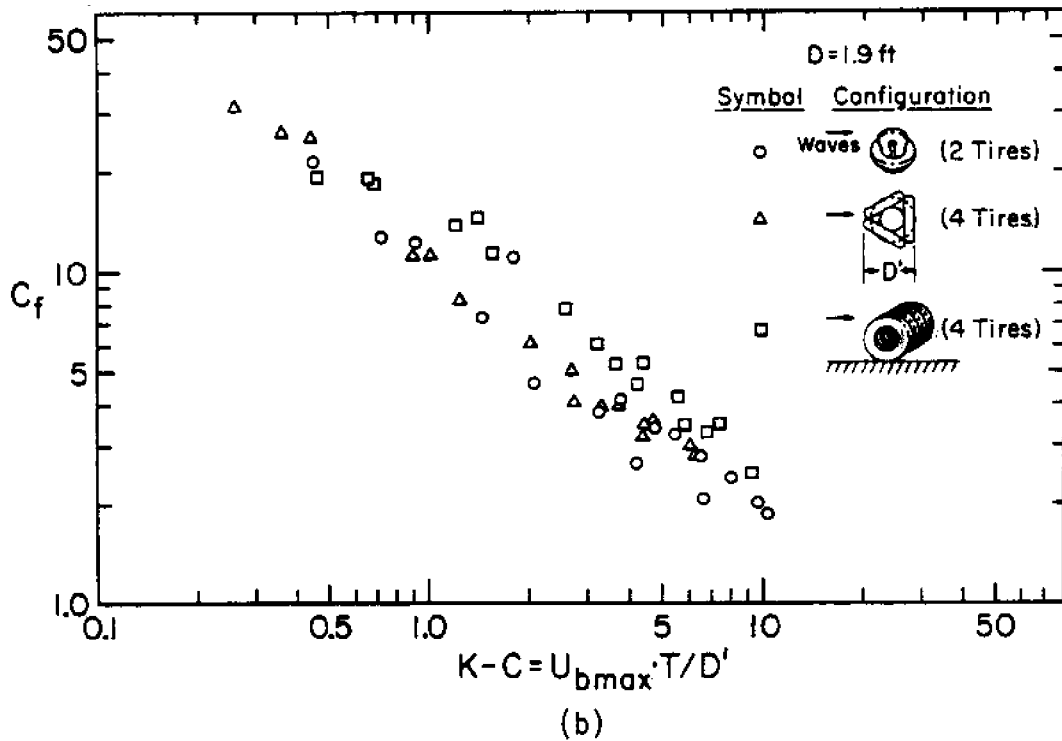
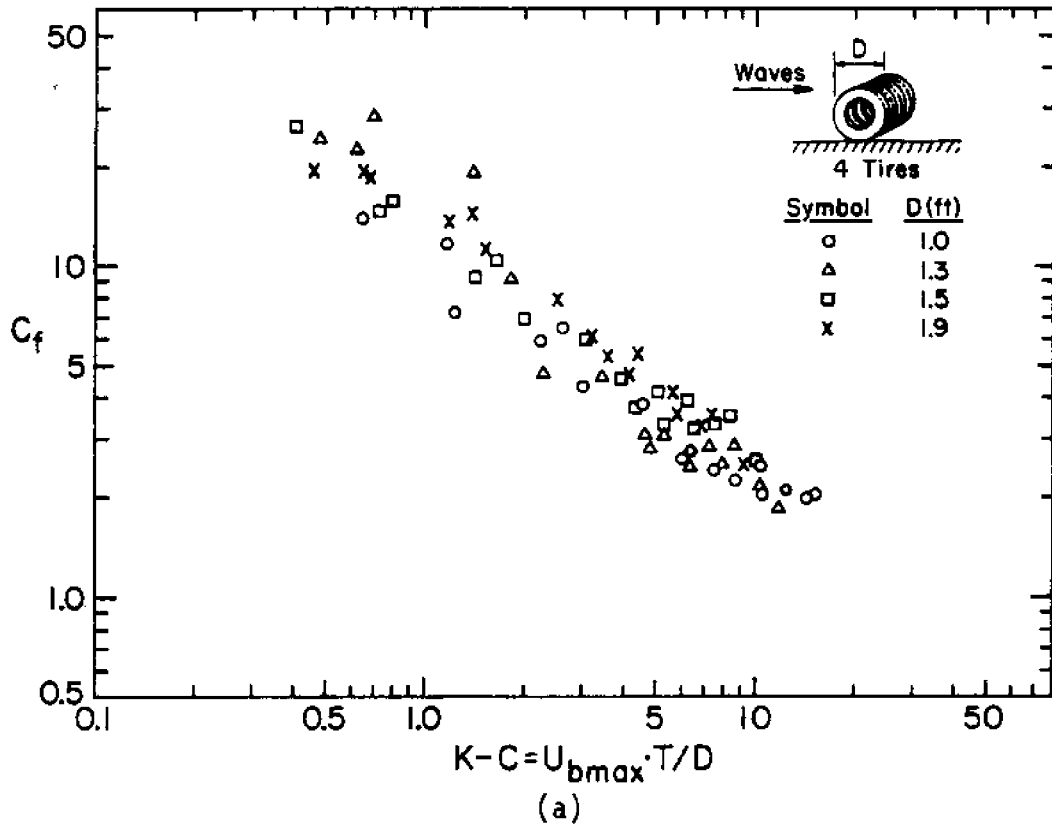


Fig. 4-9 Maximum Force Coefficients vs. K-C Number for (a) Four Tires Set Parallel to the Waves (b) Two Tires Stuffed and Four Tires Triangularly Fabricated

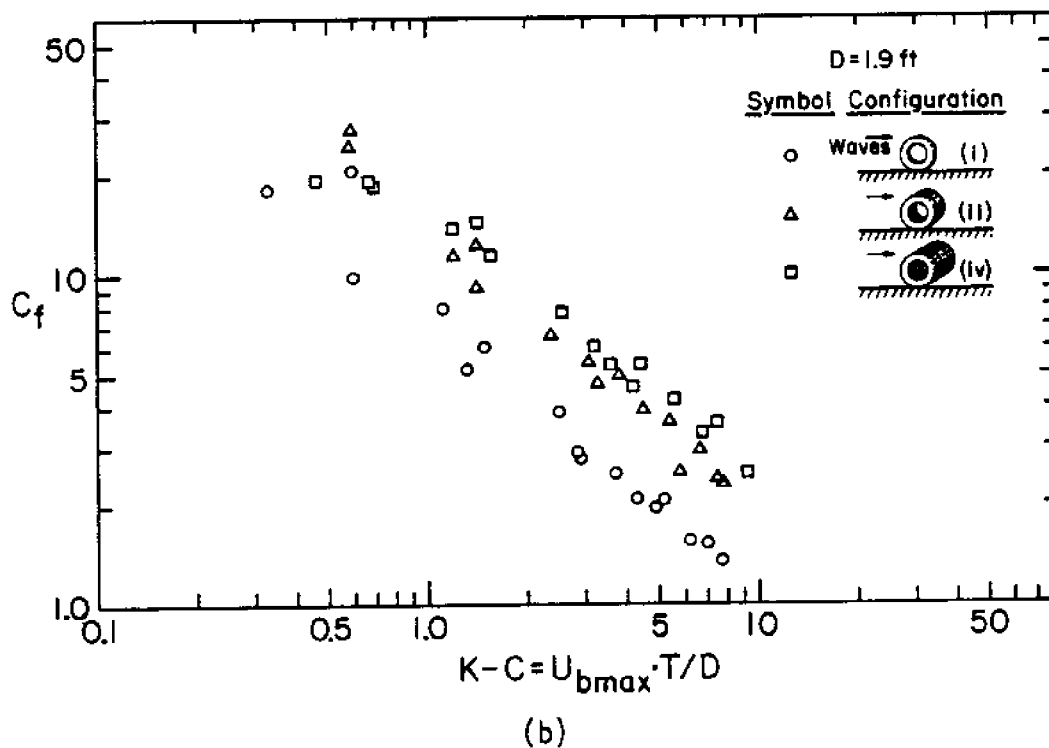
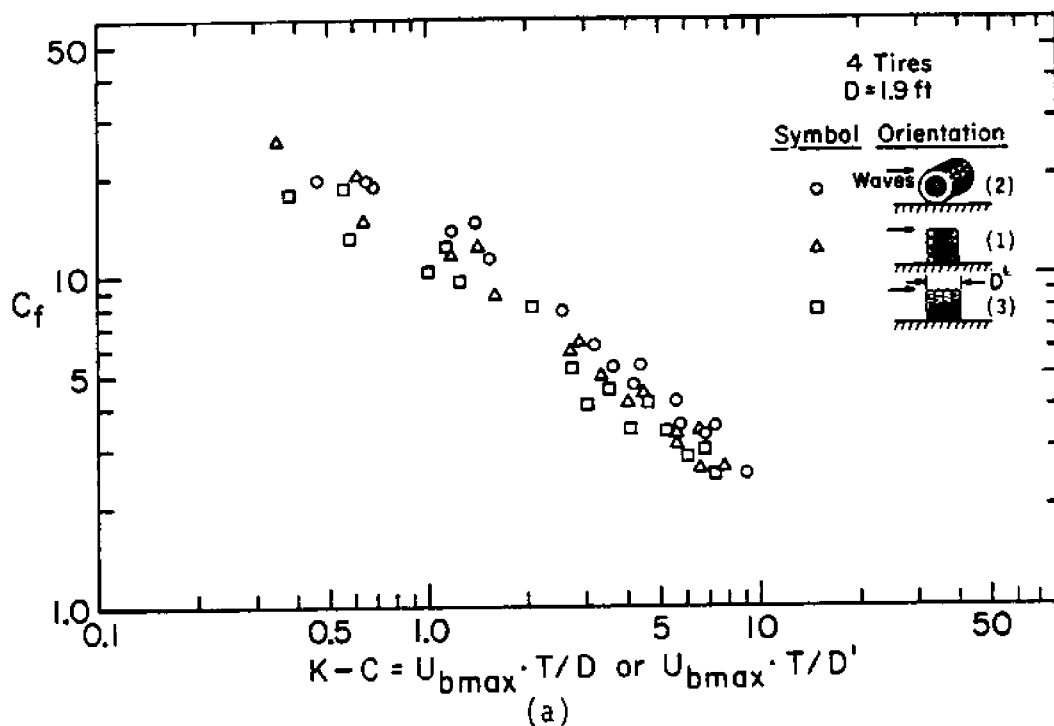
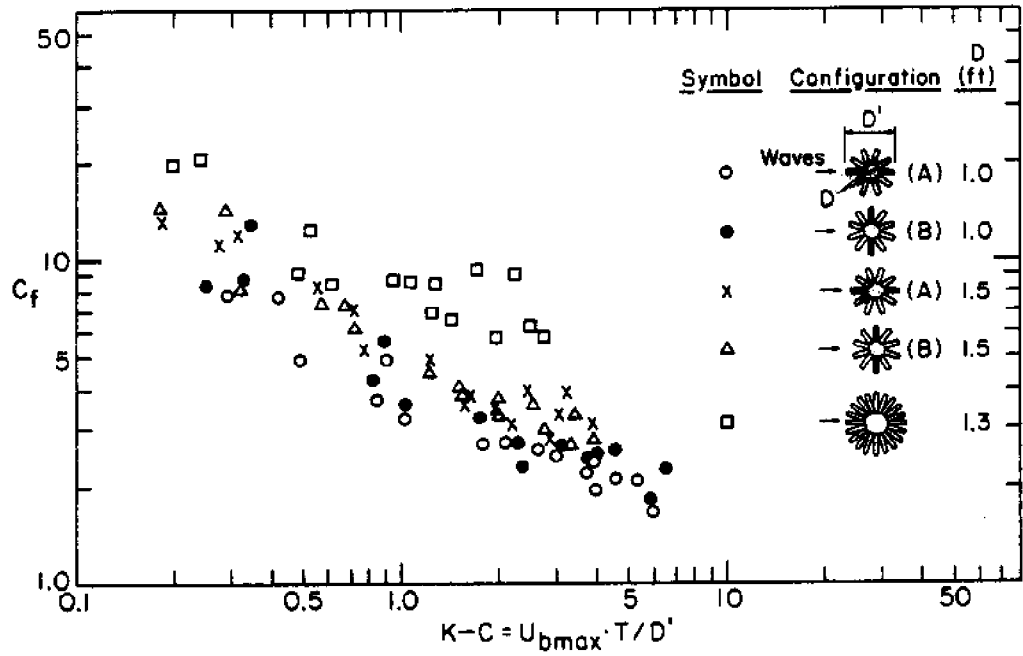
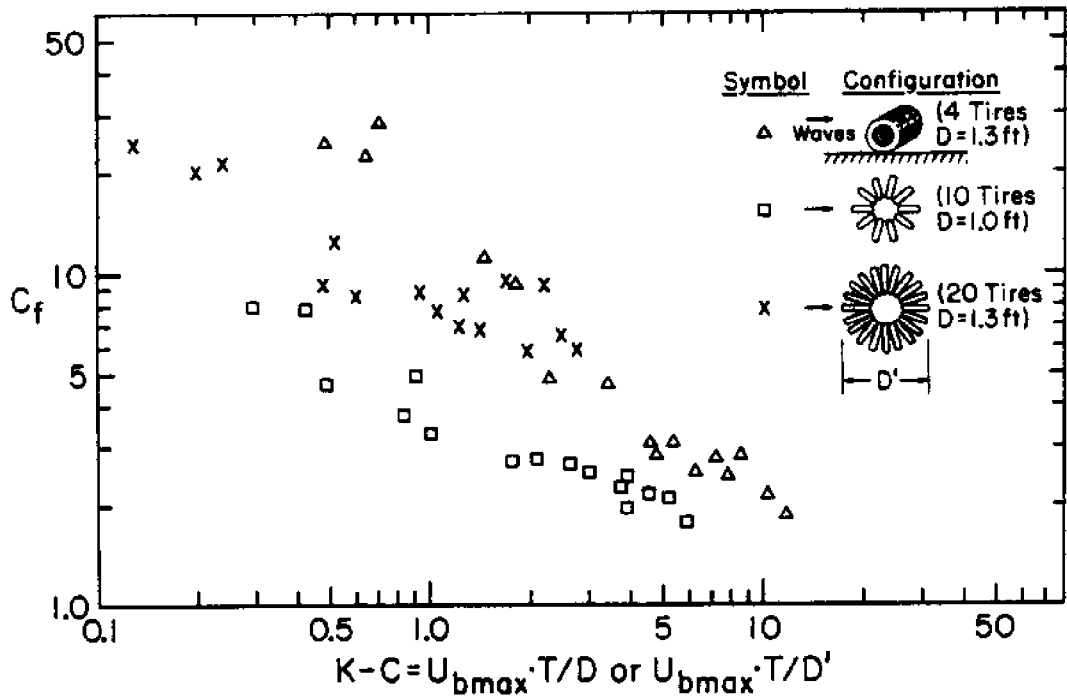


Fig. 4-10 Maximum Force Coefficients vs. K-C Number for (a) Four Tires with Different Orientations (b) Array with Different Numbers of Tires



(a)



(b)

Fig. 4-11 Maximum Force Coefficients vs. K-C Number for (a) Rosette Configurations (b) Rosette Configurations Compared with Four Tires Set Parallel to the Waves

other configuration fabricated from two tires. Two stuffed tires with $D=1.0$ ft show lower C_f values than the same configuration with $D=1.9$ ft. [See Appendix A or Fig. 4-12]

Fig. 4-10 illustrates various combinations and orientations of tires with $D=1.9$ ft: (a) variation of C_f relative to orientation for a four tire array, (b) variation of C_f relative to number of tires. All curves display similar slopes. However, the maximum force coefficients obtained from a parallel orientation(2) [See Fig. 4-10a] yield higher values of C_f , compared to the other two orientations. For a specified orientation, the maximum force coefficients increase as the number of tires increases as shown in Fig. 4-10b. The tendency shown in Fig. 4-10 is general for other configurations and orientations.

The maximum force coefficients for rosette configurations is given in Fig. 4-9b and again compared with another configuration in Fig. 4-11b. Three features are unique with rosette shape tire configurations: first, slopes of the C_f curves are less than those of other configurations; second, the slope becomes less as D' of the rosette increases; third, the magnitude of C_f increases as D' of the rosette increases. Rosettes made of ten tires were tested in two orientations which differ by 18° in rotation as shown in Fig. 4-9b. No distinguishable difference in C_f was observed between the two orientations. As shown in Fig. 4-11b, the rosette configurations display significantly smaller values of C_f than any other configurations of same tire size for Keulegan-Carpenter number smaller than 1.0.

For the convenience of further comparisons, the mean lines of maximum force coefficient data for all cases tested are shown together in Fig. 4-12 with the results of a field experiment for circular cylinders

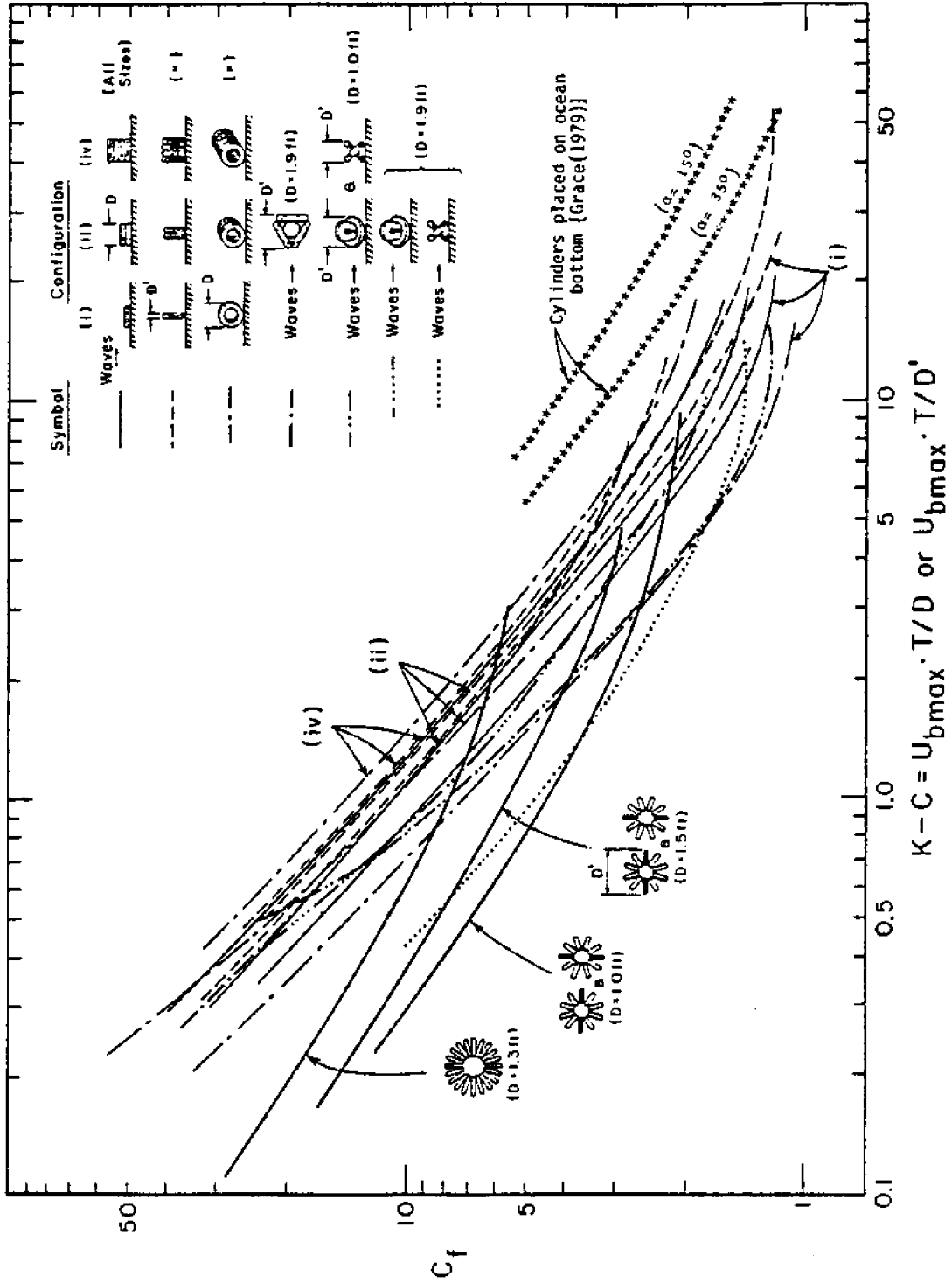


Fig. 4-12 Mean Lines of Maximum Force Coefficients vs. K-C Number

under ocean waves. [Grace(1979), See Fig.2-4b] It is interesting that the majority of the mean lines, with the exception of the rosette shape, have approximately the same slope as they decay exponentially with increasing Keulegan-Carpenter period parameter. The values of C_f display a mild leveling-off as period parameter exceeds seven. The present results appear to show similar variations of exponential decay as the circular cylinders do and have lower values of C_f in the observed range of Keulegan-Carpenter number. The C_f curves for circular cylinder level-off at higher K-C numbers than those of tire configurations.

4.3 Drag and Inertia Coefficients for Tire Units

Drag and inertia coefficients for each tire unit configuration of specified orientation were determined utilizing the maximum value method as previously discussed in Section 2.2. Eq. 2-11 can be written again for tire configurations as

$$C_D = \frac{F_{m1}}{\frac{\rho}{2} A U_{bmax}^2} \quad (4-12a)$$

$$C_I = \frac{F_{m2}}{\rho V \dot{U}_{bmax}} \quad (4-12b)$$

where F_{m1} and F_{m2} are the measured horizontal net forces at the time of $U_b = U_{bmax}$ and $U_b = 0$ (or $\dot{U}_b = \dot{U}_{bmax}$), respectively, as shown in Fig. 3-8. A and V are the projected area and volume of tire casing as listed in Table 1 and presented Fig. 3-3. The maximum near bottom velocities,

U_{bmax} , are measured directly from the records and the maximum water particle accelerations, \dot{U}_{bmax} , are graphically determined from the slope of the velocity records as discussed in Section 4.1.

The resulting C_D and C_I are found to be both Reynolds number dependent and Keulegan-Carpenter number dependent. However, a more definitive relationship was obtained relative to the K-C period parameter. The drag and inertia coefficients for selected tire unit configurations are shown in Fig. 4-13 to Fig. 4-16 as functions of Keulegan-Carpenter period parameter. The plots of C_D and C_I as function of Reynolds number are not presented here. Although it was not expected that the force coefficients for tire configurations would show any strong correlation with those for circular cylinders, the results of C_D and C_I for tire configurations are somewhat similar to that which has been observed for circular cylinders. [Sarpkaya(1976), Garrison et al. (1977)] The drag coefficients decay as the period parameter increases and attain minimum values at intermediate values of the period parameter. Beyond the minimum drag coefficient, values increase rapidly as the period parameter increases to the limit of the observed range. Inertia coefficients show gradual increases beginning between 0.5 and 0.9 and reaching relative maxima between 1.3 and 2.8 as the period parameter increases over the observed range.

The effect of tire size on C_D and C_I is presented in Fig. 4-13. For the case of maximum force coefficients, the effect of tire size on $C_{f(mes)}$ was almost negligible. However, larger tires experience generally higher C_D and C_I values than smaller ones, although this tendency is not consistent with all configurations. Another noticeable feature is that the drag coefficients attain a relative minima at lower

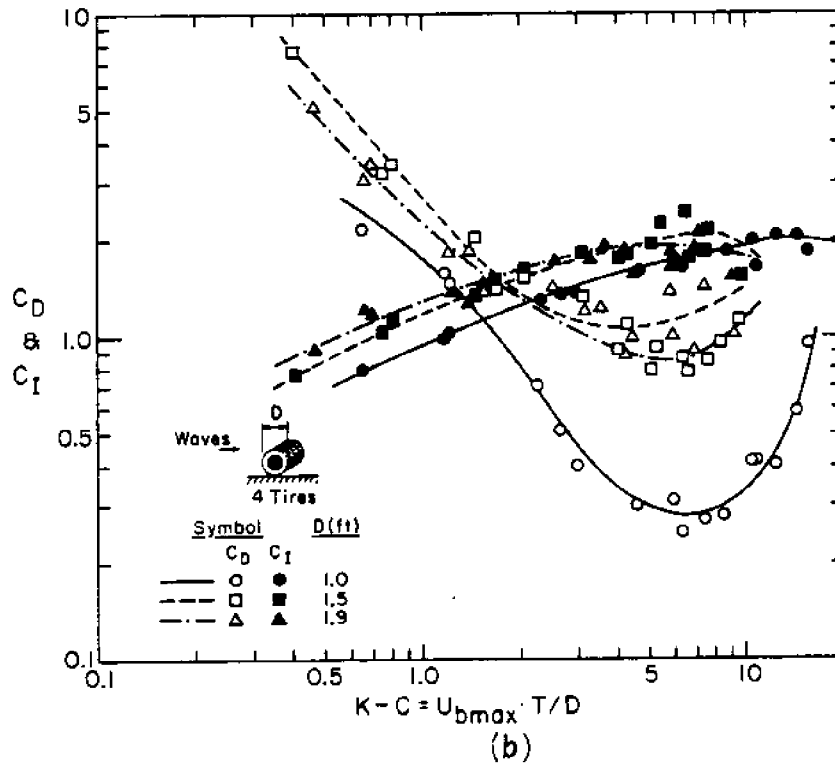
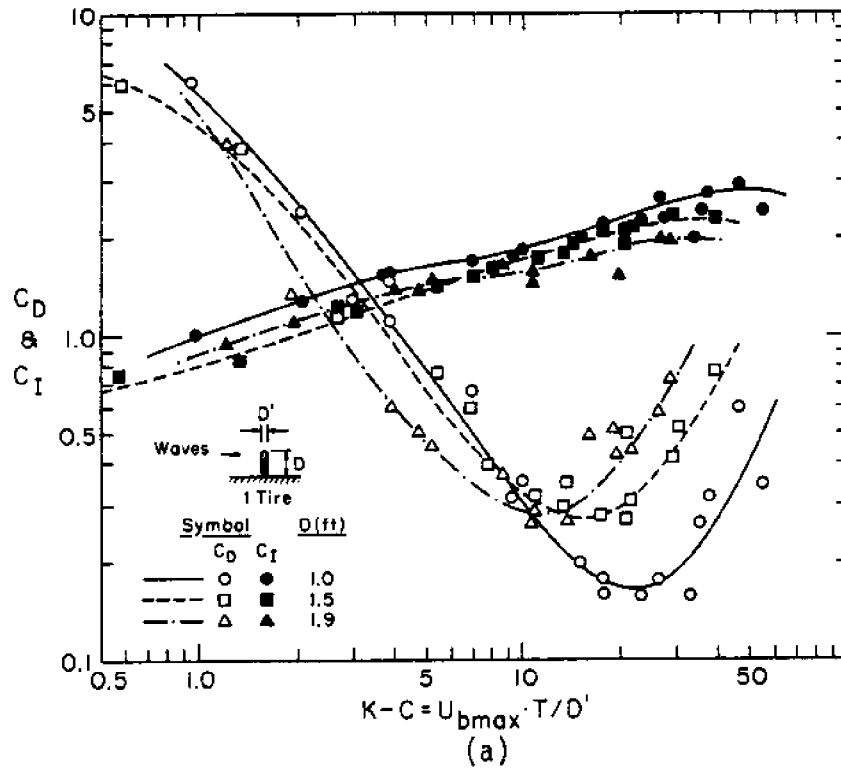


Fig. 4-13 Drag and Inertia Coefficients vs. K-C Number for
 (a) One Tire Set Perpendicular to the Waves
 (b) Four Tires Set Parallel to the Waves

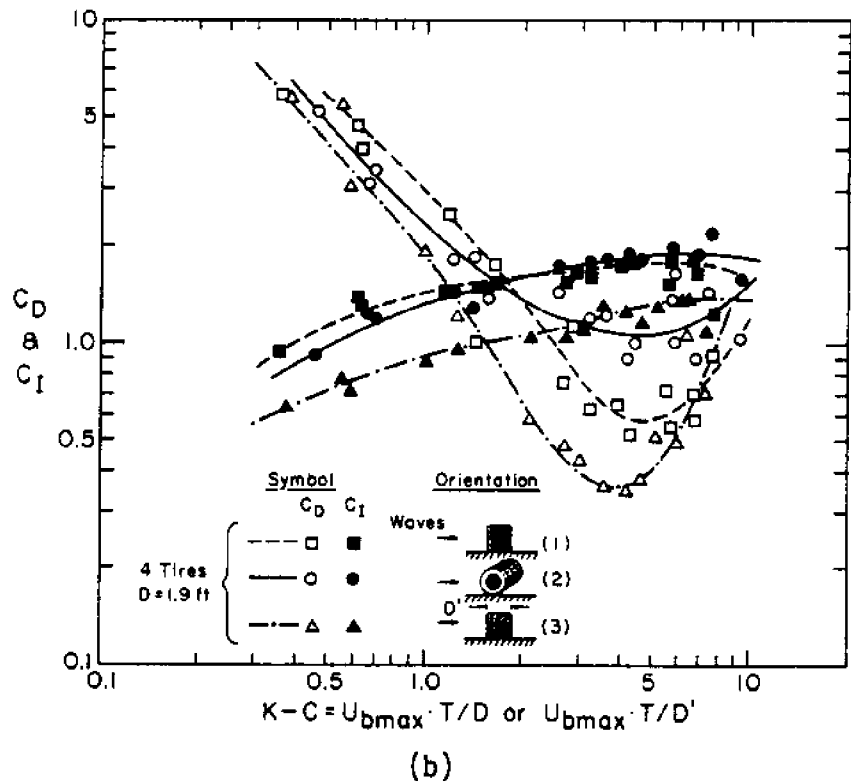
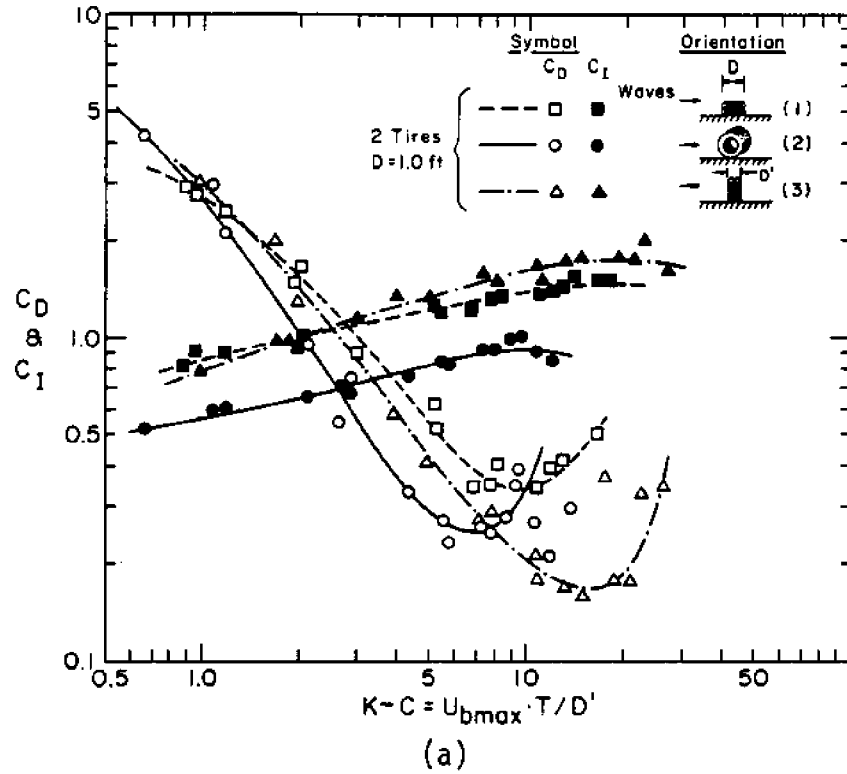


Fig. 4-14 Drag and Inertia Coefficients vs. K-C Number for
 (a) Two Tires with Different Orientations (b) Four
 Tires with Different Orientations

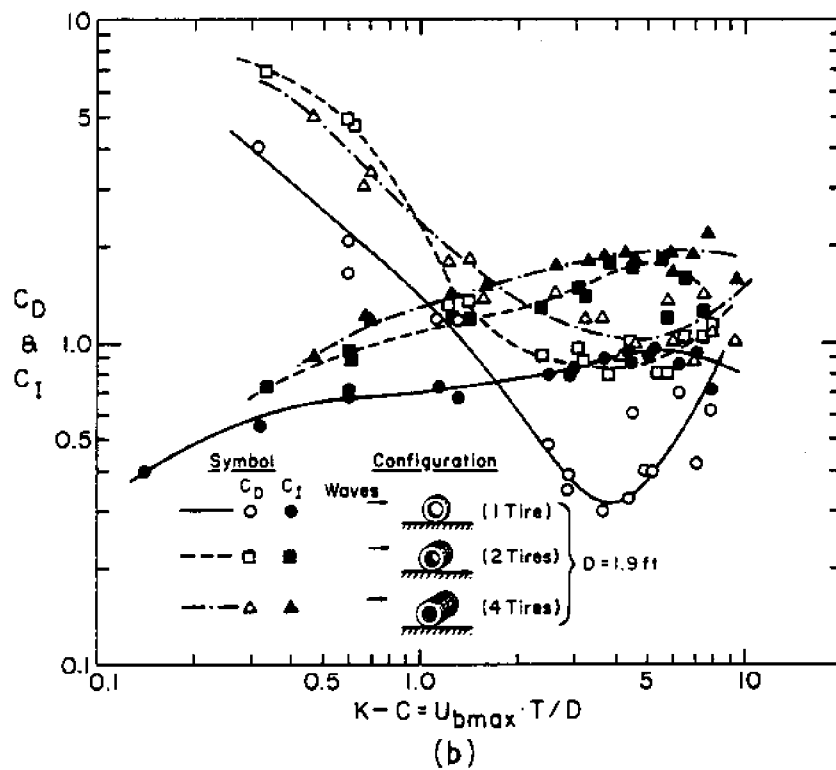
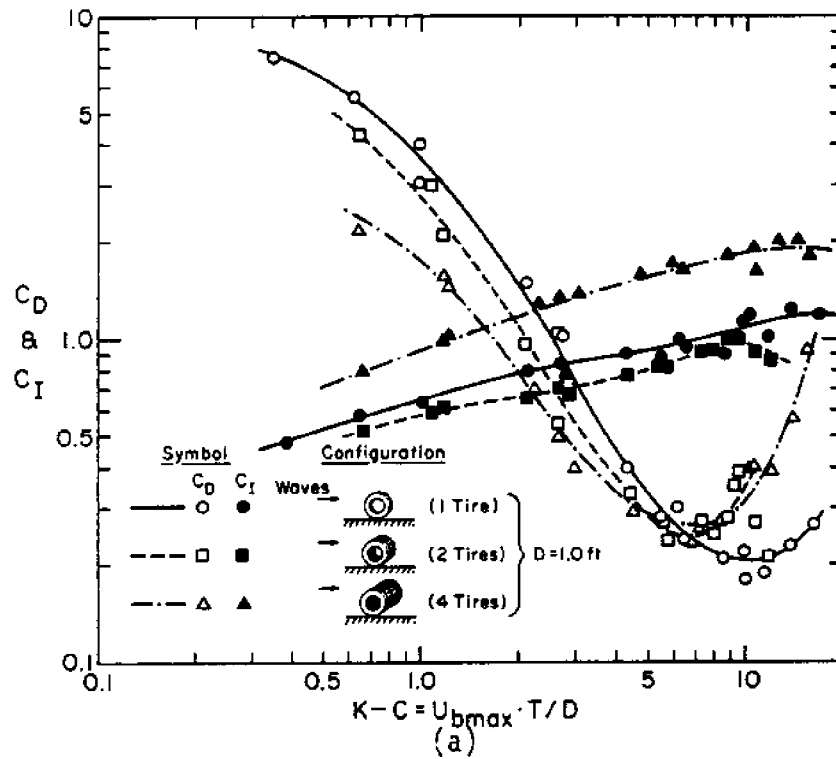


Fig. 4-15 Drag and Inertia Coefficients vs. K-C Number for Parallel Array with Different Numbers of Tires

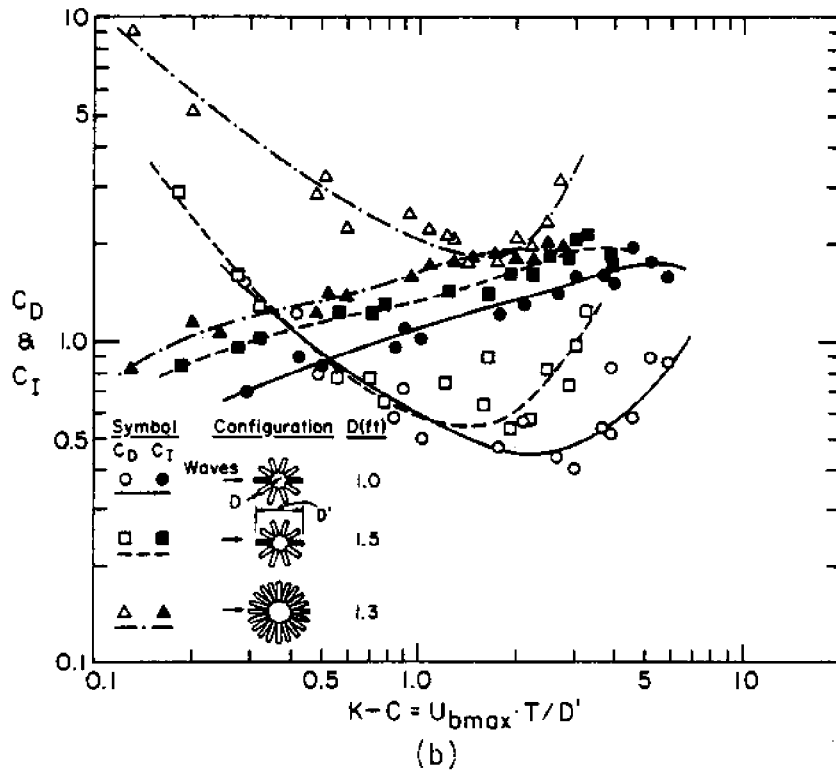
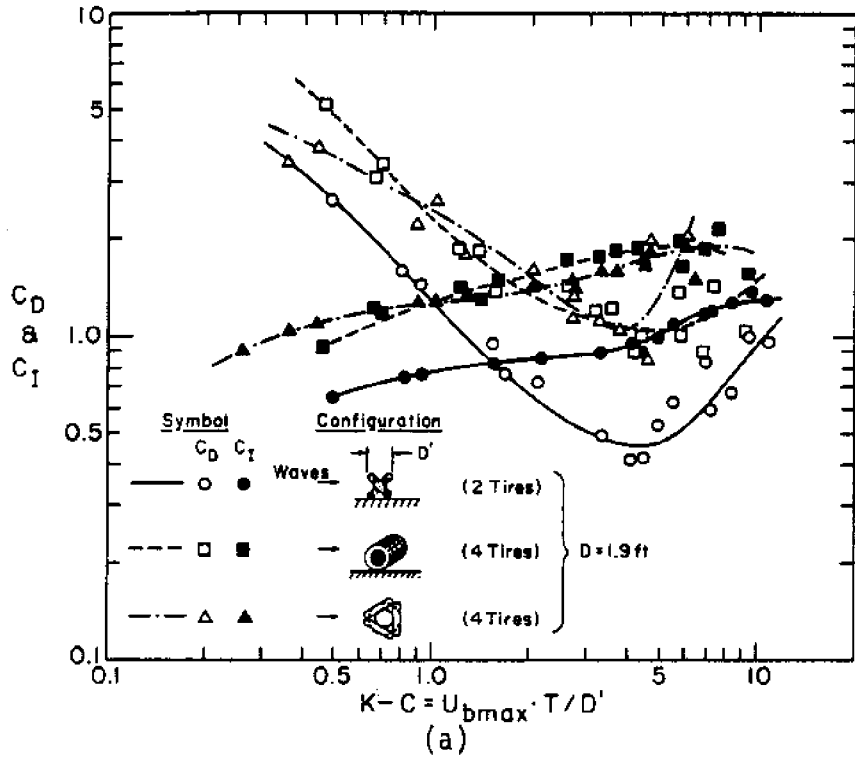


Fig. 4-16 Drag and Inertia Coefficients vs. K-C Number for
 (a) Two Tires Stuffed (b) Rosette Shape Configurations

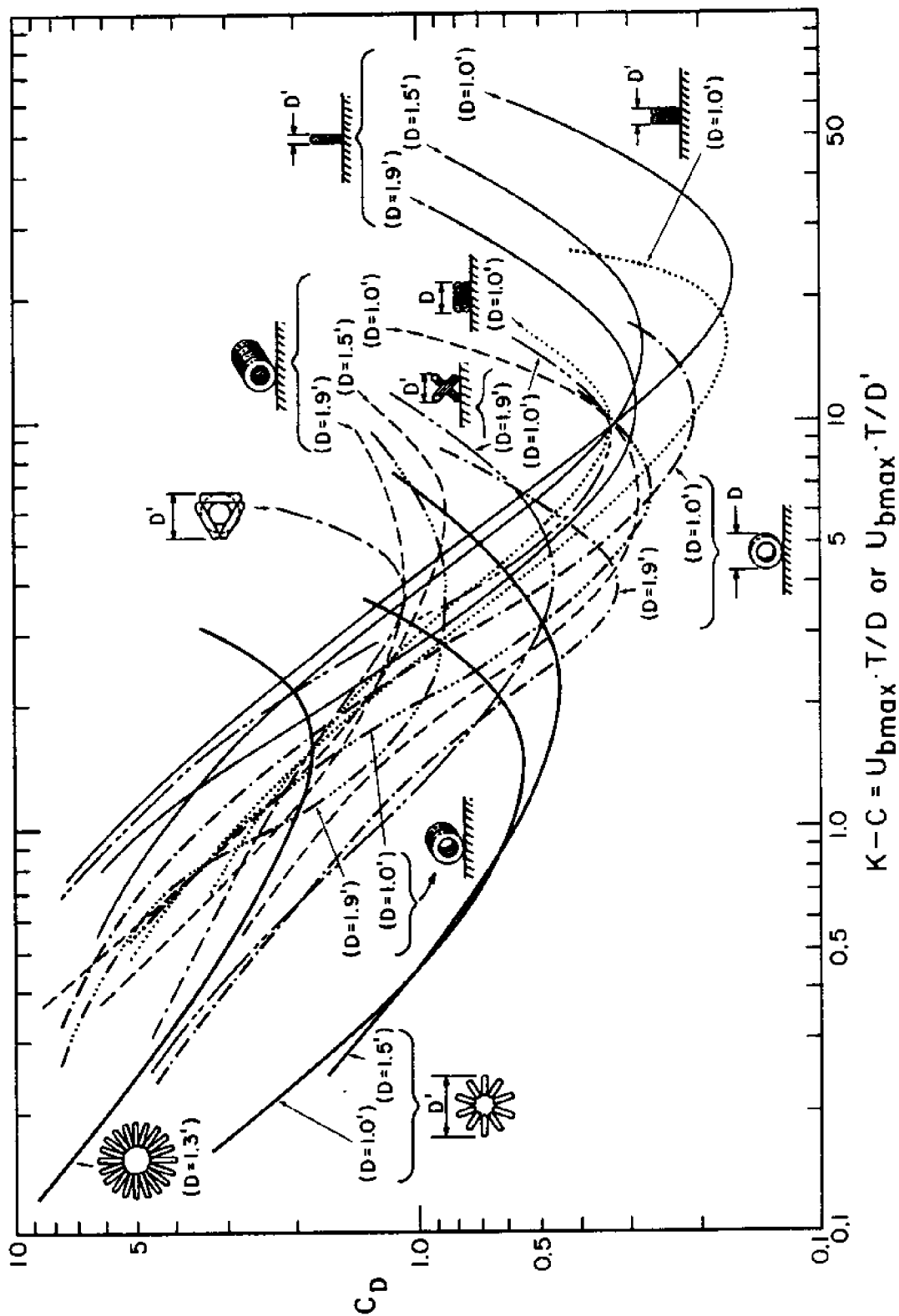


Fig. 4-17 Mean Lines of Drag Coefficients vs. K-C Number

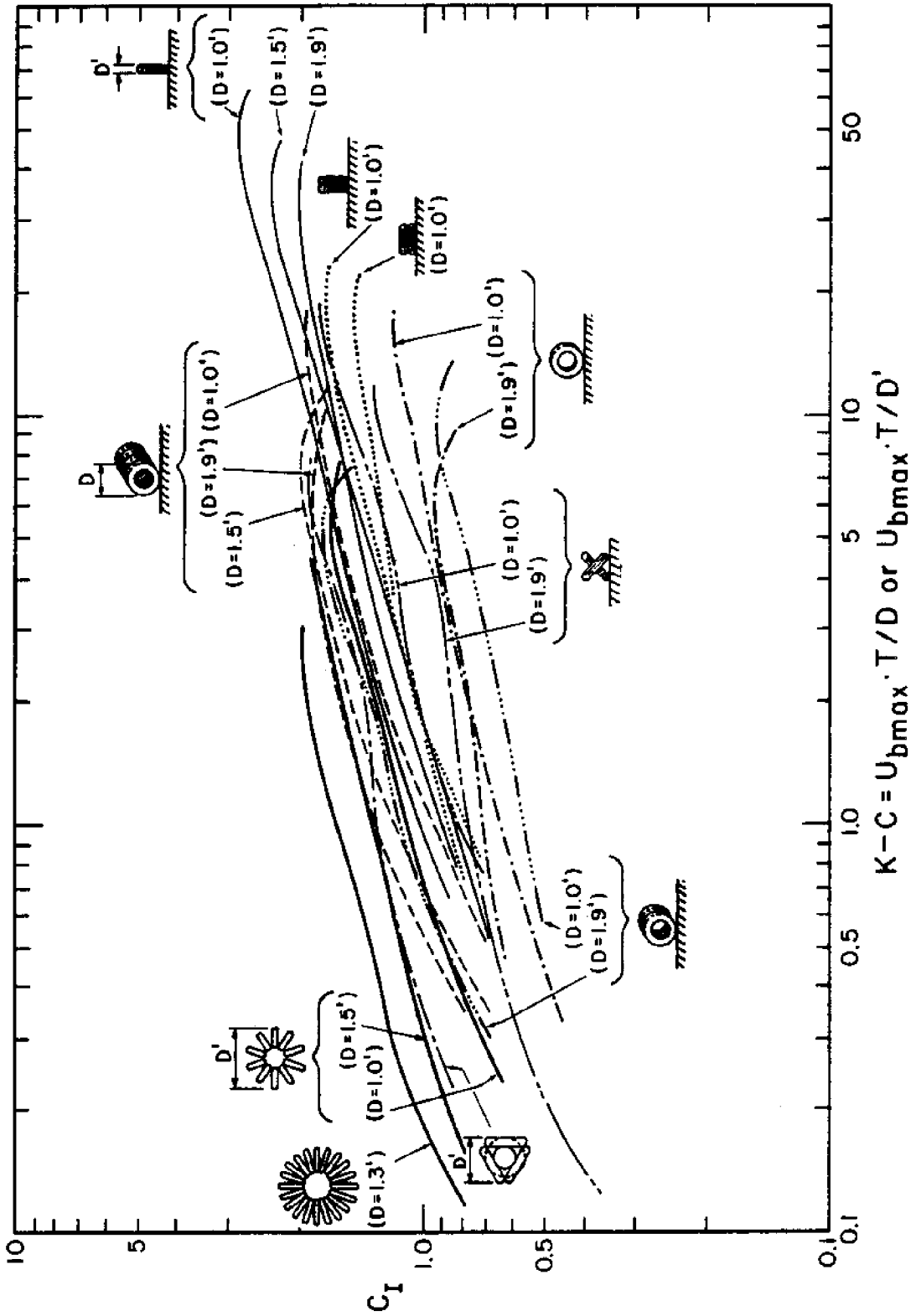


Fig. 4-18 Mean Lines of Inertia Coefficients vs. K-C Number

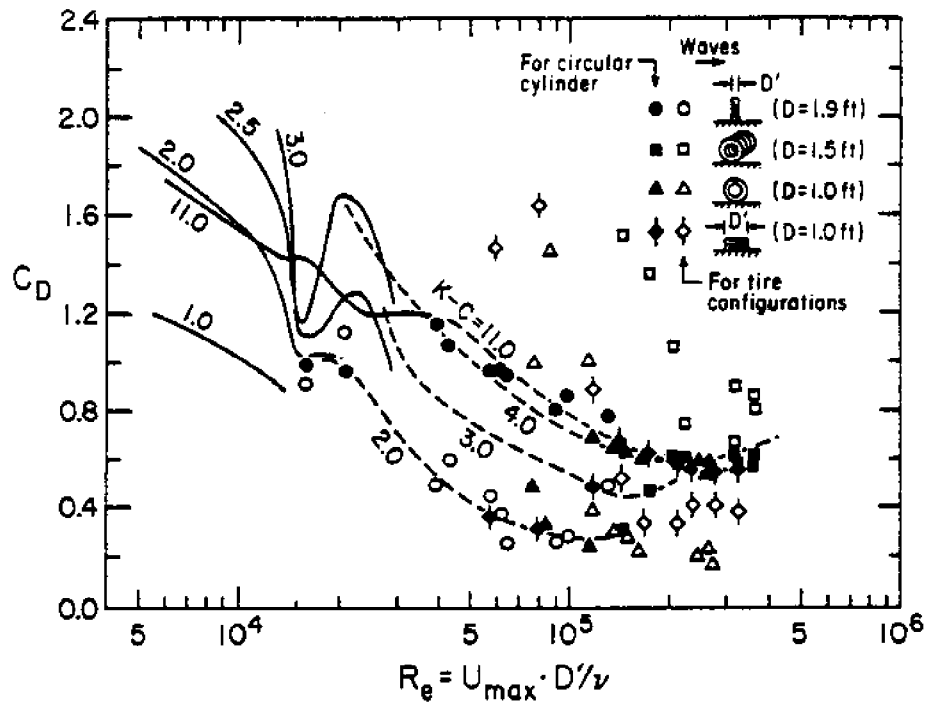
K-C numbers as the tire size increases.

Fig. 4-14 shows the effect of orientation on C_D and C_I . No consistent trends can be found. For four tire arrays, the perpendicular orientation(3) yields the lowest values of C_D and C_I among the three orientations. However, this is not the case with two tire arrays.

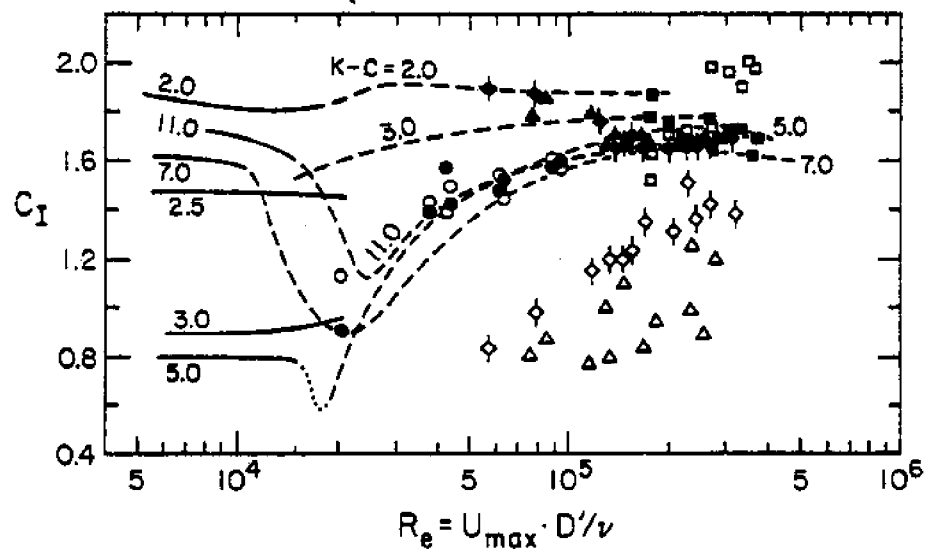
The effect of the number of tires used on C_D and C_I is shown in Fig. 4-15. For the case of $D=1.9$ ft, C_D and C_I increase as the number of tires increases. This trend is not evident with tires of $D=1.0$ ft.

Fig. 4-16a illustrates C_D and C_I of two stuffed tires and four tires fabricated from a triangular shape. The latter yields higher C_D and C_I than the former, and the magnitudes of C_D and C_I are similar to those of four tires of the same size oriented parallel to the waves, as shown in the same figure. The drag coefficients of rosette shaped configurations decay less rapidly than other configurations and rosettes with bigger D' yield higher drag coefficients as shown in Fig. 4.16b. It is also apparent that the inertia coefficients increase as D' of the rosette increases.

For the convenience of further comparisons, the mean values of C_D and C_I for various configurations and orientations are graphed as curves in Fig. 4-17 and Fig. 4-18. Drag coefficients vary between 7.6 and 0.17, with minimum coefficients occurring between $K-C=4$ and $K-C=15$. Rosette configurations display unique variations of C_D and C_I , consistent with the maximum force coefficients. This is probably due to the somewhat arbitrary definition for D' . The mean values of inertia coefficients of all the cases graphed in Fig. 4-18 show slight decreasing trends at large values of the K-C parameter. Also, the slope of the inertia coefficient curves is slightly steeper at very low values of the K-C

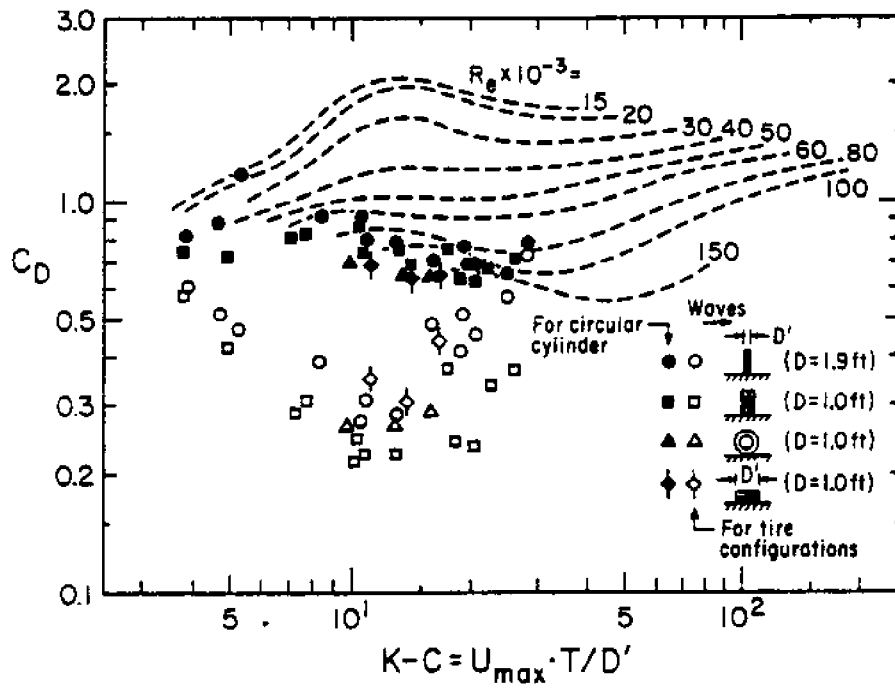


(a)

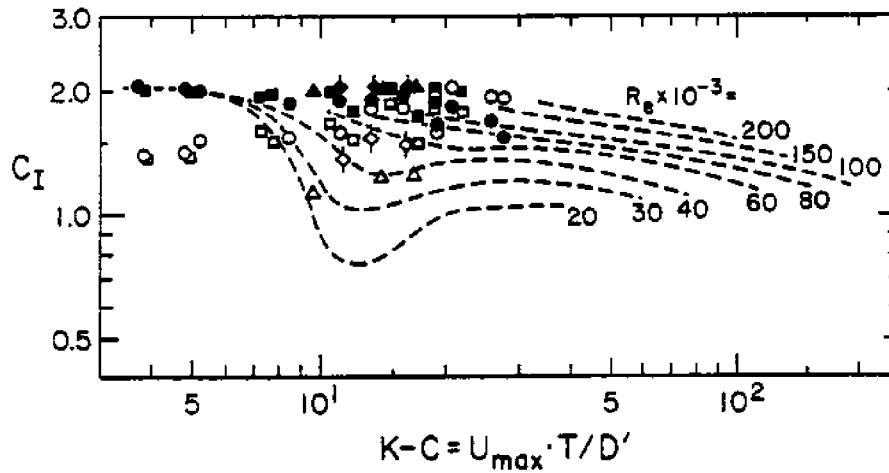


(b)

Fig. 4-19 Comparison between the Drag and Inertia Coefficients for Circular Cylinders (Garrison et al., 1977) and Those for Several Tire Unit Configurations



(a)



(b)

Fig. 4-20 Comparison between the Drag and Inertia Coefficients for Circular Cylinders (Sarpkaya, 1976) and Those for Several Tire Unit Configurations

parameter.

It is interesting to compare the obtained results with those of circular cylinders. For this purpose, values of C_D and C_I for several tire configurations are plotted in Fig. 4-19 and Fig. 4-20 along with those obtained by Garrison et al.(1977) and Sarpkaya(1976) (See Fig. 2-2 and Fig. 2-3). The open points(o, □, △, ◇ etc.) represent the values of C_D and C_I for tire configurations as functions of either Reynolds number or Keulegan-Carpenter number. The closed points(●, ■, ▲, ◆ etc.) represent the values of C_D and C_I for circular cylinders if they were placed under a flow condition with the same Reynolds number and Keulegan-Carpenter number.

The drag coefficients as a function of Reynold number show a similar exponential decay trend compared to that of circular cylinders at $Re > 1.0 \times 10^4$. However, the values of C_D are lower or higher than those of circular cylinders depending on the specific tire configuration. The inertia coefficients as a function of Reynolds number increase as Reynolds number increases and the magnitudes are lower or higher than those of circular cylinders depending on the specific tire configuration.

The drag and inertia coefficients for several tire configurations in Fig. 4-20 show lower values than those of circular cylinders observed by Sarpkaya. While C_D for circular cylinders display a mild convex peaks at approximately $K-C=10$, C_D for tire configurations display prominent concave peaks at $K-C=13$. Inertia coefficients for tire configurations generally follow the increasing trend of Sarpkaya's data as Keulegan-Carpenter number increases. However, the values are lower than those of circular cylinders. Further comparison for lower values of Reynolds number in Fig. 4-20 is limited because of the relatively high Reynolds

number of tire configurations over the range of Keulegan-Carpenter number considered.

The differences in C_D and C_I between tire configurations and circular cylinders would not be surprising if one considers the inherent difference in the shape of the two bodies and flow pattern around the bodies. However, it is concluded that results of hydrodynamic force studies for circular cylinders are useful for interpreting the results for artificial reef components.

4.4 Validity of the Morison Equation

The Morison equation, Eq. 2-4, has been widely accepted as a useful tool for the prediction of in-line wave forces on a submerged body. Past studies have indicated favorable correlations between wave force histories predicted by the Morison equation and actual force records on circular cylinders which are fixed or oscillating in water. However, the validity of the Morison equation is not assured for the case of elastic three-dimensional bodies such as reef tire configurations, responding to ocean waves.

To examine this aspect with tire configurations, the measured force records were compared with calculated force histories. The forces were calculated from Eq.2-4 by using previously obtained drag and inertia coefficients. Water particle velocities are assumed to be sinusoidal with amplitudes equal to the measured maximum velocity, U_{bmax} , so that

$$U = U_{bmax} \sin \frac{2\pi}{T}t \quad (4-13a)$$

and

$$\dot{U} = \frac{dU}{dt} = \frac{2\pi}{T} U_{bmax} \cos \frac{2\pi}{T}t \quad (4-13b)$$

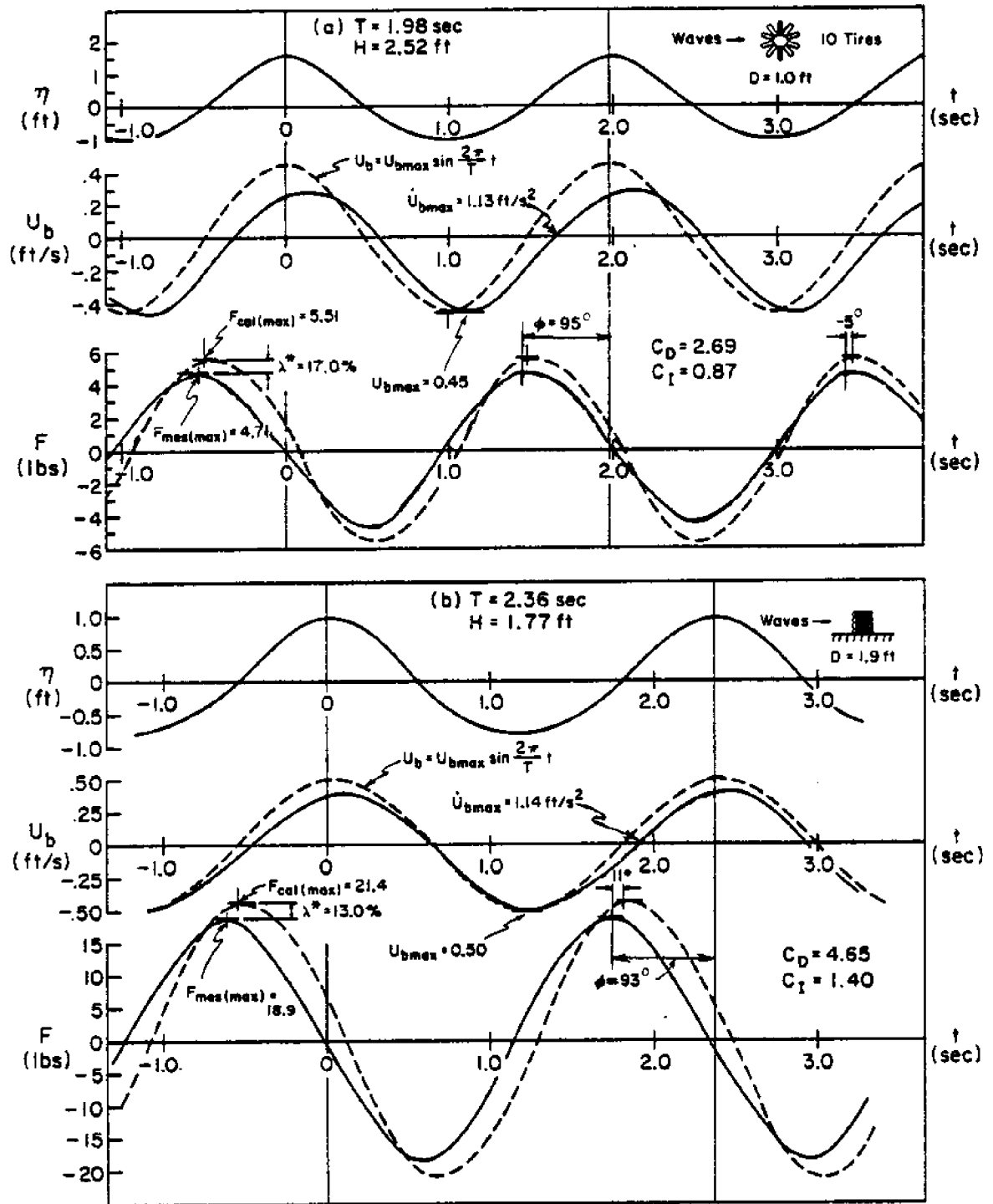


Fig. 4-21 Comparison between the Measured Force and the Calculated Force for (a) $T=1.98$ sec. (b) $T=2.36$ sec.

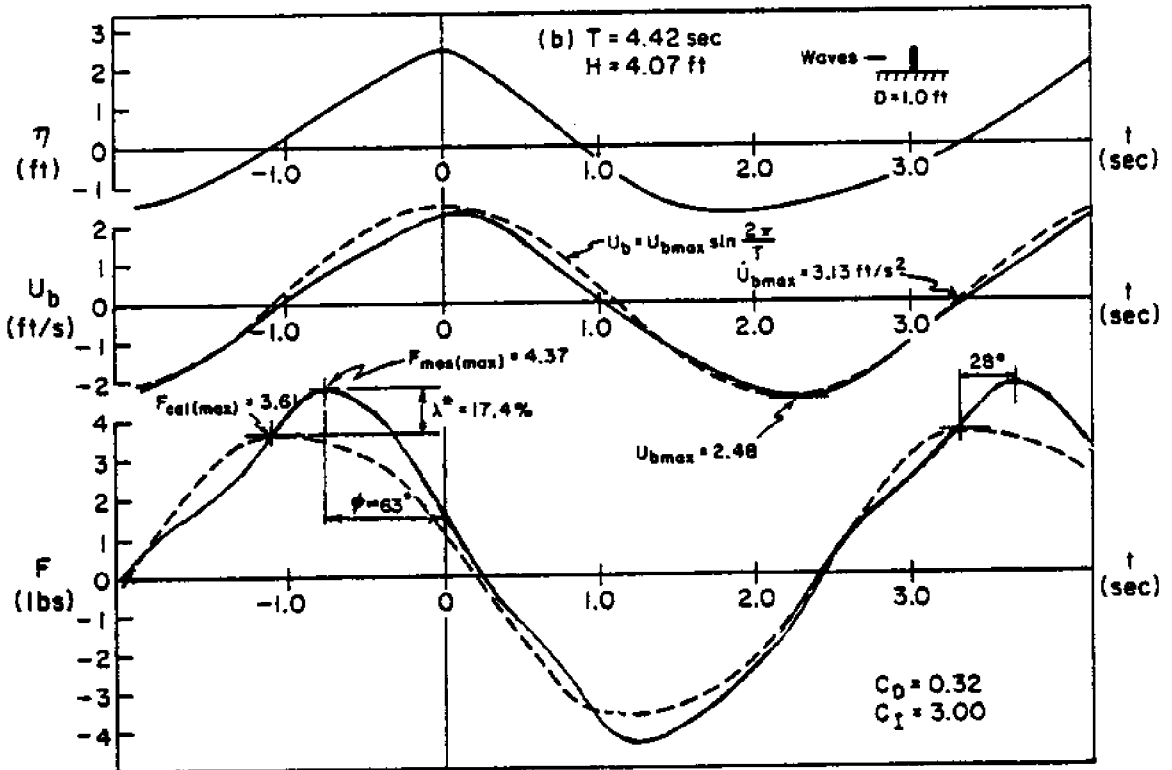
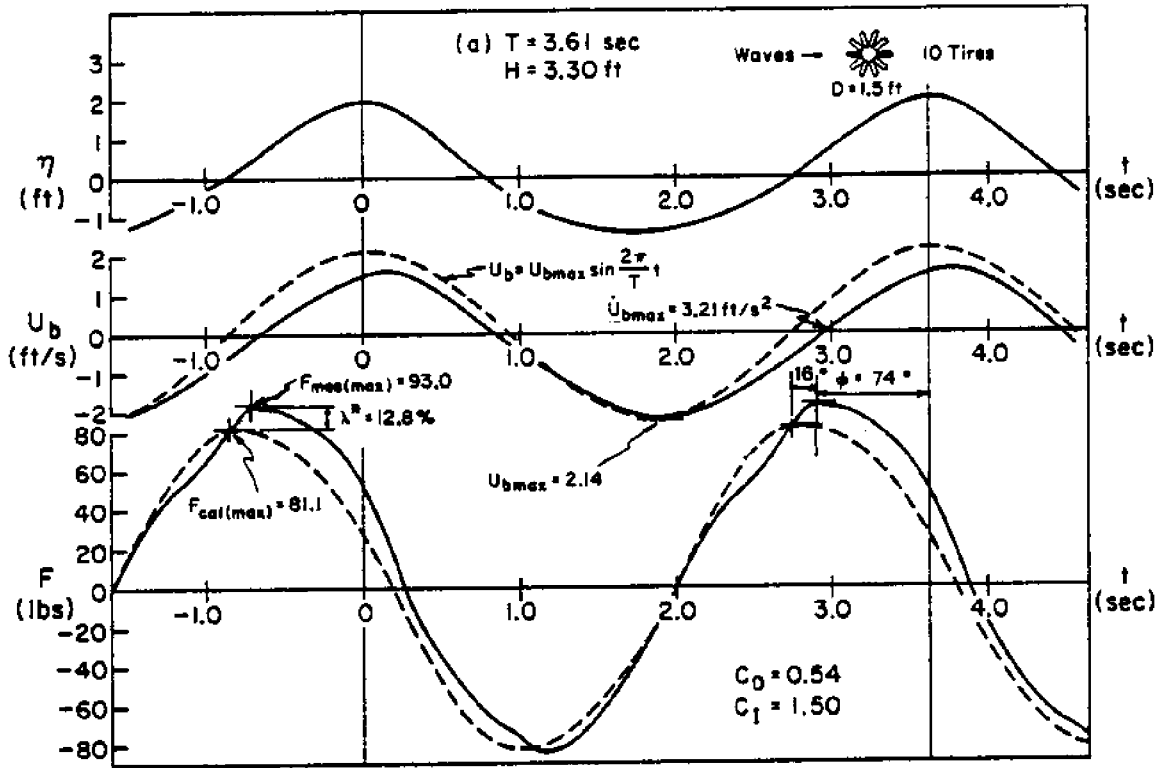


Fig. 4-22 Comparison between the Measured Force and the Calculated Force for (a) $T=3.61$ sec. (b) $T=4.42$ sec

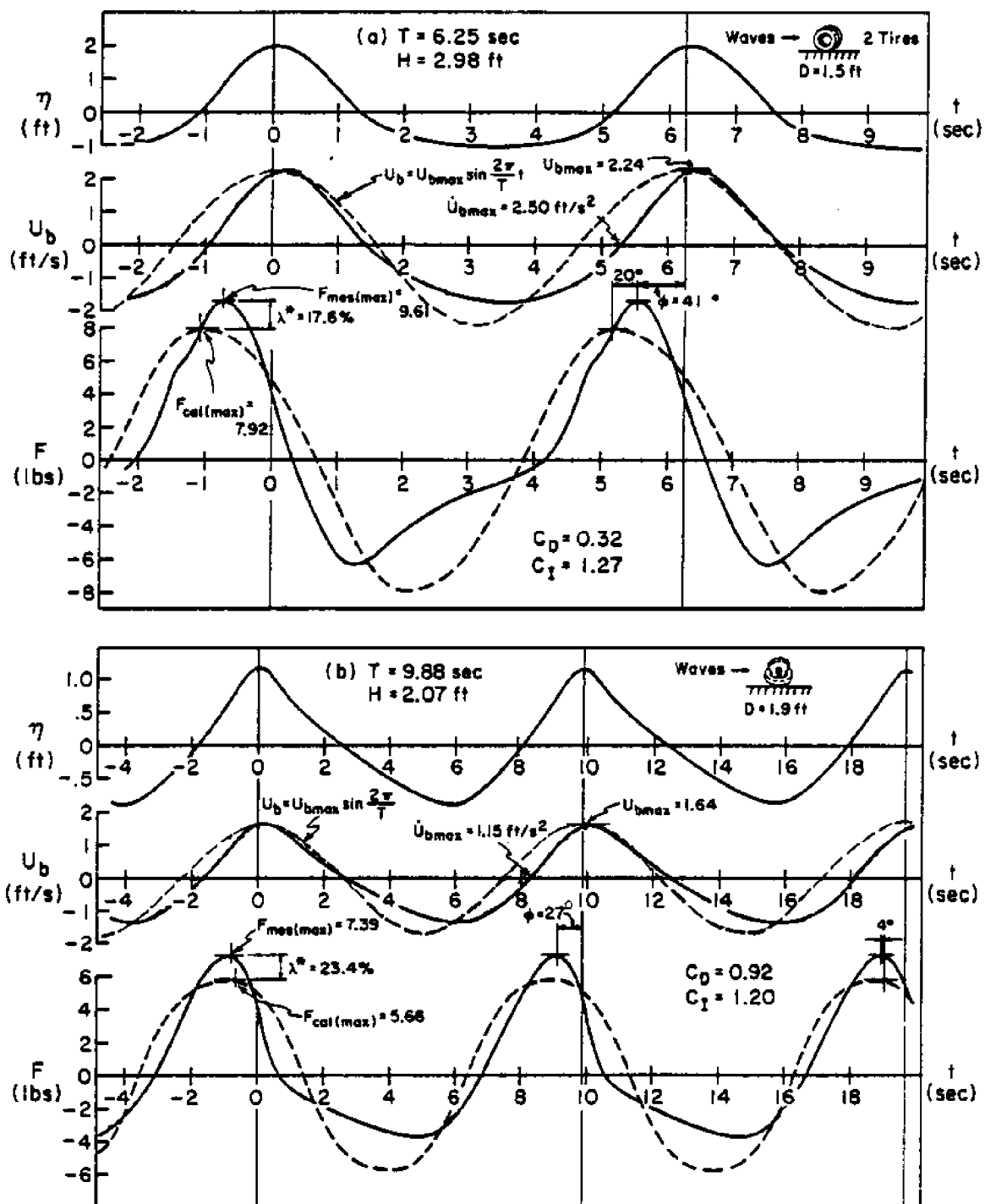


Fig. 4-23 Comparison between the Measured Force and the Calculated Force for (a) $T=6.25$ sec. (b) $T=9.88$ sec.

The results are shown from Fig. 4-21 to Fig. 4-23 for six wave periods. Tire configurations and wave heights are arbitrarily chosen for each period. The error between the measured maximum force $F_{\max(\text{mes})}$ and the calculated force $F_{\max(\text{cal})}$ is defined as

$$\lambda^* = \frac{F_{\max(\text{mes})} - F_{\max(\text{cal})}}{F_{\max(\text{mes})}} \times 100(\%) \quad (4-14)$$

Calculated force histories show good agreement in phase and magnitude for waves with period $T \leq 3.61$ seconds. However, some discrepancies in magnitude are found for longer waves. The calculated forces lead the measured forces in phase for most cases except that of $T=2.36$ seconds, however, the phase lags are below 20° , with the exception of $T=4.42$ seconds (28°). The errors between $F_{\max(\text{mes})}$ and $F_{\max(\text{cal})}$, λ^* , vary from 12.8% to 23.4%.

It can be concluded that the Morison equation estimates of dynamic in-line wave forces on tire units are approximate and some improvements in the evaluation of the drag and inertia coefficients may be required to improve the predicted force time history.

If the observed phase lags between surface wave profile and horizontal velocities are due to the frequency response of the velocity measurement system, and modifications were made to correct the velocity data, the resulting drag and inertia coefficients evaluated by the maximum value method could be considerably different. Without a velocity phase lag, the drag coefficients tend to be larger than those presently obtained values and the inertia coefficients tend to be smaller for the waves with wave periods longer than 2.36 seconds. For the waves

with wave periods less than or equal to 2.36 seconds, the opposite may occur, because the force lag exceeds the velocity phase lag. (See Fig. 3-8 and Figs. 4-19, 20, 21)

It is likely that the errors between predicted and measured force records could be further reduced by utilizing least squares procedures (See Section 2.2) to evaluate C_D and C_I . However, this improvement should also utilize relative velocities and accelerations, thereby necessitating an evaluation of tire unit displacements as a function of time. The latter is clearly beyond the scope of this study and probably exceeds practical engineering design needs. Design requirements are limited to static predictions of the maximum destabilizing force causing the onset of motion, not a time history of the dynamic force response. The maximum force is adequately evaluated by the maximum force coefficient.

The noticeable disagreements between measured and calculated force history for the cases of $T=4.42\sim 9.88$ seconds may be due to the elastic response of the tire reefs to the longer waves. Based on the present velocity measurements records, the maximum forces occur near the points of zero velocity, i. e., at the points of maximum acceleration. This behavior was verified theoretically using the Morison equation and the experimentally determined drag and inertia coefficients. It may be concluded that inertia forces dominate drag forces in Eq. 2-4 for all tire configurations and wave conditions considered in this study.

The phase differences between maximum velocity and maximum measured force, denoted by ϕ , are also shown in Fig. 4-21 to Fig. 4-23. The phase lag is defined according to:

$$U(\text{or } \eta) = U_{\max}(\text{or } \eta_{\max}) \sin \frac{2\pi}{T}t \quad (4-15a)$$

$$\text{and} \quad F = F_{\max} \sin\left(\frac{2\pi}{T}t + \phi\right) \quad (4-15b)$$

As discussed in Section 4.1, maximum velocities occur under the trough for the waves with $T=1.98\text{--}4.42$ seconds, and occur under the crest for the waves with $T=6.25\text{--}9.88$ seconds. Maximum velocities lead maximum forces for the waves with $T=1.98\text{--}4.42$ seconds, and the opposite occurs for the waves with $T=6.25\text{--}9.88$ seconds. However, ϕ is always referenced from the wave crest as defined in Eq. 4-15. The phase lags obtained from the force records are plotted against the Keulegan-Carpenter number in Fig. 4-24. Phase differences tend to decrease as the K-C number increases. For the waves with $T \leq 4.42$ seconds, the magnitude of ϕ ranges from 50° to 120° . For the waves with $T \geq 6.25$ seconds, the magnitude of ϕ ranges from 18° to 50° .

Usually, maximum forces occur at some point between maximum velocity and maximum acceleration where the algebraic sum of drag force and inertia force in Eq. 2-4 reaches its maximum. If the maximum velocity occurs at the crest, then F_{\max} leads U_{\max} and $0^\circ < \phi < 90^\circ$. This concurs with the data points corresponding to $T=6.25\text{--}9.88$ seconds in Fig. 4-24. If the maximum velocity occurs at the trough but ϕ is referenced to the wave crest, then F_{\max} will occur between the trough and the up-crossing point. The latter will yield ϕ between the up-crossing phase angle and 180° , which concurs with the data points corresponding to $T=1.98\text{--}4.24$ seconds in Fig. 4-22. However, there are some exceptions for the waves with $T=4.42$ seconds. Even though the maximum velocity occurs under the trough, data of many runs with this wave period show that the maximum

forces occur between the up-crossing points and the wave crests.

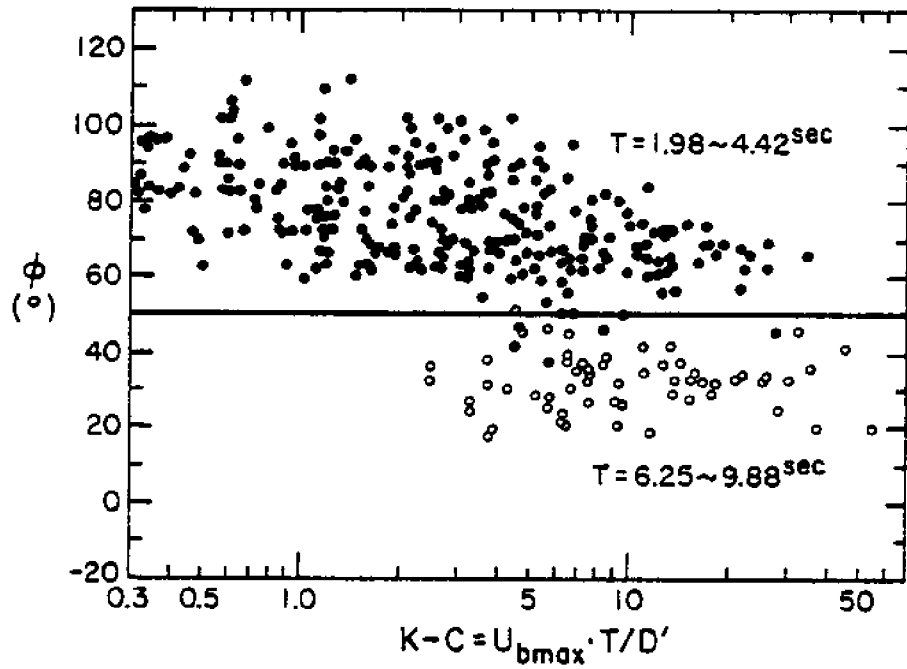


Fig. 4-25 Phase Lags between the Maximum Horizontal Velocity (Wave Crest) and the Maximum Horizontal Force vs. K-C Number

4.5 Bottom Resistance Coefficients

Bottom resistance coefficients were obtained utilizing the laboratory procedures described in Section 3.4. Each tire unit was pulled horizontally in water both on fine sand and on a concrete surface until motion was initiated. The bottom friction coefficients were calculated according to

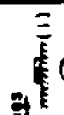







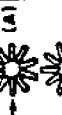





$$f = \frac{F_H}{W_{sub}} \quad (4-16)$$

where F_H is the horizontal force required to move the tire unit and W_{sub} is the submerged weight of tire unit including any added ballast.

The results are shown in Table 4. The magnitude of f varies between 0.80 and 1.28 on fine sand and between 0.46 and 0.74 on a finished concrete surface. The effect of orientation on f can be seen for each tire configurations. Orientation(1) promotes the highest values because of the relatively large contact area. Orientation(2) provides the lowest values due to rounded contact edges. For rosette shape and stuffed configurations, orientation(B) induces higher f . Bottom friction coefficients tend to decrease as tire size and number of tires increase.

Valent(1979) performed a friction test with sea-bed materials collected at various water depths. The specimens were displaced under normal loads in a direct shear test machine in contact with rough and smooth steel or rough and smooth concrete. The maximum friction coefficients vary between 0.55 and 0.65 according to the sand properties. Two test results of Valent are shown in Appendix B along with sample friction test records for two tire configurations.

Table 4 Bottom Resistance Coefficients(f) for Tire Units in Contact with Fine Sand and with Finished Concrete

| Configura- tion | f(on Fine Sand) | | | | | f(on Finished Concrete) | | | | |
|---|-----------------|----------|----------|----------|---------|-------------------------|----------|----------|----------|---------|
| | D=1.0 ft | D=1.3 ft | D=1.5 ft | D=1.9 ft | Average | D=1.0 ft | D=1.3 ft | D=1.5 ft | D=1.9 ft | Average |
| | | | | | | | | | | |
| ways  | 1.06 | 0.95 | 1.01 | 0.96 | 1.00 | 0.58 | 0.60 | 0.59 | 0.55 | 0.58 |
|  | 1.00 | 0.80 | 0.90 | 0.87 | 0.89 | 0.50 | 0.50 | 0.46 | 0.49 | 0.49 |
|  | 1.01 | 0.85 | 0.95 | 0.91 | 0.93 | 0.53 | 0.55 | 0.53 | 0.58 | 0.55 |
|  | 1.05 | 0.85 | 0.95 | 0.88 | 0.93 | 0.74 | 0.59 | 0.62 | 0.62 | 0.64 |
|  | 0.96 | 0.80 | 0.87 | 0.81 | 0.86 | 0.55 | 0.50 | 0.50 | 0.56 | 0.53 |
|  | 1.00 | 0.84 | 0.91 | 0.85 | 0.92 | 0.59 | 0.56 | 0.54 | 0.54 | 0.56 |
|  | 0.96 | 0.95 | 0.95 | 0.85 | 0.93 | 0.60 | 0.60 | 0.56 | 0.70 | 0.62 |
|  | 0.87 | 0.86 | 0.80 | 0.75 | 0.82 | 0.53 | 0.46 | 0.46 | 0.60 | 0.51 |
|  | 0.92 | 0.90 | 0.87 | 0.80 | 0.87 | 0.61 | 0.60 | 0.58 | 0.70 | 0.62 |
|  | 0.95 | 0.80 | 0.80 | - | 0.85 | 0.59 | 0.52 | 0.55 | - | 0.55 |
|  | 1.01 | 0.85 | 0.87 | - | 0.91 | 0.61 | 0.56 | 0.60 | - | 0.59 |
|  | 1.19 | 1.05 | - | 1.04 | 1.09 | 0.58 | 0.61 | - | 0.58 | 0.59 |
|  | 1.28 | 1.15 | - | 1.10 | 1.18 | 0.63 | 0.63 | - | 0.64 | 0.63 |
|  | - | 0.85 | - | 0.85 | 0.85 | - | 0.55 | - | 0.60 | 0.58 |

4.6 Field Application

In this section, the results of the present study are integrated to provide a design procedure for submerged artificial reefs fabricated from rubber tires. The required information for reef design includes: design wave conditions (wave period T , offshore wave height H_0), water depth at the reef site (h), physical characteristics of sea bottom materials, and tire sizes and configurations to be used. The design wave height in deep water, H_0 , may be taken as the significant wave height (H_s) or average wave height of highest 10 percent of all waves (H_{10}). H_s or H_{10} are used to allow occasional unit motion for the design storm without excessive ballast requirements. The deep water wave height, H_0 , should be modified to the actual wave height at the reef site, H , by considering shoaling, refraction and breaking of the incident waves.

This wave condition combined with water depth at the reef site enables the designer to predict the near bottom kinematics of water particles utilizing available wave theories. As discussed in Section 3.1, linear wave theory adequately predicts maximum sea floor water particle velocities and may be used in reef design. A dimensionless maximum water particle velocity at the sea floor $U_{bmax}/(L_0/T)$ is given in Fig. 4-25 as a function of dimensionless wave height (H/L_0) and water depth (h/L_0) in accordance with linear wave theory. L_0 represents the deep water wave length for waves with period T , $L_0 = gT^2/2\pi$.

A reef should be configured and ballasted so that it will remain stable under the maximum horizontal forces imposed upon it by the design wave. Maximum horizontal wave forces on tire reefs of specified size and configuration can be predicted in two ways: first, by using Eq. 2-5 with maximum force coefficient (C_f) and maximum near bottom water

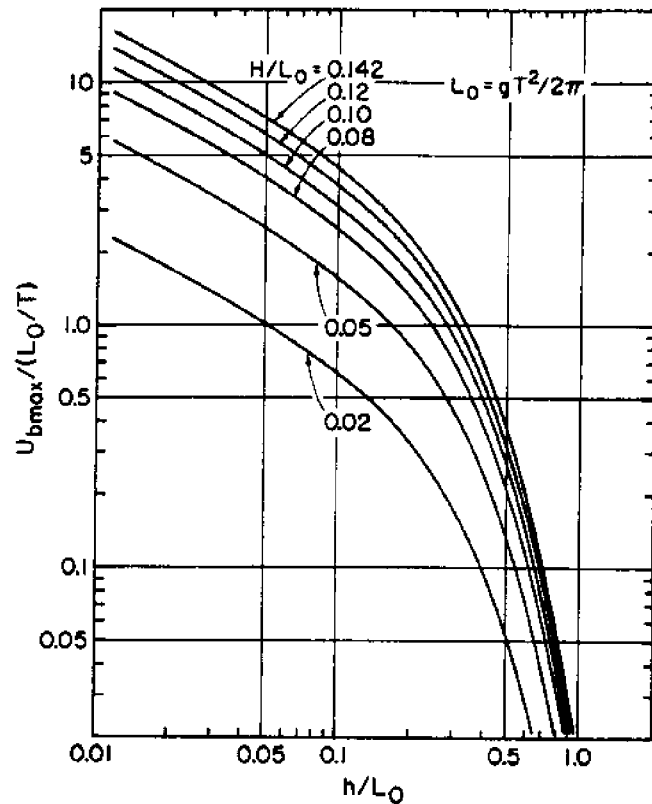


Fig. 4-25 Maximum Bottom Velocity by Linear Wave Theory for Specified Wave Height and Water Depth

particle velocity (U_{bmax}), second, by using the Morison equation (Eq. 2-4) with drag and inertia coefficients (C_D and C_I) and time-varying near bottom water particle velocity (U_b) and acceleration (\dot{U}_b). However, the former method is recommended because a designer needs the maximum force rather than a time history of force. Another reason is that predictions by the Morison equation may be accompanied by considerable errors in maximum values as was discussed in Section 4.4.

The following procedures can be used to complete a design:

- (1) Predict the maximum sea floor water particle velocity (U_{bmax}) from the design wave height (H), wave period (T) and water depth (h) by

using Fig. 4-25.

(2) Select the maximum force coefficients(C_f) and bottom resistance coefficient(f) for the tire unit configuration and orientation in question by calculating the Keulegan-Carpenter parameter and utilizing Fig. 4-12 and Table 4.

(3) Calculate the maximum horizontal force on the tire unit as

$$F_{\max} = C_f \frac{\rho}{2} A U_{b\max}^2$$

(4) Calculate the required submerged weight of the tire unit to resist the maximum horizontal forces as,

$$\text{Required } W_{\text{sub}} = F_{\max}/f.$$

(5) Calculate the ballast required to obtain stability as

$$W_{\text{ballast}}(\text{per tire}) = (\text{Required } W_{\text{sub}}) / (\text{No. of tires}) - \text{Submerged weight of single tire}$$

The submerged weight of tire units of specified size can be obtained from Fig. 3-2.

Table 5 shows the allowable deep water wave height for design waves with periods of 10, 14 and 18 seconds at six different water depths, assuming that each tire is ballasted to the bead by concrete as shown in Fig. 3-1. The allowable maximum water particle velocity is calculated by

$$\text{Allowable } U_{b\max} = \sqrt{\frac{f W_{\text{sub}}}{\frac{\rho}{2} A C_{f(\min)}}} \quad (4-17)$$

where W_{sub} = ballast in water(from Fig. 3-1) + submerged weight of tire units(from Fig. 3-2). $C_{f(\min)}$ is the lowest maximum force coefficient from Fig. 4-12 experienced by each tire unit of a specified configuration and orientation. Lowest values are taken because the resulting Keulegan-Carpenter numbers under the severe wave conditions in

field are typically high enough to exceed the highest K-C values covered by maximum force coefficients curves in Fig. 4-12.

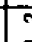

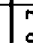
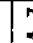

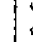
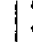


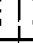
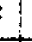

Linear wave theory maximum sea floor water particle velocities are given by Eq. 4-4. The allowable wave height in deep water can be calculated as

$$\text{Allowable } H_0 = \frac{T}{\pi} \sinh \frac{2\pi h}{L} \cdot (\text{Allowable } U_{b\max}) / K_s \quad (4.18)$$

where K_s is the shoaling coefficient and represents the variation of wave height as waves approach shore. The effects of refraction and reflection of waves are not considered in Table 5. The results show that tire reefs manufactured from most configurations can tolerate waves with periods up to 18 seconds and heights up to 15 feet at a water depth of 150 feet when ballasted by concrete to the level of the tire bead. However, additional ballast is required to obtain stability at shallower depths under severe waves. Similar tables can be presented for tire reefs with other ballast levels.

Table 5. Allowable Deep Water Wave Height (H_0) for Tire Units Ballasted by Concrete to the Level of Tire Bead

(D=1.9 ft)

| Config- uration | W_{sub} (Lbs) | $\frac{PA}{2}$ | f | Allow- able U_{max} (ft/s) | h = 30 ft | | h = 60 ft | | h = 90 ft | | h = 120 ft | | h = 150 ft | | h = 180 ft | | | | | | | | |
|--|--------------------|----------------|------|---------------------------------------|-----------|-----|-----------|-----|-----------|------|------------|------|------------|------|------------|------|----------|------|------|------|------|------|------|
| | | | | | $T=10^5$ | | $T=10^5$ | | $T=10^5$ | | $T=10^5$ | | $T=10^5$ | | $T=10^5$ | | $T=10^5$ | | | | | | |
| | | | | | 14 | 18 | 14 | 18 | 14 | 18 | 14 | 18 | 14 | 18 | 14 | 18 | 14 | 18 | 14 | 18 | | | |
| Waves  | 16.2 | .906 | 0.96 | 1.20 | 3.78 | 8.4 | 6.9 | 6.1 | 14.9 | 11.9 | 10.3 | 22.0 | 16.5 | 14.1 | 30.8 | 21.2 | 17.8 | 42.5 | 26.2 | 21.4 | 59.0 | 31.5 | 25.1 |
|  | " | .906 | 0.87 | 1.10 | 3.76 | 8.3 | 6.9 | 6.0 | 14.8 | 11.8 | 10.3 | 21.9 | 16.5 | 14.1 | 30.6 | 21.1 | 17.7 | 42.3 | 26.0 | 21.3 | 58.7 | 31.3 | 24.9 |
|  | " | 1.84 | 0.91 | 1.20 | 2.58 | 5.7 | 4.7 | 4.1 | 10.2 | 8.1 | 7.0 | 15.0 | 11.3 | 9.7 | 21.0 | 14.5 | 12.2 | 29.0 | 17.9 | 14.6 | 40.3 | 21.5 | 17.1 |
|  | 32.3 | 1.812 | 0.88 | 1.40 | 3.35 | 7.4 | 6.1 | 5.4 | 13.2 | 10.6 | 9.1 | 19.5 | 14.7 | 12.5 | 27.2 | 18.8 | 15.8 | 37.6 | 23.2 | 19.0 | 52.3 | 27.9 | 22.2 |
|  | " | 1.812 | 0.81 | 1.40 | 3.21 | 7.1 | 5.9 | 5.1 | 12.7 | 10.1 | 8.8 | 18.7 | 14.1 | 12.0 | 26.1 | 18.0 | 15.1 | 36.1 | 22.2 | 18.2 | 50.1 | 26.7 | 21.3 |
|  | " | 1.84 | 0.85 | 1.20 | 3.53 | 7.8 | 6.5 | 5.7 | 13.9 | 11.1 | 9.6 | 20.6 | 15.5 | 13.2 | 28.7 | 19.8 | 16.6 | 39.7 | 24.4 | 20.0 | 55.1 | 29.4 | 23.4 |
|  | 64.6 | 3.624 | 0.85 | 1.65 | 3.03 | 6.7 | 5.5 | 4.9 | 12.0 | 9.5 | 8.3 | 17.7 | 13.3 | 11.3 | 24.7 | 17.0 | 14.3 | 34.1 | 21.0 | 17.2 | 47.3 | 25.2 | 20.1 |
|  | " | 3.624 | 0.75 | 1.90 | 2.65 | 5.9 | 4.9 | 4.2 | 10.5 | 8.3 | 7.2 | 15.4 | 11.6 | 9.9 | 21.6 | 14.9 | 12.5 | 29.8 | 18.3 | 15.0 | 41.4 | 22.1 | 17.6 |
|  | " | 1.840 | 0.80 | 2.10 | 3.66 | 8.1 | 6.7 | 5.9 | 14.4 | 11.5 | 10.0 | 21.3 | 16.0 | 13.7 | 29.8 | 20.6 | 17.3 | 41.1 | 25.3 | 20.8 | 57.1 | 30.5 | 24.3 |
|  | 18.7 | 2.45 | 1.10 | 1.90 | 2.10 | 4.6 | 3.8 | 3.4 | 8.3 | 6.6 | 5.7 | 12.2 | 9.2 | 7.9 | 17.1 | 11.8 | 9.9 | 23.6 | 14.5 | 11.9 | 32.8 | 17.5 | 13.9 |
|  | 64.6 | 4.755 | 0.85 | 2.80 | 2.03 | 4.5 | 3.7 | 3.3 | 8.0 | 6.4 | 5.5 | 11.8 | 8.9 | 7.6 | 16.5 | 11.4 | 9.6 | 22.8 | 14.1 | 11.5 | 31.7 | 16.9 | 13.5 |
|  | 111.1 | 5.763 | 0.87 | 2.90 | 2.40 | 5.3 | 4.4 | 3.8 | 9.5 | 7.6 | 6.5 | 14.0 | 10.5 | 9.0 | 19.5 | 13.5 | 11.3 | 27.0 | 16.6 | 13.6 | 37.5 | 20.0 | 15.9 |

Allowable $U_0 = \frac{1}{n} \sinh(\frac{2\pi}{L} h) U_{bmax} \bar{K}_S$

W_{sub} = Submerged weight of ballasted tire configuration [See Fig. 3-1 and 3-2]

$$K_S = \sqrt{\frac{g T^2 \sinh(\frac{4\pi}{L} h)}{2 \pi L [\frac{4\pi}{L} h + \sinh(\frac{4\pi}{L} h)]}}$$

$$U_{bmax} = \sqrt{\frac{F \cdot W_{sub}}{\frac{\rho}{2} A C_f (min)}}$$

$$L = \frac{g T^2}{2} \tanh(\frac{2\pi}{L} h)$$

$\rho = 1.94$ slugs/ft

V. CONCLUSIONS

5.1 Summary

Engineering studies have been conducted to provide basic information required to design stable artificial reefs fabricated from scrap tires. Large scale laboratory experiments were conducted to determine maximum force coefficients, drag and inertia coefficients, and bottom friction coefficients for seven tire unit configurations and various orientations. The force coefficients are utilized to predict wave and current induced loads on individual units while the bottom friction coefficients are utilized to predict ballast requirements for resisting wave and current loads. Monochromatic waves ranging from shallow to deep water, low amplitude to breaking waves in a model depth of 10 feet were utilized in the test.

The results presented herein confirm the following conclusions:

- (1) The resulting force coefficients, relating forces to wave-current velocities, depend both on Reynolds number and Keulegan-Carpenter period parameter, however, a more definitive relationship was observed with respect to the period parameter.
- (2) The maximum force coefficients exponentially decay as the period parameter increases over the observed range (maximum 40 to minimum 1.1). The effect of tire size on the maximum force coefficients of a specified configuration is almost negligible.
- (3) The drag and inertia coefficients based on Morison equation analysis vary uniquely as a function of period parameter. The drag coefficients decay to a minimum value at an intermediate period parameter (2 to 7) and rapidly increase as the value of the period parameter increases further. Inertia coefficients increase gradually from 0.6 up to 3.0 as the period parameter increases over the observed range.

- (4) The force histories from the Morison equation using previously obtained drag and inertia coefficients agree well with measured force records, but shorter waves give better agreement than longer waves. The difference between the calculated maximum forces and measured values ranged 12.8 to 23.4 percent. Throughout the observed range of Reynolds number and Keulegan-Carpenter parameter, inertia forces dominate drag forces for all tire configurations.
- (5) The Morison equation may be used to predict the force history on tire reefs in spite of their three-dimensional shape and elastic response to the waves. However, maximum design forces may be predicted with confidence by using maximum force coefficients rather than using the Morison equation.
- (6) The bottom resistance coefficients of tire units in contact with fine sands were found to vary between 0.75 and 1.20, gradually decreasing with increasing tire size.
- (7) Observed surface wave profiles show that the experimentally generated waves were nonlinear and the Stream-function theory provided better correlation with experiments than the linear wave theory. The differences between observed profiles and those of Stream-function theory were less than 6.3 percent at the crest and 4.2 percent at the trough.
- (8) Linear wave theory yields better maximum near bottom velocities than Stream-function theory. The differences between the observed values and those of linear wave theory were up to 20 percent except the case of very short waves with $T \leq 2.0$ seconds. However, Stream-function theory yields better maximum bottom water particle acceleration than linear wave theory. The differences between observed values and theoretical values are less than 20 percent for both theories.

5.2 Application of Results

Practical application of the study results has been discussed in detail in Section 4.6 and may be briefly summarized as outlined below.

- (1) Predict significant wave height and period for return period equal to desired design life of reef using established wave forecasting techniques.
- (2) Shoal, refract and deffract the wave height to the reef site.
- (3) Tolerate same reef unit motion by using significant wave properties rather than the average of the highest 10% or 1% of the waves.
- (4) Calculate maximum bottom velocity using the linear wave theory combined with water depth, wave height and period.
- (5) Select a variety of configuration shapes to provide a diverse habitat for a range of fish sizes.
- (6) Evaluate the Keulegan-Carpenter period parameter.
- (7) Refer to the experimental results of C_f vs. K-C to obtain C_f for each configuration.
- (8) Evaluate $F_{\max} = C_f A U_{\max}^2 / 2$, utilizing A from Table 1., C_f from Step(7) and U_{\max} from Step(4).
- (9) Refer to Table 4 to obtain the bottom friction coefficient, f, for each configuration. Use the lesser of the two values(one for sand surface, the other for finished concrete surface) if the bottom properties are unknown.
- (10) Calculate $W_{\text{sub}} = F_{\max} / f$.
- (11) Add sufficient ballast to each tire to increase the total submerged weight of configuration to W_{sub} .
- (12) Repeat Step(5)-(11) for each configuration.

5.3 Future Studies

This study has responded to the need for basic engineering information required to design a stable artificial reef fabricated from scrap tires. However, additional studies could provide further refinements and increase our understanding of artificial reef behavior. Suggested additional research topics include:

- (1) Extend the range of the Keulegan-Carpenter period parameter by repeating the tests conducted in this study at the same large wave scale but with tires of smaller diameter. For this study, a smaller and more sensitive dynamometer table must be constructed.
- (2) Evaluate lift coefficients for tire unit configurations. Then evaluate the phase difference between the maximum lift force and the maximum horizontal force to determine if lift forces reduce the effective submerged weight of tires. This study requires construction of a sophisticated tire support and strain gage system.
- (3) Evaluate bottom resistance coefficients(f) for a range of sea bottom materials with various soil properties.
- (4) Repeat the tests for additional unit configurations of interest.
- (5) Monitor the elastic response of tire configurations to water particle motion and use least-squares or Fourier decomposition techniques to evaluate drag and inertia coefficients. With the results of this study, a precise force-time history could be predicted utilizing the Morison equation.
- (6) Verify the frequency response of the Novar Model 403 Streamflo propeller current meter.

REFERENCES

1. Achenbach, E., "Distribution of Local Pressure and Skin Friction around a Circular Cylinder in Cross-Flow up to $Re = 5 \times 10^5$," Journal of Fluid Mechanics, Vol. 34, 1968, pp. 625-639.
2. Airy, G. B., "Tides and Waves," Encyc. Metrop., Article No. 192, 1845, pp. 241-396.
3. Aska, D. Y., Editor, Artificial Reefs in Florida, Florida Sea Grant College, Report N. 24, May 1978.
4. Carlisle, J. G. Jr. and Turner, C. H. and Ebert, E. E., Artificial Habitat in the Marine Environment, The Resources Agency of California, Fish Bulletin 124, 1964.
5. Dean, R. G., "Stream Function Representation of Nonlinear Ocean Waves," Journal of Geophysical Research, Vol. 70, No. 8, 1965, pp. 4561-72.
6. Dean R. G., "Evaluation and Development of Water Wave Theories for Engineering Application," Special Report No. 1: U.S. Army Corps of Engineers, Coastal Engineering Research Center, Fort Belvoir, Va., Vols. I & II, November 1974.
7. Edmund, N. W., "Old Tires: the ideal material for building Fish Havens," Edmund Scientific Co., Barrington, N. J., 1967.
8. Garrison, C. J., Field, J. B. and May, M. D., "Drag and Inertia Forces on a Cylinder in Periodic Flow," J. Waterway Port Coastal and Ocean Div., ASCE, May 1977.
9. Goda, Y., "Wave Forces on Vertical Circular Cylinder: Experiments and a Proposed Method of Wave Force Computation," Report of the Port and Harbor Technical Research Institute, Japan, 1964, No. 8.
10. Grace, R. A., "Wave Forces on Submerged Objects," Miscellaneous Report No. 10, Univ. of Hawaii Look Lab-M-10, July 1974.
11. Grace, R. A., "Near-Bottom Water Motion under Ocean Waves," Proceedings, Fifteenth Conference on Coastal Engineering, Honolulu, Hawaii, July 1979, pp. 2371-2386.
12. Grace, R. A., "A Slanted Look at Ocean Wave Forces on Pipes," A report prepared for the American Gas Association, Alexandria, Va., at the Univ. of Hawaii, Honolulu., August 1979.

13. Jensen, R. E., "Finite Amplitude Deep Water Waves: A Comparison of Theoretical and Experimental Kinematics and Dynamics," A Thesis for Master of Ocean Engineering Degree at Oregon State University, Corvallis, Oregon, 1978, pp. 91-94.
14. Jones, W. T., "Forces on Submarine Pipelines from Steady Currents," ASME, Paper 71-UnT-3 presented at the Petroleum Mechanical Engineering with Underwater Technology Conference, September 1971, Houston, Texas.
15. Jones, W. T., "On-Bottom Pipeling Stability in Steady Water Current," Journal of Petroleum Technology, March 1978, pp. 475-484.
16. Keulegan, G. H., and Carpenter, L. H., "Forces on Cylinders and Plates in an Oscillation Fluid," Journal of Research of the National Bureau of Standards, Vol. 60, No. 5, May 1958.
17. Kobune, K., "Random Wave Velocity Field from Periodic Theory," A Thesis for Civil Engineer Degree at Oregon State University, Corvallis, Oregon., 1978, pp. 7, 13, 20-22.
18. Le Mehaute, B., Divoky, D. and Lin, A., "Shallow Water Waves: A Comparison of Theories and Experiments," Proceedings: Eleventh International Conference on Coastal Engineering, Vol. 1, 1968, pp. 86-107.
19. Milgram, J. H., "Waves and Wave Forces," Report of MIT Sea Grant Program, No. 76-19, November 1976.
20. Morison, J. R., O'Brien, M. P., Johnson, J. W. and Schaaf, S. A., "The Force Exerted by Surface Waves on Piles," Petroleum Transactions, AIME, Vol. 189, 1950.
21. Nath, J. H., Yamamoto, T. and Wright, J. C., "Wave Forces on Pipes Near the Ocean Bottom," Proceedings, Eighth Annual Offshore Technology Conference, Dallas, Texas, May 1976, Paper No. OTC 2496.
22. Parker, R. O. Jr. and Buchanan, C. C. and Stemile, F. W. Jr., "How to Build Marine Artificial Reefs," Fishery Facts 10, U.S. Department of Commerce, National Oceanic and Atmospheric Administration/National Fisheries Service, Seattle, Wash., December 1974.
23. Sarpkaya, T., "Forces on Cylinders and Spheres in a Sinusoidally Oscillating Fluid," Journal of Applied Mechanics, ASME, Vol. 42, No. 1, March 1975, pp. 32-37.

24. Sarpkaya, T., "Vortex Shedding and Resistance in Harmonic Flow about Smooth and Rough Cylinders at High Reynolds Numbers," Rept. No. NPS-59 SL76021, U. S. Naval Post Graduate School, Monterey, Calif., 1976.
25. Shore Protection Manual, U.S.Army Coastal Engineering Research Center, Vol. III, 1977.
26. Valent, P. J., "Coefficients of Friction between Calcareous Sands and Some Building Materials, and Their Significance," TN no. N-1542, Civil Engineering Laboratory, Port Hueneme, Cal., January 1979.
27. Yamamoto, T., Nath, J. H. and Slotta, L. S., "Wave Forces on Cylinders Near Plane Boundary," J. Waterway Port Coastal and Ocean Div., ASCE, November 1974, pp. 345-359.
28. Yamamoto, T. and Nath, J. H., "High Reynolds Number Oscillating Flow by Cylinders," Proceedings, Fifteenth Coastal Engineering Conference, Honolulu, Hawaii, July 1976, Vol. 3, pp. 2321-2340.

APPENDIX A

Tables of Measured Data and
Resulted Force Coefficients

Governing Parameters

$$\text{Reynolds Number: } R_e = \frac{U_{bmax} \cdot D'}{\nu} \quad (\text{Eq. 2-2})$$

$$\text{Keulegan-Carpenter Number: } K-C = \frac{U_{bmax} \cdot T}{D'} \quad (\text{Eq. 2-19})$$

Force Coefficients

$$\text{Maximum Force Coefficients: } C_f = \frac{F_{max}}{\rho A U_{bmax}^2 / 2} \quad (\text{Eq. 4-11})$$

$$\text{Drag Coefficients: } C_D = \frac{F_{m1}}{\rho A U_{bmax}^2 / 2} \quad (\text{Eq. 4-12a})$$

$$\text{Inertia Coefficients: } C_I = \frac{F_{m2}}{\rho V U_{bmax}} \quad (\text{Eq. 4-12b})$$

where $\rho = 1.936 \text{ slugs/ft}^3$ (at 70°F)

$\nu = 1.059 \times 10^{-5} \text{ ft}^2/\text{sec}$ (at 70°F)

CASE A-1 $D'=1.0 \text{ ft}$ $\rho A/2 = .2643$ $\frac{\text{Waves}}{\text{min}}$ $(D=1.0 \text{ ft})$

| T(sec) | H(ft) | U_{bmax} (ft/s) | F_{max} (lbs) | C_f | $R_e (\times 10^5)$ | K-C |
|--------|-------|-------------------|-----------------|-------|---------------------|-------|
| 1.98 | 1.88 | .34 | .18 | 5.96 | .32 | .67 |
| | 2.69 | .47 | .52 | 8.89 | .44 | .93 |
| 2.36 | 1.81 | .49 | .47 | 7.51 | .46 | 1.15 |
| | 2.80 | .84 | .58 | 3.11 | .79 | 1.97 |
| | 3.60 | 1.14 | .90 | 2.63 | 1.08 | 2.39 |
| 3.13 | 1.80 | .75 | .84 | 5.67 | .71 | 2.34 |
| | 3.59 | 1.80 | 1.65 | 1.92 | 1.70 | 5.64 |
| | 5.07 | 2.61 | 2.56 | 1.42 | 2.47 | 8.18 |
| 3.61 | 2.18 | 1.23 | .65 | 1.50 | 1.21 | 4.62 |
| | 3.27 | 1.96 | 1.86 | 1.83 | 1.85 | 7.07 |
| | 4.76 | 2.92 | 3.22 | 1.43 | 2.76 | 10.54 |
| 4.42 | 2.05 | 1.21 | 1.02 | 2.62 | 1.14 | 5.36 |
| | 4.28 | 2.68 | 2.13 | 1.12 | 2.53 | 11.85 |
| 6.25 | 2.16 | 1.50 | 1.22 | 2.03 | 1.42 | 9.40 |
| | 2.92 | 2.16 | 1.92 | 1.56 | 2.04 | 13.48 |
| 9.88 | 2.00 | 1.57 | .97 | 1.34 | 1.48 | 15.48 |

Run No. 532-547

CASE A-2 $D' = .292\text{ft}$ $\rho A/2 = .5856$ $V = .176\text{ft}^2$ $\phi = 90^\circ$ ($D = 1.0\text{ft}$)

| T (sec) | H (ft) | U_{bmax} (ft/s) | \dot{U}_{bmax} (ft/s ²) | F_{max} (lbs) | F_{m1} (lbs) | F_{m2} (lbs) | C_f | C_D | C_I | ϕ (°) | R_0 ($\times 10^5$) | K-C |
|------------|-----------|----------------------|--|--------------------|-------------------|-------------------|-------|-------|-------|---------------|----------------------------|-------|
| 1.98 | 1.73 | .30 | .75 | .36 | .13 | .33 | 6.85 | 2.47 | 1.30 | 89 | .08 | 2.04 |
| | 2.49 | .57 | 1.02 | .86 | .28 | .55 | 4.52 | 1.47 | 1.60 | 82 | .16 | 3.87 |
| 2.36 | 1.57 | .48 | 1.22 | .70 | .15 | .67 | 5.20 | 1.11 | 1.60 | 95 | .13 | 3.89 |
| | 2.67 | .86 | 1.99 | 1.20 | .30 | 1.15 | 2.77 | .59 | 1.70 | 95 | .24 | 6.96 |
| | 3.27 | 1.22 | 2.50 | 1.70 | .31 | 1.64 | 1.95 | .36 | 1.85 | 77 | .34 | 9.87 |
| 3.13 | 1.55 | .86 | 1.50 | 1.03 | .14 | .98 | 2.39 | .32 | 1.80 | 80 | .24 | 9.23 |
| | 3.40 | 1.67 | 3.25 | 2.72 | .26 | 2.56 | 1.66 | .16 | 2.40 | 67 | .46 | 17.92 |
| | 4.87 | 2.47 | 4.25 | 4.10 | .64 | 3.91 | 1.15 | .18 | 2.70 | 62 | .68 | 26.51 |
| 3.61 | 2.03 | 1.22 | 2.19 | 1.53 | .17 | 1.49 | 1.77 | .20 | 2.00 | 74 | .34 | 15.10 |
| | 3.07 | 1.37 | 2.90 | 2.79 | .33 | 2.28 | 1.36 | .16 | 2.30 | 68 | .52 | 23.15 |
| | 4.47 | 2.67 | 4.25 | 7.43 | .37 | 2.89 | 1.78 | .16 | 2.00 | 66 | .74 | 33.05 |
| 4.42 | 1.91 | 1.24 | 1.80 | 1.62 | .15 | 1.54 | 1.47 | .18 | 2.37 | 68 | .34 | 17.75 |
| | 4.07 | 2.48 | 3.13 | 4.37 | 1.18 | 3.20 | 1.21 | .32 | 3.00 | 63 | .68 | 37.58 |
| 6.25 | 2.10 | 1.64 | 1.80 | 1.79 | .43 | 1.54 | 1.14 | .27 | 2.50 | 36 | .45 | 35.14 |
| | 2.80 | 2.15 | 2.70 | 3.47 | 1.66 | 2.76 | 1.28 | .61 | 3.00 | 41 | .59 | 46.07 |
| 9.88 | 2.00 | 1.64 | 1.50 | 1.30 | .56 | 1.21 | .82 | .35 | 2.37 | 10 | .45 | 55.53 |

Run No. 56-66, 79-84

CASE A-3 $D' = 1.0\text{ft}$ $\rho A/2 = .2643$ $V = .229\text{ft}^2$ $\phi = 90^\circ$ ($D = 1.0\text{ft}$)

| T (sec) | H (ft) | U_{bmax} (ft/s) | \dot{U}_{bmax} (ft/s ²) | F_{max} (lbs) | F_{m1} (lbs) | F_{m2} (lbs) | C_f | C_D | C_I | ϕ (°) | R_0 ($\times 10^5$) | K-C |
|------------|-----------|----------------------|--|--------------------|-------------------|-------------------|-------|-------|-------|---------------|----------------------------|-------|
| 1.98 | 1.77 | .32 | .90 | .35 | .15 | .23 | 12.90 | 5.60 | .58 | 96 | .30 | .63 |
| | 2.60 | .50 | 1.20 | .67 | .20 | .34 | 10.19 | 3.03 | .64 | 89 | .47 | .99 |
| 2.36 | 1.70 | .41 | 1.03 | .41 | .18 | .31 | 9.14 | 4.00 | .68 | 91 | .39 | .97 |
| | 2.63 | .90 | 1.90 | .76 | .32 | .73 | 3.53 | 1.49 | .87 | 91 | .95 | 2.12 |
| | 3.33 | 1.16 | 2.30 | .80 | .36 | .77 | 2.24 | 1.01 | .76 | 98 | 1.10 | 2.74 |
| 3.13 | 1.70 | .84 | 1.50 | .64 | .19 | .56 | 3.42 | 1.02 | .80 | 102 | .79 | 2.63 |
| | 3.27 | 1.71 | 3.29 | 1.30 | .22 | 1.25 | 1.68 | .28 | .86 | 94 | 1.62 | 5.35 |
| | 4.93 | 2.67 | 5.00 | 2.08 | .40 | 2.00 | 1.10 | .21 | .90 | 82 | 2.52 | 8.36 |
| 3.61 | 2.07 | 1.21 | 1.95 | .72 | .16 | .69 | 1.86 | .40 | .80 | 102 | 1.14 | 4.37 |
| | 3.03 | 1.78 | 2.90 | 1.25 | .20 | 1.20 | 1.50 | .24 | .94 | 86 | 1.68 | 6.43 |
| | 4.57 | 2.77 | 4.10 | 3.17 | .36 | 2.13 | 1.56 | .18 | 1.20 | 74 | 2.62 | 10.00 |
| 4.42 | 1.93 | 1.40 | 1.90 | .90 | .15 | .84 | 1.74 | .30 | 1.00 | 63 | 1.32 | 6.19 |
| | 4.13 | 2.57 | 3.80 | 1.75 | .33 | 1.69 | 1.01 | .19 | 1.00 | 65 | 2.43 | 11.36 |
| 6.25 | 1.80 | 1.58 | 1.60 | .89 | .15 | .80 | 1.34 | .22 | 1.13 | 50 | 1.49 | 9.58 |
| | 2.90 | 2.20 | 2.20 | 1.57 | .29 | 1.22 | 1.23 | .23 | 1.25 | 41 | 2.08 | 13.75 |
| 9.88 | 1.91 | 1.64 | 1.05 | .68 | .19 | .56 | .96 | .27 | 1.20 | 32 | 1.55 | 16.20 |

Run No. 67-78, 85-90

CASE B-1 $D' = 1.47$ ft $\rho A/2 = .5605$ $V = 3.500$ ft/sec (D = 1.5 ft)

| T (sec) | H (ft) | U_{bmax} (ft/s) | F_{max} (lbs) | C_f | R_e ($\times 10^5$) | K-C |
|---------|--------|-------------------|-----------------|-------|-------------------------|-------|
| 1.98 | 1.80 | .40 | .87 | 9.71 | .56 | .54 |
| | 2.53 | .47 | 1.49 | 12.06 | .66 | .63 |
| 2.36 | 1.71 | .45 | 1.55 | 13.63 | .63 | .72 |
| | 2.80 | .80 | 2.77 | 7.73 | 1.12 | 1.28 |
| | 3.65 | 1.22 | 3.55 | 4.26 | 1.70 | 1.95 |
| 3.13 | 1.73 | .75 | 2.29 | 7.27 | 1.05 | 1.59 |
| | 3.40 | 1.95 | 5.72 | 2.68 | 2.72 | 4.13 |
| | 5.03 | 2.54 | 7.24 | 2.00 | 3.55 | 5.38 |
| 3.61 | 2.26 | 1.23 | 3.07 | 3.62 | 1.72 | 3.00 |
| | 3.20 | 2.09 | 4.64 | 1.89 | 2.92 | 5.10 |
| | 4.82 | 2.88 | 8.51 | 1.93 | 4.02 | 7.03 |
| 4.42 | 2.00 | 1.28 | 2.88 | 3.13 | 1.79 | 3.83 |
| | 4.40 | 2.86 | 6.39 | 1.39 | 3.99 | 8.55 |
| 6.25 | 2.17 | 1.63 | 2.68 | 1.80 | 2.28 | 6.89 |
| | 3.03 | 2.10 | 4.56 | 1.84 | 2.93 | 8.87 |
| 9.88 | 1.42 | 1.58 | 1.88 | 1.34 | 2.21 | 10.56 |

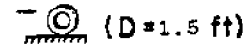
Run No. 372-387

CASE B-2 $D' = 1.17$ ft $\rho A/2 = 1.3465$ $V = 3.500$ ft/sec (D = 1.5 ft)

| T (sec) | H (ft) | U_{bmax} (ft/s) | \dot{U}_{bmax} (ft/s ²) | F_{max} (lbs) | F_{m1} (lbs) | F_{m2} (lbs) | C_f | C_D | C_I | ϕ (°) | R_e ($\times 10^5$) | K-C |
|---------|--------|-------------------|---------------------------------------|-----------------|----------------|----------------|-------|-------|-------|------------|-------------------------|-------|
| 1.98 | 1.70 | .28 | .85 | .94 | .40 | .79 | 8.92 | 3.79 | .83 | 96 | .11 | .33 |
| | 2.72 | .55 | 1.20 | 2.01 | .46 | 1.66 | 4.94 | 1.13 | 1.23 | 39 | .22 | 2.61 |
| 2.36 | 1.70 | .52 | 1.10 | 1.98 | .47 | 1.48 | 5.44 | 1.29 | 1.20 | 91 | .21 | 2.95 |
| | 2.64 | .95 | 2.00 | 3.38 | .94 | 3.17 | 2.78 | .77 | 1.41 | 89 | .37 | 5.38 |
| | 3.37 | 1.22 | 2.40 | 3.92 | 1.20 | 3.85 | 1.96 | .60 | 1.42 | 77 | .48 | 6.91 |
| 3.13 | 2.13 | 1.03 | 1.85 | 4.01 | .50 | 3.43 | 2.81 | .40 | 1.65 | 80 | .41 | 7.74 |
| | 3.40 | 1.76 | 3.30 | 7.23 | 1.23 | 6.67 | 1.73 | .29 | 1.80 | 62 | .69 | 13.22 |
| | 4.50 | 2.78 | 4.57 | 13.06 | 2.33 | 10.76 | 1.25 | .27 | 2.10 | 67 | 1.09 | 20.88 |
| 3.61 | 2.07 | 1.26 | 2.10 | 4.48 | .63 | 4.24 | 2.10 | .32 | 1.80 | 85 | .50 | 10.91 |
| | 3.10 | 2.00 | 2.90 | 8.55 | 1.54 | 6.84 | 1.59 | .28 | 2.10 | 74 | .79 | 17.33 |
| | 4.50 | 2.53 | 4.60 | 17.99 | 2.71 | 11.35 | 2.09 | .31 | 2.20 | 66 | 1.00 | 21.92 |
| 4.42 | 1.85 | 1.29 | 1.80 | 3.84 | .78 | 3.75 | 1.71 | .35 | 1.85 | 64 | .51 | 13.58 |
| | 4.13 | 2.68 | 4.20 | 13.07 | 4.07 | 10.92 | 1.35 | .42 | 2.32 | 46 | 1.06 | 28.43 |
| 6.25 | 2.07 | 1.36 | 1.85 | 4.87 | 1.24 | 3.90 | 1.95 | .50 | 1.88 | 32 | .54 | 20.40 |
| | 2.30 | 2.00 | 2.55 | 8.71 | 2.79 | 6.62 | 1.62 | .52 | 2.31 | 32 | .79 | 30.00 |
| 9.88 | 1.63 | 1.33 | 1.15 | 4.11 | 2.75 | 2.96 | 1.15 | .77 | 2.29 | 20 | .64 | 38.65 |

Run No. 34-44, 97-102

CASE B-3

 $D' = 1.29 \text{ ft}$ $\rho A/2 = .5605$  (D = 1.5 ft)

| T (sec) | H (ft) | U_{bmax} (ft/s) | F_{max} (lbs) | C_f | $R_e (x 10^5)$ | K-C |
|---------|--------|-------------------|-----------------|-------|----------------|-------|
| 1.98 | 1.69 | .29 | .72 | 15.23 | .41 | .39 |
| | 2.63 | .55 | 1.85 | 10.89 | .77 | .74 |
| 2.36 | 1.64 | .43 | 1.25 | 12.07 | .60 | .69 |
| | 2.62 | .88 | 2.08 | 4.79 | 1.23 | 1.40 |
| | 3.33 | 1.16 | 2.77 | 3.68 | 1.62 | 1.85 |
| 3.13 | 1.65 | .75 | 1.53 | 4.87 | 1.05 | 1.59 |
| | 3.33 | 1.74 | 3.60 | 2.12 | 2.43 | 3.68 |
| | 4.93 | 2.52 | 5.11 | 1.44 | 3.52 | 5.33 |
| 3.61 | 2.03 | 1.26 | 1.74 | 1.96 | 1.76 | 3.08 |
| | 3.07 | 1.38 | 2.37 | 1.45 | 2.63 | 4.59 |
| | 4.53 | 2.79 | 6.42 | 1.47 | 3.90 | 6.81 |
| 4.42 | 1.93 | 1.37 | 2.08 | 1.98 | 1.91 | 4.09 |
| | 4.20 | 2.58 | 4.59 | 1.23 | 3.60 | 7.71 |
| 6.25 | 2.10 | 1.48 | 2.09 | 1.71 | 2.07 | 6.25 |
| | 2.87 | 2.13 | 3.37 | 1.33 | 2.98 | 9.00 |
| 9.88 | 1.97 | 1.55 | 1.19 | .88 | 2.17 | 10.35 |

Run No. 45-55, 103-108

CASE C-1

 $D' = 1.29 \text{ ft}$ $\rho A/2 = .906$  (D = 1.9 ft)

| T (sec) | H (ft) | U_{bmax} (ft/s) | F_{max} (lbs) | C_f | $R_e (x 10^5)$ | K-C |
|---------|--------|-------------------|-----------------|-------|----------------|------|
| 1.98 | 1.81 | .32 | 1.67 | 17.51 | .58 | .34 |
| | 2.63 | .52 | 3.09 | 12.78 | .93 | .54 |
| 2.36 | 1.80 | .58 | 2.82 | 9.27 | 1.04 | .72 |
| | 2.79 | .80 | 5.31 | 9.07 | 1.44 | 1.00 |
| | 3.56 | 1.15 | 6.73 | 5.62 | 2.06 | 1.43 |
| 3.13 | 1.80 | .72 | 4.53 | 9.75 | 1.28 | 1.18 |
| | 3.47 | 1.83 | 9.34 | 3.09 | 3.27 | 3.02 |
| | 5.23 | 2.70 | 15.22 | 2.30 | 4.84 | 4.46 |
| 3.61 | 2.17 | 1.40 | 6.18 | 3.50 | 2.50 | 2.65 |
| | 3.15 | 2.26 | 9.27 | 2.00 | 4.05 | 4.31 |
| | 4.31 | 3.02 | 17.84 | 2.16 | 5.41 | 5.75 |
| 4.42 | 2.00 | 1.47 | 5.08 | 2.60 | 2.63 | 3.42 |
| | 4.32 | 2.77 | 11.75 | 1.69 | 4.96 | 6.46 |
| 6.25 | 2.18 | 1.83 | 5.67 | 1.97 | 3.27 | 6.03 |
| | 2.90 | 2.04 | 3.08 | 2.14 | 3.66 | 6.74 |
| 9.88 | 2.04 | 1.58 | 3.76 | 1.66 | 2.83 | 8.25 |

Run No. 420-435

CASE C-2 $D' = 525 \text{ ft}$ $\rho A/2 = 1.8402$ $V = .998 \text{ ft}^{-1}$ $(D = 1.9 \text{ ft})$

| T (sec) | H (ft) | U_{bmax} (ft/s) | U_{bmax} (ft/s ²) | F_{max} (lbs) | F_{m1} (lbs) | F_{m2} (lbs) | C_f | C_D | C_I | ϕ (°) | R_e ($\times 10^5$) | K-C |
|---------|--------|-------------------|---------------------------------|-----------------|----------------|----------------|-------|-------|-------|------------|-------------------------|-------|
| 1.98 | 1.75 | .32 | .90 | .59 | .75 | 1.55 | 8.42 | 4.00 | .89 | 75 | .15 | 1.21 |
| | 2.50 | .47 | - | - | - | - | - | - | - | - | .23 | 1.77 |
| 2.36 | 1.70 | .43 | 1.10 | 2.96 | .46 | 2.45 | 8.71 | 1.35 | 1.15 | 78 | .21 | 1.93 |
| | 2.64 | .87 | 2.00 | 5.94 | .84 | 5.41 | 4.26 | .60 | 1.40 | 90 | .43 | 3.91 |
| | 3.53 | 1.15 | 2.40 | 7.75 | 1.13 | 6.94 | 3.19 | .46 | 1.50 | 90 | .57 | 5.17 |
| 3.13 | 1.53 | .79 | 1.65 | 4.47 | .58 | 4.45 | 3.89 | .51 | 1.40 | 60 | .39 | 4.71 |
| | 3.27 | 1.81 | 3.56 | 12.19 | 1.76 | 11.34 | 2.02 | .29 | 1.50 | 63 | .90 | 10.79 |
| | 4.73 | 2.70 | 4.30 | 21.41 | 6.68 | 14.87 | 1.60 | .50 | 1.79 | 64 | 1.34 | 16.10 |
| 3.61 | 2.03 | 1.23 | 2.00 | 6.54 | 1.05 | 5.95 | 2.35 | .38 | 1.54 | 65 | .61 | 8.46 |
| | 3.09 | 1.97 | 3.00 | 12.70 | 1.98 | 10.45 | 1.78 | .27 | 1.80 | 72 | .98 | 13.55 |
| | 4.57 | 2.79 | 4.40 | 25.31 | 6.00 | 16.34 | 1.77 | .42 | 1.92 | 69 | 1.38 | 19.18 |
| 4.42 | 1.93 | 1.27 | 1.90 | 5.74 | .75 | 2.17 | 1.93 | .26 | 1.43 | 50 | .63 | 10.69 |
| | 3.80 | 2.57 | 3.50 | 20.08 | 5.52 | 13.22 | 1.65 | .45 | 1.95 | 62 | 1.27 | 21.64 |
| 6.25 | 2.13 | 1.61 | 1.75 | 7.24 | 2.49 | 5.25 | 1.52 | .52 | 1.55 | 32 | .80 | 19.17 |
| | 2.80 | 2.22 | 2.40 | 12.72 | 5.24 | 9.33 | 1.40 | .58 | 2.01 | 32 | 1.10 | 26.43 |
| 9.88 | 2.07 | 1.51 | 1.20 | 5.84 | 3.11 | 4.65 | 1.39 | .74 | 2.00 | 25 | .75 | 28.42 |

Run No. 12-22, 109-114

CASE C-3 $D' = 398 \text{ ft}$ $\rho A/2 = .906$ $V = .925 \text{ ft}^{-1}$ $(D = 1.9 \text{ ft})$

| T (sec) | H (ft) | U_{bmax} (ft/s) | U_{bmax} (ft/s ²) | F_{max} (lbs) | F_{m1} (lbs) | F_{m2} (lbs) | C_f | C_D | C_I | ϕ (°) | R_e ($\times 10^5$) | K-C |
|---------|--------|-------------------|---------------------------------|-----------------|----------------|----------------|-------|-------|-------|------------|-------------------------|------|
| 1.98 | 1.77 | .32 | .80 | 1.68 | .56 | 1.07 | 18.06 | 4.00 | .56 | 96 | .57 | .33 |
| | 2.53 | .57 | 1.15 | 2.94 | 1.08 | 2.37 | 9.99 | 2.09 | .72 | 84 | 1.02 | .60 |
| 2.36 | 1.63 | .48 | 1.05 | 4.35 | .72 | 2.10 | 20.84 | 1.65 | .70 | 106 | .86 | .60 |
| | 2.64 | .90 | 1.85 | 5.82 | .95 | 3.93 | 7.93 | 1.17 | .74 | 101 | 1.61 | 1.12 |
| | 3.40 | 1.20 | 2.30 | 7.86 | .80 | 5.77 | 6.02 | .61 | .87 | 96 | 2.15 | 1.49 |
| 3.13 | 1.70 | .80 | 1.60 | 3.02 | .58 | 2.91 | 5.20 | 1.17 | .64 | 93 | 1.43 | 1.32 |
| | 3.46 | 1.72 | 3.20 | 7.78 | .93 | 7.70 | 2.90 | .35 | .84 | 82 | 3.08 | 2.84 |
| | 4.77 | 2.64 | 4.45 | 13.11 | 2.10 | 12.02 | 2.08 | .33 | .94 | 75 | 4.73 | 4.36 |
| 3.61 | 2.03 | 1.31 | 2.05 | 5.98 | .72 | 4.89 | 3.95 | .48 | .80 | 94 | 2.35 | 2.49 |
| | 3.11 | 1.94 | 3.00 | 8.41 | 1.00 | 7.71 | 2.47 | .30 | .90 | 98 | 3.47 | 3.69 |
| | 4.58 | 2.74 | 4.40 | 14.17 | 2.71 | 12.18 | 2.08 | .40 | .96 | 78 | 4.91 | 5.22 |
| 4.42 | 2.00 | 1.24 | 1.80 | 3.92 | .55 | 4.29 | 2.82 | .39 | .83 | 68 | 2.22 | 2.89 |
| | 4.27 | 2.67 | 3.30 | 10.09 | 1.69 | 8.32 | 1.56 | .70 | .76 | 50 | 4.78 | 6.22 |
| 6.25 | 2.11 | 1.49 | 1.60 | 3.92 | .81 | 3.82 | 1.95 | .40 | .83 | 45 | 2.67 | 4.91 |
| | 2.87 | 2.15 | 2.20 | 6.35 | 1.76 | 5.90 | 1.52 | .42 | .93 | 34 | 3.85 | 7.09 |
| 9.88 | 1.95 | 1.50 | 1.20 | 2.75 | 1.27 | 2.44 | 1.35 | .62 | .71 | 33 | 2.69 | 7.82 |

Run No. 23-33, 115-119

CASE D-1 $D' = 1.0$ ft $\rho A/2 = .5285$ $V = .458$ ft/s $(D = 1.0$ ft)

| T (sec) | H (ft) | U_{bmax} (ft/s) | U_{bmax}^2 (ft/s ²) | F_{max} (lbs) | F_{m1} (lbs) | F_{m2} (lbs) | C_f | C_D | C_I | ϕ (°) | R_e (x10 ⁵) | K-C |
|------------|-----------|----------------------|--------------------------------------|--------------------|-------------------|-------------------|-------|-------|-------|---------------|------------------------------|-------|
| 1.98 | 1.81 | .44 | .90 | 1.43 | .30 | .65 | 14.00 | 2.93 | .81 | 89 | .42 | .87 |
| | 2.77 | .48 | 1.20 | 1.63 | .34 | .96 | 13.35 | 2.79 | .90 | 89 | .45 | .95 |
| 2.36 | 1.85 | .50 | 1.25 | 1.53 | .32 | 1.00 | 11.56 | 2.42 | .90 | 83 | .47 | 1.18 |
| | 2.80 | .85 | 1.90 | 2.26 | .63 | 2.03 | 8.92 | 1.65 | .99 | 101 | .80 | 2.01 |
| | 3.52 | 1.27 | 2.45 | 2.58 | .77 | 2.50 | 3.03 | .90 | 1.15 | 101 | 1.20 | 3.00 |
| 3.13 | 1.80 | .62 | 1.70 | 1.90 | .32 | 1.39 | 9.33 | 1.48 | .83 | 93 | .59 | 1.94 |
| | 3.47 | 1.62 | 3.40 | 3.94 | .88 | 3.70 | 2.85 | .63 | 1.23 | 35 | 1.53 | 5.07 |
| | 5.07 | 2.58 | 4.80 | 8.00 | 1.45 | 5.75 | 2.27 | .41 | 1.35 | 62 | 2.44 | 8.08 |
| 3.61 | 2.20 | 1.42 | 2.16 | 2.77 | .55 | 2.31 | 2.60 | .52 | 1.20 | 78 | 1.34 | 5.13 |
| | 3.27 | 2.15 | 3.16 | 4.45 | .86 | 3.64 | 1.82 | .35 | 1.30 | 74 | 2.03 | 7.76 |
| | 4.91 | 3.31 | 4.80 | 6.98 | 2.32 | 5.75 | 1.21 | .40 | 1.39 | 72 | 3.13 | 11.95 |
| 4.42 | 2.00 | 1.50 | 2.00 | 2.25 | .38 | 2.13 | 1.39 | .32 | 1.20 | 62 | 1.42 | 6.63 |
| | 4.39 | 2.88 | 3.80 | 4.92 | 1.84 | 4.76 | 1.12 | .42 | 1.42 | 56 | 2.72 | 12.73 |
| 6.25 | 2.16 | 1.74 | 1.76 | 2.30 | .56 | 2.09 | 1.44 | .35 | 1.34 | 34 | 1.64 | 10.88 |
| | 2.93 | 2.20 | 2.40 | 3.37 | .77 | 3.22 | 1.32 | .30 | 1.51 | 32 | 2.08 | 13.75 |
| 9.88 | 2.09 | 1.63 | 1.14 | 1.93 | .71 | 1.51 | 1.34 | .50 | 1.49 | 28 | 1.56 | 16.30 |

Run No. 328-343

CASE D-2 $D' = .563$ ft $\rho A/2 = .5856$ $V = .353$ ft/s $(D = 1.0$ ft)

| T (sec) | H (ft) | U_{bmax} (ft/s) | U_{bmax}^2 (ft/s ²) | F_{max} (lbs) | F_{m1} (lbs) | F_{m2} (lbs) | C_f | C_D | C_I | ϕ (°) | R_e (x10 ⁵) | K-C |
|------------|-----------|----------------------|--------------------------------------|--------------------|-------------------|-------------------|-------|-------|-------|---------------|------------------------------|-------|
| 1.98 | 1.85 | .29 | .90 | .52 | .15 | .49 | 1.07 | 3.03 | .80 | -- | .15 | .98 |
| | 2.53 | .50 | 1.29 | 1.27 | .29 | .83 | 3.69 | 2.00 | 1.00 | 89 | .28 | 1.70 |
| 2.36 | 1.78 | .47 | 1.15 | .85 | .17 | .73 | 6.55 | 1.30 | .99 | 89 | .26 | 1.90 |
| | 2.73 | .95 | 1.95 | 1.90 | .30 | 1.31 | 3.59 | .57 | 1.35 | 89 | .52 | 3.34 |
| | 3.47 | 1.22 | 2.44 | 2.35 | .35 | 2.25 | 2.69 | .42 | 1.35 | 71 | .67 | 4.94 |
| 3.13 | 2.50 | 1.33 | 2.44 | 2.69 | .30 | 2.67 | 2.60 | .28 | 1.60 | 62 | .73 | 7.14 |
| | 3.39 | 1.97 | 3.90 | 4.82 | .48 | 4.53 | 2.12 | .21 | 1.70 | 75 | 1.09 | 10.57 |
| | 4.97 | 2.72 | 4.72 | 5.99 | .70 | 5.82 | 1.38 | .16 | 1.80 | 62 | 1.50 | 14.60 |
| 3.61 | 2.11 | 1.27 | 1.95 | 2.15 | .28 | 2.00 | 2.28 | .30 | 1.50 | 74 | .70 | 7.86 |
| | 3.10 | 2.10 | 2.95 | 3.56 | .44 | 3.49 | 1.38 | .17 | 1.73 | 71 | 1.16 | 13.00 |
| | 4.37 | 3.03 | 4.70 | 6.87 | .96 | 5.71 | 1.28 | .18 | 1.78 | 68 | 1.67 | 18.75 |
| 4.42 | 1.96 | 1.40 | 1.83 | 1.95 | .20 | 1.86 | 1.70 | .18 | 1.50 | 69 | .77 | 10.81 |
| | 4.33 | 2.77 | 4.00 | 4.95 | .80 | 4.30 | 1.11 | .18 | 1.75 | 56 | 1.53 | 20.99 |
| 6.25 | 2.17 | 1.62 | 1.70 | 1.99 | .58 | 1.73 | 1.30 | .37 | 1.49 | 34 | .89 | 17.36 |
| | 2.87 | 2.07 | 2.50 | 3.46 | .83 | 3.41 | 1.38 | .33 | 2.00 | 32 | 1.14 | 22.18 |
| 9.88 | 2.00 | 1.55 | 1.20 | 1.60 | .50 | 1.31 | 1.13 | .35 | 1.60 | 33 | .85 | 26.25 |

Run No. 137-152

CASE D-3 $D' = 1.0 \text{ ft}$ $\rho A / 2 = 5285$ $V = .358 \text{ ft}^3 - \text{min}$ ($D = 1.0 \text{ ft}$)


| T (sec) | H (ft) | U_{bmax} (ft/s) | \dot{U}_{bmax} (ft/s ²) | F_{max} (lbs) | F_{m1} (lbs) | F_{m2} (lbs) | C_f | C_D | C_I | ϕ (°) | R_e ($\times 10^5$) | K-C |
|---------|--------|-------------------|---------------------------------------|-----------------|----------------|----------------|-------|-------|-------|------------|-------------------------|-------|
| 1.98 | 1.73 | .33 | .80 | .79 | .25 | .37 | 13.69 | 4.34 | .52 | 89 | .31 | .65 |
| | 2.63 | .55 | 1.20 | 1.54 | .48 | .54 | 9.53 | 3.00 | .60 | 89 | .52 | 1.09 |
| 2.36 | 1.73 | .50 | 1.40 | 1.12 | .28 | .77 | 3.45 | 2.10 | .62 | 80 | .47 | 1.13 |
| | 2.67 | .89 | 2.00 | 1.76 | .40 | 1.16 | 4.19 | .93 | .55 | 88 | .84 | 2.10 |
| | 3.40 | 1.19 | 2.50 | 2.33 | .53 | 1.51 | 3.18 | .71 | .68 | 84 | 1.12 | 2.51 |
| 3.13 | 1.37 | .34 | 1.72 | 1.55 | .20 | 1.06 | 4.13 | .54 | .70 | 80 | .79 | 2.63 |
| | 3.47 | 1.84 | 3.40 | 3.54 | .43 | 2.41 | 1.98 | .24 | .80 | 75 | 1.74 | 5.75 |
| | 4.32 | 2.55 | 4.39 | 5.74 | .86 | 3.51 | 1.96 | .25 | .90 | 65 | 2.41 | 7.98 |
| 3.61 | 2.11 | 1.20 | 2.19 | 1.53 | .25 | 1.48 | 2.01 | .33 | .77 | 86 | 1.13 | 4.33 |
| | 3.00 | 2.03 | 3.22 | 3.34 | .30 | 2.57 | 1.53 | .27 | .90 | 70 | 1.92 | 7.33 |
| | 4.47 | 2.94 | 4.35 | 6.90 | .95 | 3.44 | 1.51 | .21 | .89 | 65 | 2.78 | 10.61 |
| 4.42 | 1.91 | 1.23 | 1.96 | 1.66 | .23 | 1.31 | 2.07 | .28 | .82 | 59 | 1.16 | 5.44 |
| | 4.16 | 2.67 | 3.92 | 5.17 | .80 | 2.95 | 1.37 | .21 | .85 | 62 | 2.52 | 11.80 |
| 6.25 | 2.15 | 1.39 | 1.80 | 1.61 | .40 | 1.60 | 1.58 | .39 | 1.00 | 32 | 1.42 | 9.33 |
| | 2.20 | 1.50 | 1.83 | 2.09 | .33 | 1.62 | 1.75 | .28 | 1.00 | 36 | 1.31 | 8.69 |
| 9.88 | 1.47 | .90 | .76 | .68 | .15 | .67 | 1.60 | .35 | .97 | 39 | .65 | 8.39 |

Run No. 121-136

CASE E-1 $D' = .479 \text{ ft}$ $\rho A / 2 = 1.1209$ $V = .358 \text{ ft}^3 - \text{min}$ ($D = 1.5 \text{ ft}$)


| T (sec) | H (ft) | U_{bmax} (ft/s) | F_{max} (lbs) | C_f | R_e ($\times 10^5$) | K-C |
|---------|--------|-------------------|-----------------|-------|-------------------------|------|
| 1.98 | 1.80 | .37 | 2.26 | 14.70 | .52 | .50 |
| | 2.61 | .58 | 4.25 | 11.27 | .81 | .78 |
| 2.36 | 1.73 | .52 | 3.55 | 11.72 | .73 | .33 |
| | 2.76 | .85 | 6.16 | 7.61 | 1.19 | 1.36 |
| | 3.67 | 1.08 | 8.68 | 6.69 | 1.50 | 1.72 |
| 3.13 | 1.71 | .77 | 5.52 | 8.23 | 1.08 | 1.64 |
| | 3.53 | 1.64 | 11.16 | 3.70 | 2.29 | 3.47 |
| | 5.10 | 2.24 | 17.34 | 3.09 | 3.12 | 4.73 |
| 3.61 | 2.13 | 1.17 | 7.83 | 5.15 | 1.63 | 2.34 |
| | 3.20 | 1.77 | 11.30 | 3.23 | 2.47 | 4.31 |
| | 4.78 | 2.65 | 20.98 | 2.67 | 3.70 | 6.47 |
| 4.42 | 2.00 | 1.24 | 5.73 | 3.31 | 1.74 | 3.71 |
| | 4.35 | 2.53 | 15.28 | 2.13 | 3.53 | 7.55 |
| 6.25 | 2.10 | 1.42 | 7.08 | 3.13 | 1.99 | 6.00 |
| | 2.93 | 1.83 | 10.32 | 2.74 | 2.56 | 7.75 |
| 9.88 | --- | --- | 4.48 | --- | --- | --- |

Run No. 388-403

CASE E-2 $D' = .933$ ft $\rho A/2 = 1.3465$  (D=1.5 ft)

| T (sec) | H (ft) | U_{bmax} (ft/s) | F_{max} (lbs) | C_f | $R_e (x 10^5)$ | K-C |
|---------|--------|-------------------|-----------------|-------|----------------|-------|
| 1.98 | 1.80 | .35 | 1.74 | 10.52 | .28 | .83 |
| | 2.67 | .37 | 3.14 | 7.17 | .45 | 1.35 |
| 2.36 | 1.73 | .48 | 2.91 | 9.39 | .38 | 1.36 |
| | 2.73 | .93 | 5.26 | 4.52 | .73 | 2.63 |
| | 3.40 | 1.30 | 7.15 | 3.14 | 1.02 | 3.68 |
| 3.13 | 1.73 | .85 | 3.98 | 4.10 | .57 | 3.19 |
| | 3.47 | 1.88 | 10.32 | 2.17 | 1.48 | 7.06 |
| | 4.93 | 2.67 | 16.67 | 1.74 | 2.10 | 10.03 |
| 3.61 | 2.15 | 1.33 | 5.48 | 2.30 | 1.05 | 5.76 |
| | 3.30 | 2.11 | 11.85 | 1.93 | 1.66 | 9.14 |
| | 4.82 | 2.85 | 21.03 | 1.91 | 2.25 | 12.39 |
| 4.42 | 2.05 | 1.50 | 5.13 | 1.69 | 1.18 | 7.96 |
| | 4.27 | 2.78 | 16.43 | 1.58 | 2.19 | 14.75 |
| 6.25 | 2.15 | 1.50 | 6.57 | 2.17 | 1.18 | 11.25 |
| | 2.87 | 2.07 | 11.19 | 1.94 | 1.63 | 15.53 |
| 9.88 | 2.00 | 1.62 | 4.95 | 1.40 | 1.27 | 19.22 |

Run No. 169-184

CASE E-3 $D' = .479$ ft $\rho A/2 = 1.1209$  (D=1.5 ft)

| T (sec) | H (ft) | U_{bmax} (ft/s) | F_{max} (lbs) | C_f | $R_e (x 10^5)$ | K-C |
|---------|--------|-------------------|-----------------|-------|----------------|-------|
| 1.98 | 1.87 | .31 | 2.09 | 19.37 | .43 | .42 |
| | 2.63 | .60 | 3.70 | 9.17 | .84 | .30 |
| 2.36 | 1.77 | .55 | 3.36 | 9.92 | .77 | .88 |
| | 2.80 | .90 | 5.53 | 6.09 | 1.26 | 1.44 |
| | 3.40 | 1.21 | 7.27 | 4.43 | 1.69 | 1.93 |
| 3.13 | 1.76 | .88 | 4.14 | 4.77 | 1.23 | 1.86 |
| | 3.52 | 1.88 | 10.65 | 2.89 | 2.33 | 3.98 |
| | 5.08 | 2.64 | 16.07 | 2.06 | 3.69 | 5.39 |
| 3.61 | 2.22 | 1.31 | 6.18 | 3.21 | 1.33 | 3.20 |
| | 3.25 | 2.05 | 10.10 | 2.14 | 2.86 | 5.00 |
| | 4.77 | 3.19 | 18.52 | 1.62 | 4.46 | 7.79 |
| 4.42 | 2.07 | 1.46 | 5.62 | 2.35 | 2.04 | 4.36 |
| | 4.29 | 2.73 | 15.78 | 1.89 | 3.61 | 8.16 |
| 6.25 | 2.19 | 1.68 | 5.15 | 1.63 | 2.35 | 7.10 |
| | 2.98 | 2.24 | 9.51 | 1.71 | 3.13 | 9.47 |
| 9.88 | 2.09 | 1.68 | 4.53 | 1.43 | 2.35 | 11.22 |

Run No. 153-168

CASE F-1 $D' \approx .59 \text{ ft}$ $\rho A/2 = 1.8121$ $\frac{1}{\text{min}}$ ($D = 1.9 \text{ ft}$)

| T (sec) | H (ft) | U_{bmax} (ft/s) | F_{max} (lbs) | C_f | $R_e (\times 10^5)$ | K-C |
|---------|--------|-------------------|-----------------|-------|---------------------|------|
| 1.98 | 1.87 | .31 | 4.70 | 27.34 | .55 | .32 |
| | 2.77 | .45 | 7.94 | 21.74 | .60 | .47 |
| 2.36 | 1.80 | .44 | 7.72 | 22.11 | .79 | .55 |
| | 2.69 | .87 | 13.57 | 9.97 | 1.55 | 1.08 |
| | 3.48 | 1.25 | 19.82 | 6.96 | 2.25 | 1.56 |
| 3.13 | 1.73 | .83 | 10.88 | 8.82 | 1.48 | 1.36 |
| | 3.49 | 1.95 | 26.83 | 3.90 | 3.49 | 3.22 |
| | 5.13 | 2.68 | 39.00 | 3.00 | 4.80 | 4.42 |
| 3.61 | 2.20 | 1.44 | 16.79 | 4.49 | 2.57 | 2.74 |
| | 3.19 | 1.83 | 26.34 | 4.35 | 3.27 | 3.43 |
| | 4.73 | 3.07 | 43.91 | 2.57 | 5.50 | 5.85 |
| 4.42 | 1.97 | 1.54 | 13.04 | 3.05 | 2.75 | 3.58 |
| | 4.40 | 2.92 | 31.00 | 1.34 | 5.23 | 6.81 |
| 6.25 | 2.18 | 1.28 | 14.13 | 4.80 | 2.28 | 4.20 |
| | 2.98 | 1.96 | 20.66 | 2.97 | 3.51 | 6.46 |
| 9.88 | 1.97 | 1.34 | 8.67 | 2.68 | 2.39 | 6.97 |

Run No. 436-451

CASE F-2 $D' \approx 1.05 \text{ ft}$ $\rho A/2 = 1.8402$ $\frac{1}{\text{min}}$ ($D = 1.9 \text{ ft}$)

| T (sec) | H (ft) | U_{bmax} (ft/s) | F_{max} (lbs) | C_f | $R_e (\times 10^5)$ | K-C |
|---------|--------|-------------------|-----------------|-------|---------------------|-------|
| 1.98 | 1.90 | .34 | 4.13 | 19.42 | .18 | .64 |
| | 2.63 | .60 | 7.10 | 10.72 | .60 | 1.13 |
| 2.36 | 1.87 | .50 | 5.09 | 11.06 | .50 | 1.12 |
| | 2.89 | 1.00 | 9.77 | 5.31 | .99 | 2.25 |
| | 3.67 | 1.24 | 17.01 | 3.01 | 1.23 | 2.79 |
| 3.13 | 1.79 | .83 | 8.67 | 6.84 | .32 | 2.47 |
| | 3.53 | 1.90 | 20.78 | 3.13 | 1.86 | 5.67 |
| | 4.93 | 2.96 | 32.97 | 2.05 | 2.94 | 8.82 |
| 3.61 | 2.20 | 1.25 | 11.72 | 4.08 | 1.24 | 4.30 |
| | 3.27 | 2.05 | 20.05 | 2.59 | 2.03 | 7.05 |
| | 4.70 | 2.90 | 37.27 | 2.41 | 2.88 | 9.97 |
| 4.42 | 2.11 | 1.43 | 10.45 | 2.82 | 1.41 | 5.98 |
| | 4.27 | 2.86 | 27.85 | 1.35 | 2.84 | 12.04 |
| 6.25 | 2.23 | 1.60 | 12.48 | 2.55 | 1.59 | 9.52 |
| | 3.00 | 2.16 | 18.08 | 2.11 | 2.14 | 12.86 |
| 9.88 | 1.98 | 1.68 | 8.76 | 1.69 | 1.57 | 13.31 |

Run No. 201-216

CASE F-3 $D' = 1.496$ ft $\rho A/2 = 1.8121$ $V = 2.964$ ft/s $\phi = 90^\circ$ (D = 1.9 ft)

| T (sec) | H (ft) | U_{bmax} (ft/s) | \dot{U}_{bmax} (ft/s ²) | F_{max} (lbs) | F_{m1} (lbs) | F_{m2} (lbs) | C_f | C_D | C_I | ϕ (°) | R_e ($\times 10^5$) | K-C |
|---------|--------|-------------------|---------------------------------------|-----------------|----------------|----------------|-------|-------|-------|------------|-------------------------|------|
| 1.98 | 1.90 | .32 | 1.00 | 11.92 | 1.29 | 3.33 | 64.25 | 6.95 | .73 | 96 | .57 | .33 |
| | 2.69 | .57 | 1.25 | 16.18 | 2.93 | 3.64 | 27.48 | 4.98 | .95 | 104 | 1.02 | .60 |
| 2.36 | 1.34 | .48 | 1.15 | 11.63 | 2.07 | 9.19 | 27.35 | 4.96 | .91 | 102 | .86 | .60 |
| | 2.92 | .98 | 2.00 | 20.16 | 2.30 | 16.45 | 11.59 | 1.33 | 1.18 | 109 | 1.76 | 1.22 |
| | 3.53 | 1.13 | 2.80 | 29.11 | 3.10 | 19.30 | 12.58 | 1.34 | 1.20 | 92 | 2.02 | 1.41 |
| 3.13 | 1.80 | .85 | 1.70 | 12.06 | .25 | 11.00 | 9.21 | .19 | .97 | 112 | 1.52 | 1.40 |
| | 3.51 | 1.85 | 3.50 | 33.75 | 5.97 | 29.51 | 5.44 | .95 | 1.47 | 98 | 3.31 | 3.05 |
| | 5.06 | 2.73 | 4.70 | 52.40 | 13.90 | 46.73 | 3.88 | 1.02 | 1.73 | 89 | 4.89 | 4.51 |
| 3.61 | 2.15 | 1.25 | 1.90 | 18.57 | 2.60 | 13.93 | 6.56 | .92 | 1.28 | 90 | 2.24 | 2.38 |
| | 3.25 | 1.98 | 3.00 | 35.34 | 5.60 | 30.34 | 4.97 | .79 | 1.78 | 86 | 3.55 | 3.77 |
| | 4.75 | 2.86 | 4.10 | 53.03 | 12.43 | 43.55 | 3.53 | .82 | 1.85 | 82 | 5.12 | 5.45 |
| 4.42 | 2.03 | 1.35 | 1.85 | 15.66 | 2.90 | 14.87 | 4.74 | .88 | 1.40 | 62 | 2.42 | 3.15 |
| | 4.29 | 2.32 | 3.90 | 41.95 | 14.90 | 35.30 | 2.91 | 1.04 | 1.59 | 54 | 5.05 | 6.57 |
| 6.25 | 2.20 | 1.75 | 1.70 | 13.83 | 4.55 | 11.50 | 2.49 | .82 | 1.18 | 39 | 3.13 | 5.77 |
| | 2.97 | 2.27 | 2.80 | 22.60 | 9.00 | 19.48 | 2.42 | 1.05 | 1.21 | 34 | 4.06 | 7.48 |
| 9.88 | 2.03 | 1.50 | 1.20 | 9.54 | 4.73 | 7.51 | 2.34 | 1.16 | 1.09 | 26 | 2.69 | 7.82 |

Run No. 185-200

CASE I-1 $D' = 1.283$ ft $\rho A/2 = 1.6069$ $\phi = 90^\circ$ (D = 1.3 ft)

| T (sec) | H (ft) | U_{bmax} (ft/s) | F_{max} (lbs) | C_f | R_e ($\times 10^5$) | K-C |
|---------|--------|-------------------|-----------------|-------|-------------------------|-------|
| 1.98 | 1.95 | .37 | 3.18 | 14.78 | .44 | .56 |
| | 2.54 | .63 | 5.16 | 8.16 | .76 | .97 |
| 2.36 | 1.93 | .62 | 5.87 | 9.62 | .75 | 1.13 |
| | 2.81 | .97 | 9.96 | 6.64 | 1.17 | 1.78 |
| | 3.53 | 1.25 | 13.21 | 5.23 | 1.52 | 2.31 |
| 3.13 | 1.80 | .84 | 8.25 | 7.26 | 1.02 | 2.05 |
| | 3.55 | 1.85 | 20.94 | 3.79 | 2.25 | 4.52 |
| | 4.55 | 2.21 | 32.92 | 4.21 | 2.67 | 5.38 |
| 3.61 | 2.17 | 1.24 | 11.21 | 4.53 | 1.50 | 3.49 |
| | 3.20 | 1.96 | 20.99 | 3.40 | 2.37 | 5.51 |
| | 4.45 | 2.21 | 32.92 | 4.21 | 3.02 | 7.02 |
| 4.42 | 2.13 | 1.31 | 10.65 | 3.89 | 1.58 | 4.50 |
| | 4.32 | 2.37 | 36.22 | 4.01 | 2.87 | 6.16 |
| 6.25 | 2.10 | 1.70 | 11.92 | 2.57 | 2.06 | 8.27 |
| | 2.93 | 2.21 | 22.49 | 2.87 | 2.67 | 10.75 |
| 9.88 | 2.01 | 1.55 | 8.22 | 2.12 | 1.88 | 11.97 |

Run No. 628-643

CASE I-2 $D'=1373\text{ft}$ $\rho A/2 = .9351$  (D=1.3ft)


| T (sec) | H (ft) | U_{bmax} (ft/s) | F_{max} (lbs) | C_f | $R_o (\times 10^5)$ | K-C |
|---------|--------|-------------------|-----------------|-------|---------------------|-------|
| 1.98 | 1.80 | .24 | 2.05 | 38.04 | .31 | .35 |
| | 2.48 | .54 | 3.72 | 13.48 | .70 | .78 |
| 2.36 | 1.84 | .41 | 3.93 | 25.39 | .53 | .70 |
| | 2.73 | .93 | 6.20 | 7.71 | 1.20 | 1.59 |
| | 3.58 | 1.22 | 6.95 | 4.99 | 1.58 | 2.10 |
| 3.13 | 1.70 | .77 | 5.28 | 9.58 | 1.00 | 1.75 |
| | 3.41 | 1.88 | 11.33 | 3.43 | 2.43 | 4.28 |
| | 4.61 | 2.48 | 17.75 | 3.08 | 3.22 | 5.66 |
| 3.61 | 2.19 | 1.20 | 7.59 | 5.62 | 1.56 | 3.16 |
| | 3.26 | 2.04 | 16.27 | 4.19 | 2.54 | 5.36 |
| | 4.21 | 2.67 | 19.38 | 2.98 | 3.46 | 7.02 |
| 4.42 | 2.10 | 1.31 | 5.07 | 3.31 | 1.69 | 4.20 |
| | 4.23 | 2.70 | 17.64 | 2.59 | 3.50 | 8.68 |
| 6.25 | 2.07 | 1.61 | 7.08 | 2.91 | 2.09 | 7.34 |
| | 2.90 | 1.97 | 11.72 | 3.22 | 2.56 | 8.98 |
| 9.88 | 2.00 | 1.50 | 5.65 | 2.68 | 1.95 | 10.81 |

Run No. 644-659

CASE I-3 $D'=1283\text{ft}$ $\rho A/2 = 1.6069$  (D=1.3 ft)


| T (sec) | H (ft) | U_{bmax} (ft/s) | F_{max} (lbs) | C_f | $R_o (\times 10^5)$ | K-C |
|---------|--------|-------------------|-----------------|-------|---------------------|-------|
| 1.98 | 1.85 | .31 | 3.83 | 24.33 | .38 | .48 |
| | 2.57 | .41 | 6.19 | 22.57 | .50 | .64 |
| 2.36 | 1.83 | .38 | 6.66 | 28.84 | .46 | .70 |
| | 2.83 | .78 | 10.79 | 10.92 | .95 | 1.44 |
| | 3.37 | 1.24 | 11.79 | 4.76 | 1.50 | 2.29 |
| 3.13 | 1.77 | .75 | 8.29 | 9.17 | .91 | 1.83 |
| | 3.48 | 1.88 | 17.52 | 3.08 | 2.28 | 4.59 |
| | 4.57 | 2.56 | 29.41 | 2.79 | 3.10 | 7.20 |
| 3.61 | 2.23 | 1.21 | 10.83 | 4.62 | 1.46 | 3.40 |
| | 3.22 | 1.89 | 17.71 | 3.07 | 2.29 | 5.33 |
| | 4.43 | 2.56 | 29.41 | 2.79 | 3.10 | 7.20 |
| 4.42 | 2.07 | 1.39 | 8.76 | 2.82 | 1.69 | 4.79 |
| | 4.30 | 2.48 | 27.88 | 2.82 | 3.01 | 8.55 |
| 6.25 | 2.21 | 1.60 | 10.11 | 2.46 | 1.94 | 7.79 |
| | 2.93 | 2.12 | 15.46 | 2.14 | 2.57 | 10.34 |
| 9.88 | 2.07 | 1.54 | 6.99 | 1.85 | 1.86 | 11.82 |

Run No. 660-675

CASE J-1 $D'=1.0$ ft $\rho A/2=1.0571$  (D = 1.0ft)


| T(sec) | H(ft) | U_{bmax} (ft/s) | F_{max} (lbs) | C_f | $R_e(x10^5)$ | K-C |
|--------|-------|-------------------|-----------------|-------|--------------|-------|
| 1.98 | 1.80 | .30 | 1.71 | 17.92 | .28 | .59 |
| | 2.57 | .55 | 3.33 | 10.41 | .52 | 1.09 |
| 2.36 | 1.76 | .47 | 2.67 | 11.44 | .44 | 1.11 |
| | 2.67 | .95 | 4.95 | 5.18 | .90 | 2.24 |
| | 3.40 | 1.38 | 5.68 | 2.82 | 1.30 | 3.26 |
| 3.13 | 1.70 | .80 | 3.60 | 5.33 | .76 | 2.50 |
| | 3.47 | 1.88 | 7.12 | 1.90 | 1.78 | 5.88 |
| | 4.96 | 2.68 | 12.18 | 1.60 | 2.53 | 8.39 |
| 3.61 | 2.03 | 1.28 | 5.07 | 2.93 | 1.21 | 4.52 |
| | 3.20 | 2.12 | 8.43 | 1.77 | 2.00 | 7.65 |
| | 4.83 | 2.98 | 16.54 | 1.76 | 2.81 | 10.76 |
| 4.42 | 1.93 | 1.33 | 5.77 | 3.09 | 1.26 | 5.88 |
| | 4.33 | 2.75 | 13.73 | 1.72 | 2.60 | 12.16 |
| 6.25 | 2.12 | 1.66 | 5.43 | 1.86 | 1.57 | 10.38 |
| | 2.89 | 2.30 | 8.01 | 1.43 | 2.17 | 14.38 |
| 9.88 | 2.00 | 1.49 | 4.59 | 1.96 | 1.41 | 14.72 |

Run No. 344-359

CASE J-2 $D'=1.667$ ft $\rho A/2 = .5856$  (D = 1.0ft)


| T(sec) | H(ft) | U_{bmax} (ft/s) | F_{max} (lbs) | C_f | $R_e(x10^5)$ | K-C |
|--------|-------|-------------------|-----------------|-------|--------------|-------|
| 1.98 | 1.77 | .26 | .92 | 23.27 | .29 | .44 |
| | 2.65 | .55 | 1.35 | 7.60 | .61 | .93 |
| 2.36 | 1.81 | .46 | 1.48 | 11.90 | .51 | .93 |
| | 2.76 | .87 | 3.23 | 7.29 | .96 | 1.76 |
| | 3.39 | 1.24 | 4.40 | 4.88 | 1.37 | 2.51 |
| 3.13 | 1.71 | .85 | 2.54 | 6.00 | .94 | 2.28 |
| | 3.45 | 1.89 | 6.39 | 3.06 | 2.08 | 3.07 |
| | 4.97 | 2.52 | 9.84 | 2.64 | 2.78 | 6.76 |
| 3.61 | 2.12 | 1.22 | 3.23 | 3.71 | 1.34 | 3.78 |
| | 3.16 | 2.00 | 6.16 | 2.63 | 2.20 | 6.19 |
| | 4.69 | 2.33 | 10.49 | 2.24 | 3.12 | 4.55 |
| 4.42 | 2.02 | 1.20 | 2.34 | 3.36 | 1.32 | 4.55 |
| | 4.23 | 2.57 | 7.72 | 2.00 | 2.63 | 9.74 |
| 6.25 | 2.11 | 1.26 | 3.61 | 3.88 | 1.39 | 6.75 |
| | 2.91 | 1.87 | 6.02 | 2.94 | 2.06 | 10.02 |
| 9.88 | 2.07 | 1.20 | 2.46 | 2.91 | 1.32 | 10.16 |

Run No. 233-248

CASE J-3 $D'=1.0$ ft $\rho A/2 = 1.0571$ $V = .916$ ft³ -  (D = 1.0ft)


| T (sec) | H (ft) | U_{bmax} (ft/s) | \dot{U}_{bmax} (ft/s ²) | F_{max} (lbs) | F_{m1} (lbs) | F_{m2} (lbs) | C_f | C_D | C_I | ϕ (°) | R_e ($\times 10^5$) | K-C |
|---------|--------|-------------------|---------------------------------------|-----------------|----------------|----------------|-------|-------|-------|------------|-------------------------|-------|
| 1.98 | 1.83 | .33 | .87 | 1.59 | .25 | 1.23 | 13.79 | 2.17 | .80 | 82 | .31 | .65 |
| | 2.60 | .61 | 1.15 | 2.84 | .57 | 2.11 | 7.23 | 1.45 | 1.03 | 75 | .58 | 1.21 |
| 2.36 | 1.76 | .50 | 1.15 | 3.05 | .42 | 2.05 | 11.56 | 1.59 | 1.00 | 77 | .47 | 1.18 |
| | 2.89 | .96 | 1.95 | 5.78 | .69 | 4.49 | 5.93 | .70 | 1.30 | 77 | .91 | 2.27 |
| | 3.63 | 1.27 | 2.50 | 7.34 | .67 | 6.04 | 4.30 | .40 | 1.36 | 60 | 1.20 | 3.00 |
| 3.13 | 1.32 | .84 | 1.75 | 4.86 | .36 | 4.17 | 6.51 | .51 | 1.34 | 62 | .79 | 2.63 |
| | 3.59 | 1.90 | 3.50 | 9.80 | 1.22 | 9.00 | 2.57 | .32 | 1.45 | 66 | 1.79 | 5.95 |
| | 4.97 | 2.73 | 4.75 | 17.75 | 2.20 | 15.34 | 2.25 | .28 | 1.82 | 66 | 2.58 | 8.55 |
| 3.61 | 2.23 | 1.27 | 2.10 | 6.45 | .51 | 5.97 | 3.79 | .30 | 1.60 | 74 | 1.20 | 4.59 |
| | 3.23 | 2.05 | 3.00 | 10.69 | 1.18 | 9.86 | 2.41 | .27 | 1.95 | 70 | 1.94 | 7.40 |
| | 4.67 | 2.86 | 4.00 | 21.20 | 3.53 | 14.17 | 2.45 | .40 | 2.00 | 67 | 2.70 | 10.33 |
| 4.42 | 2.09 | 1.43 | 1.85 | 5.50 | .54 | 5.41 | 2.55 | .25 | 1.65 | 67 | 1.35 | 6.32 |
| | 4.27 | 2.78 | 3.80 | 17.73 | 3.32 | 13.82 | 2.18 | .40 | 2.05 | 61 | 2.63 | 12.29 |
| 6.25 | 2.21 | 1.69 | 1.70 | 6.08 | 1.25 | 4.92 | 2.01 | .41 | 1.63 | 41 | 1.60 | 10.56 |
| | 2.82 | 2.28 | 2.45 | 10.83 | 3.20 | 8.78 | 1.97 | .58 | 2.02 | 29 | 2.15 | 14.25 |
| 9.88 | 1.97 | 1.55 | 1.20 | 5.19 | 2.43 | 3.90 | 2.05 | .96 | 1.83 | 37 | 1.46 | 15.31 |

Run No. 217-232

CASE K-1 $D'=1479$ ft $\rho A/2 = 2.2419$ $V = 1.1$ ft³ -  (D = 1.5ft)


| T (sec) | H (ft) | U_{bmax} (ft/s) | F_{max} (lbs) | C_f | R_e ($\times 10^5$) | K-C |
|---------|--------|-------------------|-----------------|-------|-------------------------|------|
| 1.98 | 1.85 | .26 | 5.82 | 39.64 | .36 | .34 |
| | 2.77 | .60 | 10.36 | 13.01 | .83 | .80 |
| 2.36 | 1.77 | .44 | 9.41 | 21.29 | .62 | .71 |
| | 2.80 | .92 | 17.34 | 9.16 | 1.28 | 1.47 |
| | 3.56 | 1.23 | 24.68 | 7.30 | 1.72 | 1.96 |
| 3.13 | 1.74 | .80 | 12.72 | 8.78 | 1.12 | 1.70 |
| | 3.60 | 1.97 | 32.77 | 3.77 | 2.75 | 4.17 |
| | 5.11 | 2.75 | 45.47 | 2.68 | 3.35 | 5.83 |
| 3.61 | 2.20 | 1.29 | 18.07 | 4.84 | 1.80 | 3.15 |
| | 3.27 | 2.07 | 29.46 | 3.05 | 2.90 | 5.06 |
| | 4.83 | 3.13 | 53.46 | 2.43 | 4.38 | 7.65 |
| 4.42 | 1.99 | 1.28 | 14.37 | 3.94 | 1.78 | 3.81 |
| | 4.33 | 2.95 | 43.76 | 2.25 | 4.11 | 8.80 |
| 6.25 | 2.16 | 1.44 | 14.36 | 3.10 | 2.01 | 6.07 |
| | 2.95 | 2.13 | 24.90 | 2.46 | 2.97 | 8.98 |
| 9.88 | 2.08 | 1.37 | 10.72 | 2.53 | 1.92 | 9.18 |

Run No. 404-419

CASE K-2 $D' = .667$ ft $\rho A/2 = 1.3465$  (D = 1.5 ft)

| T (sec) | H (ft) | U_{bmax} (ft/s) | F_{max} (lbs) | C_f | R_e ($\times 10^5$) | K-C |
|---------|--------|-------------------|-----------------|-------|-------------------------|------|
| 1.98 | 1.85 | .28 | 3.43 | 32.52 | .44 | .34 |
| | 2.65 | .60 | 5.91 | 12.19 | .94 | .71 |
| 2.36 | 1.77 | .42 | 5.18 | 21.79 | .66 | .60 |
| | 2.70 | .83 | 9.82 | 10.59 | 1.31 | 1.20 |
| | 3.60 | 1.26 | 13.98 | 6.54 | 1.98 | 1.80 |
| 3.13 | 1.69 | .90 | 8.65 | 7.93 | 1.42 | 1.70 |
| | 3.53 | 1.90 | 20.48 | 4.21 | 2.99 | 3.60 |
| | 5.07 | 2.70 | 31.99 | 3.26 | 4.25 | 5.10 |
| 3.61 | 2.13 | 1.26 | 11.85 | 5.54 | 1.98 | 2.70 |
| | 3.33 | 2.15 | 20.75 | 3.33 | 3.38 | 4.70 |
| | 4.77 | 3.00 | 37.23 | 3.07 | 4.72 | 6.50 |
| 4.42 | 2.07 | 1.30 | 9.93 | 4.37 | 2.05 | 3.40 |
| | 4.27 | 2.77 | 27.82 | 2.69 | 4.36 | 7.30 |
| 6.25 | 2.17 | 1.72 | 11.98 | 3.01 | 2.71 | 6.40 |
| | 2.95 | 2.28 | 18.80 | 2.69 | 3.59 | 8.50 |
| 9.88 | 2.08 | 1.67 | 8.62 | 2.30 | 2.63 | 9.90 |

Run No. 264-279

CASE K-3 $D' = .479$ ft $\rho A/2 = 2.2419$ $V = 22.56$ ft/s  (D = 1.5 ft)

| T (sec) | H (ft) | U_{bmax} (ft/s) | \dot{U}_{bmax} (ft/s ²) | F_{max} (lbs) | F_{m1} (lbs) | F_{m2} (lbs) | C_f | C_D | C_I | ϕ (°) | R_e ($\times 10^5$) | K-C |
|---------|--------|-------------------|---------------------------------------|-----------------|----------------|----------------|-------|-------|-------|------------|-------------------------|------|
| 1.98 | 1.82 | .30 | .87 | 5.25 | 1.55 | 3.69 | 26.0 | 7.68 | .76 | 82 | .42 | .40 |
| | 2.73 | .55 | 1.20 | 9.86 | 2.17 | 6.76 | 14.5 | 3.20 | 1.02 | 84 | .77 | .74 |
| 2.36 | 1.73 | .50 | 1.15 | 8.65 | 1.92 | 6.89 | 15.4 | 3.43 | 1.08 | 83 | .70 | .80 |
| | 2.72 | .90 | 1.90 | 17.00 | 3.64 | 14.20 | 9.36 | 2.00 | 1.35 | 83 | 1.26 | 1.44 |
| | 3.48 | 1.26 | 2.45 | 24.75 | 5.41 | 20.38 | 6.95 | 1.52 | 1.50 | 81 | 1.76 | 2.01 |
| 3.13 | 1.73 | .79 | 1.70 | 14.22 | 2.03 | 13.17 | 10.2 | 1.45 | 1.40 | 84 | 1.10 | 1.67 |
| | 3.47 | 1.89 | 3.40 | 36.27 | 7.25 | 33.02 | 4.53 | .90 | 1.75 | 66 | 2.64 | 4.00 |
| | 5.07 | 2.37 | 4.80 | 52.18 | 8.50 | 51.68 | 4.14 | .68 | 1.94 | 62 | 3.31 | 5.02 |
| 3.61 | 2.17 | 1.26 | 2.10 | 21.39 | 4.90 | 19.23 | 5.95 | 1.38 | 1.65 | 78 | 1.76 | 3.08 |
| | 3.13 | 2.17 | 2.95 | 35.23 | 9.80 | 32.70 | 3.34 | .92 | 2.00 | 65 | 3.03 | 5.30 |
| | 4.73 | 2.58 | 4.05 | 57.98 | 12.98 | 48.26 | 3.89 | .87 | 2.15 | -- | 3.60 | 6.30 |
| 4.42 | 2.05 | 1.43 | 1.85 | 17.14 | 5.00 | 17.47 | 3.74 | 1.09 | 1.70 | 69 | 2.00 | 4.27 |
| | 4.28 | 2.51 | 3.80 | 46.75 | 11.86 | 45.35 | 3.31 | .84 | 2.15 | -- | 3.51 | 7.50 |
| 6.25 | 2.11 | 1.55 | 1.70 | 17.45 | 4.15 | 16.25 | 3.24 | .77 | 1.72 | 39 | 2.17 | 6.55 |
| | 2.83 | 1.95 | 2.45 | 29.62 | 8.18 | 27.73 | 3.47 | .96 | 2.04 | -- | 2.72 | 8.24 |
| 9.88 | 1.91 | 1.49 | 1.20 | 12.76 | 5.53 | 10.16 | 2.56 | 1.11 | 1.53 | 26 | 2.08 | 9.95 |

Run No. 249-263

CASE L-1 $D'=1.896$ ft $\rho A/2 = 3.6242$ $V=5.928$ ft $\frac{1}{\text{min}}$ (D=1.9 ft)


| T (sec) | H (ft) | U_{bmax} (ft/s) | \dot{U}_{bmax} (ft/s ²) | F_{max} (lbs) | F_{m1} (lbs) | F_{m2} (lbs) | C_f | C_D | C_I | ϕ (°) | R_e ($\times 10^5$) | K-C |
|---------|--------|-------------------|---------------------------------------|-----------------|----------------|----------------|-------|-------|-------|------------|-------------------------|------|
| 1.98 | 1.87 | .34 | .90 | 11.1 | 2.39 | 9.56 | 26.43 | 5.70 | .93 | 77 | .61 | .36 |
| | 2.62 | .62 | 1.10 | 20.8 | 5.52 | 16.39 | 15.09 | 3.96 | 1.30 | 82 | 1.10 | .64 |
| 2.36 | 1.77 | .30 | 1.14 | 18.9 | 4.52 | 18.28 | 20.76 | 4.35 | 1.40 | 93 | .90 | .52 |
| | 2.67 | .96 | 1.90 | 38.9 | 8.20 | 31.45 | 11.63 | 2.46 | 1.44 | 92 | 1.72 | 1.20 |
| | 3.47 | 1.31 | 2.45 | 54.9 | 10.83 | 43.64 | 8.89 | 1.74 | 1.55 | 87 | 2.34 | 1.63 |
| 3.13 | 1.71 | .37 | 1.60 | 33.6 | 2.75 | 27.54 | 12.18 | 1.00 | 1.50 | 85 | 1.56 | 1.44 |
| | 3.33 | 1.98 | 3.20 | 70.6 | 8.78 | 59.07 | 5.00 | .62 | 1.61 | 80 | 3.54 | 3.26 |
| | 4.87 | 2.64 | 4.50 | 109.7 | 13.40 | 94.23 | 4.35 | .53 | 1.82 | 89 | 4.72 | 4.36 |
| 3.61 | 2.14 | 1.41 | 1.90 | 42.5 | 5.55 | 33.75 | 5.90 | .77 | 1.55 | 90 | 2.52 | 2.69 |
| | 3.11 | 2.09 | 2.95 | 65.2 | 10.30 | 58.24 | 4.12 | .65 | 1.72 | 82 | 3.74 | 3.98 |
| | 4.77 | 3.00 | 4.10 | 102.2 | 17.93 | 84.30 | 3.12 | .55 | 1.79 | 74 | 5.38 | 5.72 |
| 4.42 | 2.00 | 1.23 | 1.80 | 34.2 | 6.00 | 33.00 | 6.26 | 1.10 | 1.60 | 62 | 2.20 | 2.86 |
| | 4.23 | 2.84 | 3.80 | 76.2 | 20.20 | 72.40 | 2.60 | .69 | 1.66 | 56 | 5.09 | 6.53 |
| 6.25 | 2.03 | 1.70 | 2.03 | 34.7 | 7.50 | 32.80 | 3.32 | .72 | 1.41 | 39 | 3.04 | 5.60 |
| | 2.75 | 2.09 | 2.50 | 54.2 | 9.24 | 51.71 | 3.43 | .58 | 1.80 | 45 | 3.74 | 6.39 |
| 9.88 | 2.03 | 1.47 | 1.20 | 20.1 | 7.13 | 16.96 | 2.57 | .91 | 1.23 | 33 | 2.63 | 7.55 |

Run No. 452-467

CASE L-2 $D'=2.10$ ft $\rho A/2 = 1.8402$ $V=3.992$ ft $\frac{1}{\text{min}}$ (D=1.9 ft)


| T (sec) | H (ft) | U_{bmax} (ft/s) | \dot{U}_{bmax} (ft/s ²) | F_{max} (lbs) | F_{m1} (lbs) | F_{m2} (lbs) | C_f | C_D | C_I | ϕ (°) | R_e ($\times 10^5$) | K-C |
|---------|--------|-------------------|---------------------------------------|-----------------|----------------|----------------|-------|-------|-------|------------|-------------------------|------|
| 1.98 | 1.80 | .40 | .33 | 5.19 | 1.70 | 4.02 | 17.63 | 5.77 | .63 | 96 | .79 | .38 |
| | 2.60 | .63 | 1.20 | 9.61 | 2.24 | 6.65 | 13.16 | 3.07 | .72 | 89 | 1.25 | .59 |
| 2.36 | 1.78 | .50 | 1.20 | 8.59 | 2.49 | 7.22 | 18.67 | 5.41 | .78 | 101 | .99 | .56 |
| | 2.78 | .90 | 2.00 | 15.02 | 2.90 | 13.65 | 10.20 | 1.95 | .88 | 89 | 1.78 | 1.01 |
| | 3.50 | 1.12 | 2.70 | 22.44 | 2.80 | 10.15 | 9.72 | 1.21 | .96 | 89 | 2.22 | 1.26 |
| 3.13 | 1.77 | .77 | 1.65 | 13.30 | .85 | 11.71 | 12.19 | .78 | .92 | 75 | 1.53 | 1.15 |
| | 3.40 | 1.83 | 3.20 | 32.18 | 2.96 | 25.40 | 5.22 | .48 | 1.03 | 80 | 3.63 | 2.73 |
| | 4.96 | 2.78 | 4.60 | 48.71 | 4.98 | 44.23 | 3.42 | .40 | 1.24 | 69 | 5.51 | 4.14 |
| 3.61 | 2.07 | 1.22 | 2.10 | 22.01 | 1.60 | 17.15 | 8.04 | .58 | 1.05 | 75 | 2.42 | 2.10 |
| | 3.22 | 2.06 | 3.15 | 33.71 | 2.81 | 29.17 | 4.32 | .36 | 1.20 | 78 | 4.09 | 3.54 |
| | 4.70 | 3.00 | 4.60 | 55.28 | 8.48 | 46.16 | 3.34 | .51 | 1.30 | 70 | 5.95 | 5.16 |
| 4.42 | 2.02 | 1.45 | 2.03 | 19.00 | 1.70 | 17.28 | 4.91 | .44 | 1.10 | 68 | 2.88 | 3.05 |
| | 4.23 | 2.86 | 3.70 | 42.57 | 7.45 | 39.65 | 2.83 | .49 | 1.39 | 57 | 5.67 | 6.02 |
| 6.25 | 2.10 | 1.55 | 1.80 | 18.47 | 1.70 | 16.05 | 4.18 | .38 | 1.15 | 52 | 3.07 | 4.61 |
| | 2.79 | 2.15 | 2.70 | 30.03 | 9.19 | 28.63 | 3.53 | 1.08 | 1.40 | 39 | 4.26 | 6.40 |
| 9.88 | 1.87 | 1.55 | 1.25 | 11.27 | 3.08 | 10.61 | 2.55 | .70 | 1.10 | 36 | 3.07 | 7.29 |

Run No. 312-327

CASE L-3 $D' = 2.99 \text{ ft}$ $\rho A/2 = 3.6242$ $V = 35.320 \text{ ft}^2$  ($D = 1.9 \text{ ft}$)


| T (sec) | H (ft) | U_{bmax} (ft/s) | \dot{U}_{bmax} (ft/s ²) | F_{max} (lbs) | F_{m1} (lbs) | F_{m2} (lbs) | C_f | C_D | C_I | ϕ (°) | R_0 ($\times 10^5$) | K-C |
|---------|--------|-------------------|---------------------------------------|-----------------|----------------|----------------|-------|-------|-------|------------|-------------------------|------|
| 1.98 | 1.85 | .44 | .90 | 13.7 | -- | 9.53 | 19.56 | 5.20 | .92 | -- | .79 | .46 |
| | 2.67 | .63 | 1.15 | 27.5 | -- | 16.08 | 19.13 | 3.41 | 1.22 | 111 | 1.13 | .66 |
| 2.36 | 1.80 | .55 | 1.15 | 20.6 | -- | 15.80 | 18.83 | 3.42 | 1.20 | -- | .99 | .69 |
| | 2.83 | .97 | 1.90 | 47.2 | 6.20 | 31.00 | 13.85 | 1.82 | 1.40 | 96 | 1.74 | 1.21 |
| | 3.55 | 1.25 | 2.70 | 64.0 | 7.73 | 45.56 | 11.30 | 1.37 | 1.47 | 90 | 2.24 | 1.56 |
| 3.13 | 1.80 | .85 | 1.70 | 38.2 | 4.83 | 25.08 | 14.59 | 1.84 | 1.29 | 80 | 1.52 | 1.40 |
| | 3.49 | 1.92 | 3.40 | 80.5 | 16.03 | 69.42 | 6.02 | 1.20 | 1.78 | 84 | 3.44 | 3.17 |
| | 5.00 | 2.67 | 4.80 | 138.5 | 25.85 | 98.92 | 5.36 | 1.00 | 1.80 | -- | 4.78 | 4.41 |
| 3.61 | 2.20 | 1.34 | 2.16 | 51.1 | 9.35 | 43.48 | 7.86 | 1.44 | 1.75 | 74 | 2.40 | 2.55 |
| | 3.34 | 2.30 | 3.20 | 81.3 | 13.75 | 79.14 | 4.63 | .90 | 1.87 | -- | 3.94 | 4.19 |
| | 4.82 | 2.93 | 4.70 | 130.5 | 42.43 | 109.9 | 4.18 | 1.36 | 2.00 | -- | 5.25 | 5.78 |
| 4.42 | 2.17 | 1.54 | 1.90 | 45.2 | 10.50 | 40.28 | 5.26 | 1.22 | 1.85 | 55 | 2.76 | 3.59 |
| | 4.27 | 2.93 | 3.80 | 103.8 | 28.15 | 81.50 | 3.34 | .90 | 1.87 | 50 | 5.25 | 6.83 |
| 6.25 | 2.24 | 1.77 | 1.90 | 40.0 | 11.45 | 35.80 | 3.53 | 1.01 | 1.64 | 46 | 3.17 | 5.84 |
| | 2.97 | 2.25 | 2.50 | 64.2 | 26.09 | 61.83 | 3.50 | 1.42 | 2.15 | 34 | 4.03 | 7.42 |
| 9.88 | 2.07 | 1.77 | 1.20 | 28.5 | 11.63 | 21.26 | 2.51 | 1.02 | 1.54 | 26 | 3.17 | 9.22 |

Run No. 296-311

CASE M-1 $D' = 2.720 \text{ ft}$ $\rho A/2 = 2.633$ $V = 2.29 \text{ ft}^2$  ($D = 1.0 \text{ ft}$)


| T (sec) | H (ft) | U_{bmax} (ft/s) | \dot{U}_{bmax} (ft/s ²) | F_{max} (lbs) | F_{m1} (lbs) | F_{m2} (lbs) | C_f | C_D | C_I | ϕ (°) | R_0 ($\times 10^5$) | K-C |
|---------|--------|-------------------|---------------------------------------|-----------------|----------------|----------------|-------|-------|-------|------------|-------------------------|------|
| 1.98 | 1.85 | .40 | .90 | 3.39 | .65 | 2.80 | 7.96 | 1.53 | .70 | 94 | 1.03 | .29 |
| | 2.63 | .68 | 1.25 | 6.07 | .97 | 4.66 | 5.00 | .80 | .84 | 59 | 1.74 | .49 |
| 2.36 | 1.73 | .49 | 1.10 | 4.80 | .76 | 4.39 | 7.72 | 1.22 | .90 | 83 | 1.25 | .42 |
| | 2.69 | .97 | 1.90 | 9.31 | 1.44 | 8.06 | 3.74 | .58 | .96 | 72 | 2.50 | .84 |
| | 3.51 | 1.18 | 2.40 | 11.87 | 1.84 | 10.81 | 3.27 | .50 | 1.02 | 59 | 3.02 | 1.02 |
| 3.13 | 1.73 | .78 | 1.60 | 8.01 | 1.17 | 7.84 | 4.95 | .72 | 1.10 | 63 | 2.01 | .90 |
| | 3.45 | 1.83 | 3.20 | 23.93 | 4.89 | 18.55 | 2.72 | .56 | 1.31 | 62 | 4.70 | 2.10 |
| | 5.12 | 2.61 | 4.70 | 44.72 | 14.62 | 33.42 | 2.49 | .40 | 1.60 | 63 | 6.71 | 3.01 |
| 3.61 | 2.13 | 1.34 | 2.00 | 12.97 | 2.22 | 10.73 | 2.73 | .47 | 1.21 | 56 | 3.45 | 1.78 |
| | 3.19 | 1.99 | 3.35 | 27.36 | 4.59 | 20.59 | 2.62 | .44 | 1.39 | 72 | 5.11 | 2.64 |
| | 4.73 | 2.94 | 4.40 | 55.61 | 11.77 | 33.55 | 2.44 | .52 | 1.72 | 66 | 7.55 | 3.90 |
| 4.42 | 2.04 | 1.38 | 1.80 | 11.30 | 2.70 | 10.50 | 2.26 | .54 | 1.31 | 68 | 3.54 | 3.69 |
| | 4.25 | 2.81 | 3.90 | 44.46 | 12.00 | 34.10 | 2.14 | .58 | 1.97 | 41 | 7.22 | 4.57 |
| 6.25 | 2.13 | 1.70 | 1.95 | 14.93 | 6.25 | 12.97 | 1.97 | .82 | 1.50 | 32 | 4.38 | 3.90 |
| | 2.83 | 2.25 | 2.30 | 27.83 | 11.84 | 21.98 | 2.10 | .89 | 1.76 | 29 | 5.77 | 5.16 |
| 9.88 | 2.03 | 1.61 | 1.23 | 11.34 | 5.88 | 3.66 | 1.73 | .86 | 1.59 | 25 | 4.15 | 5.86 |

Run No. 468-483

CASE M-2 $D'=2.72$ ft $\rho A/2 = 2.633$ $V=2.29$ ft³ -  (D=1.0 ft)


| T (sec) | H (ft) | U _{bmax} (ft/s) | U _{bmax} (ft/s ²) | F _{max} (lbs) | F _{m1} (lbs) | F _{m2} (lbs) | C _f | C _D | C _I | φ (°) | R _e (x10 ⁵) | K-C |
|---------|--------|--------------------------|--|------------------------|-----------------------|-----------------------|----------------|----------------|----------------|-------|------------------------------------|------|
| 1.98 | 1.80 | .35 | .80 | 2.64 | 1.09 | 2.75 | 8.43 | 3.48 | .77 | 81 | .89 | .25 |
| | 2.52 | .45 | 1.13 | 4.71 | 1.43 | 4.38 | 8.86 | 2.69 | .87 | 95 | 1.15 | .33 |
| 2.36 | 1.79 | .39 | 1.00 | 5.18 | .84 | 4.43 | 13.14 | 2.13 | 1.00 | 84 | .99 | .34 |
| | 2.90 | .94 | 2.00 | 9.72 | 1.84 | 9.00 | 4.22 | .80 | 1.01 | 83 | 2.40 | .81 |
| | 3.60 | 1.18 | 2.60 | 13.17 | 2.51 | 12.50 | 3.62 | .69 | 1.08 | 71 | 3.02 | 1.02 |
| 3.13 | 1.80 | .77 | 1.60 | 8.95 | 1.50 | 7.52 | 5.69 | .95 | 1.06 | 71 | 1.99 | .89 |
| | 3.60 | 1.96 | 3.40 | 28.14 | 7.93 | 22.54 | 2.77 | .78 | 1.49 | 63 | 5.04 | 2.26 |
| | 5.03 | 2.72 | 4.70 | 52.16 | 15.20 | 35.35 | 2.69 | .78 | 1.70 | 59 | 6.98 | 3.13 |
| 3.61 | 2.20 | 1.31 | 2.19 | 14.31 | 2.57 | 12.65 | 3.30 | .57 | 1.30 | 62 | 3.35 | 1.73 |
| | 2.68 | 1.44 | 2.80 | 33.10 | 3.80 | 19.85 | 6.09 | 1.39 | 1.60 | 74 | 3.69 | 1.91 |
| | 4.80 | 3.00 | 4.70 | 60.35 | 20.63 | 41.00 | 2.54 | .87 | 1.97 | 58 | 7.72 | 3.99 |
| 4.42 | 2.00 | 1.44 | 1.80 | 12.49 | 3.28 | 11.13 | 2.30 | .60 | 1.40 | 61 | 3.69 | 2.34 |
| | 4.27 | 2.74 | 3.90 | 52.38 | 17.90 | 31.90 | 2.64 | .90 | 1.84 | 54 | 7.05 | 4.46 |
| 6.25 | 1.79 | 1.64 | 1.89 | 17.01 | 7.06 | 12.10 | 2.42 | 1.00 | 1.44 | 29 | 4.20 | 3.76 |
| | 2.31 | 2.19 | 2.50 | 32.08 | 18.79 | 16.43 | 2.54 | 1.49 | 1.48 | 20 | 5.62 | 6.48 |
| 9.88 | 2.00 | 1.60 | 1.23 | 12.42 | 7.63 | 8.76 | 1.83 | 1.13 | 1.61 | 23 | 4.12 | 5.83 |

Run No. 484-499

CASE N-1 $D'=4.02$ ft $\rho A/2 = 5.760$ $V=7.16$ ft³ -  (D=1.5 ft)


| T (sec) | H (ft) | U _{bmax} (ft/s) | U _{bmax} (ft/s ²) | F _{max} (lbs) | F _{m1} (lbs) | F _{m2} (lbs) | C _f | C _D | C _I | φ (°) | R _e (x10 ⁵) | K-C |
|---------|--------|--------------------------|--|------------------------|-----------------------|-----------------------|----------------|----------------|----------------|-------|------------------------------------|------|
| 1.98 | 1.87 | .37 | .90 | 10.9 | 2.32 | 10.00 | 13.79 | 2.95 | .80 | 90 | 1.41 | .18 |
| | 2.81 | .56 | 1.20 | 20.5 | 2.89 | 18.35 | 11.41 | 1.60 | .96 | 76 | 2.12 | .28 |
| 2.36 | 1.73 | .54 | 1.15 | 20.2 | 2.19 | 18.08 | 12.13 | 1.30 | 1.03 | 86 | 2.04 | .32 |
| | 2.75 | .95 | 1.90 | 43.2 | 4.06 | 32.25 | 8.31 | .78 | 1.22 | 91 | 3.61 | .56 |
| | 3.53 | 1.31 | 2.40 | 51.9 | 6.47 | 43.73 | 5.29 | .66 | 1.31 | 98 | 4.96 | .77 |
| 3.13 | 1.74 | .91 | 1.70 | 34.0 | 3.71 | 28.34 | 7.07 | .78 | 1.20 | 80 | 3.47 | .71 |
| | 3.65 | 2.03 | 3.25 | 88.2 | 15.28 | 65.32 | 3.73 | .64 | 1.50 | 69 | 7.70 | 1.58 |
| | 5.11 | 2.81 | 5.10 | 142.2 | 26.30 | 102.48 | 3.13 | .58 | 1.60 | 66 | 10.67 | 2.19 |
| 3.61 | 2.20 | 1.37 | 1.90 | 54.6 | 8.13 | 37.38 | 5.03 | .75 | 1.42 | 70 | 5.22 | 1.23 |
| | 3.30 | 2.14 | 3.20 | 93.0 | 14.32 | 66.54 | 3.54 | .54 | 1.50 | 74 | 8.11 | 1.92 |
| | 4.79 | 3.20 | 4.20 | 165.2 | 43.63 | 105.10 | 2.80 | .74 | 1.80 | 69 | 12.16 | 2.88 |
| 4.42 | 2.00 | 1.47 | 1.85 | 47.2 | 11.19 | 35.95 | 3.81 | .90 | 1.40 | 68 | 5.57 | 1.61 |
| | 4.28 | 2.74 | 3.80 | 144.3 | 42.75 | 110.15 | 3.33 | .99 | 2.09 | 61 | 10.41 | 3.02 |
| 6.25 | 2.13 | 1.59 | 1.90 | 58.8 | 12.20 | 51.05 | 4.03 | .84 | 1.94 | 36 | 6.05 | 2.48 |
| | 2.88 | 2.09 | 2.70 | 98.3 | 31.79 | 79.68 | 3.91 | 1.27 | 2.13 | 26 | 7.93 | 3.25 |
| 9.88 | 1.96 | 1.57 | 1.20 | 43.9 | 25.48 | 30.11 | 3.11 | 1.80 | 1.81 | 18 | 5.95 | 3.85 |

Run No. 500-515

CASE N-2 $D' = 4.02$ ft $\rho A/2 = 5.760$ $V = 7.16$ ft³  ($D = 1.3$ ft)

| T (sec) | H (ft) | U _{bmax} (ft/s) | U _{bmax} (ft/s ²) | F _{max} (lbs) | F _{m1} (lbs) | F _{m2} (lbs) | C _f | C _D | C _I | φ (°) | R _e (x10 ⁵) | K-C |
|---------|--------|--------------------------|--|------------------------|-----------------------|-----------------------|----------------|----------------|----------------|-------|------------------------------------|------|
| 1.98 | 1.81 | .37 | .80 | 11.2 | 2.32 | 9.92 | 4.58 | 3.00 | .89 | 85 | 1.39 | .18 |
| | 2.60 | .65 | 1.25 | 20.1 | 3.63 | 20.06 | 8.34 | 1.50 | 1.16 | 81 | 2.46 | .32 |
| 2.36 | 1.83 | .50 | 1.15 | 20.9 | 3.16 | 18.56 | 4.78 | 2.20 | 1.16 | 90 | 1.88 | .29 |
| | 2.87 | .97 | 1.95 | 39.6 | 6.00 | 34.00 | 7.39 | 1.11 | 1.26 | 89 | 3.67 | .57 |
| | 3.60 | 1.23 | 2.63 | 53.8 | 9.03 | 49.29 | 6.21 | 1.04 | 1.35 | 77 | 4.66 | .72 |
| 3.13 | 1.80 | .87 | 1.50 | 31.4 | 5.05 | 27.39 | 7.27 | 1.16 | 1.32 | 71 | 3.29 | .68 |
| | 3.61 | 1.96 | 3.00 | 90.6 | 15.16 | 68.81 | 4.08 | .68 | 1.65 | 60 | 7.46 | 1.53 |
| | 4.99 | 2.55 | 4.40 | 138.4 | 22.33 | 122.16 | 3.69 | .60 | 2.00 | 67 | 9.70 | 1.99 |
| 3.61 | 2.13 | 1.37 | 2.00 | 49.9 | 10.35 | 42.73 | 4.60 | .96 | 1.54 | 67 | 5.22 | 1.23 |
| | 3.24 | 2.22 | 3.30 | 92.8 | 22.87 | 82.37 | 3.28 | .80 | 1.80 | 67 | 8.43 | 1.99 |
| | 4.83 | 3.07 | 4.25 | 161.2 | 40.48 | 122.65 | 2.97 | .75 | 2.08 | 65 | 11.66 | 2.76 |
| 4.42 | 2.01 | 1.44 | 1.90 | 46.6 | 10.70 | 35.54 | 3.93 | .90 | 1.35 | 62 | 5.46 | 1.53 |
| | 4.43 | 3.00 | 4.10 | 141.1 | 44.09 | 114.90 | 2.72 | .85 | 2.02 | 38 | 11.40 | 3.30 |
| 6.25 | 2.16 | 1.64 | 1.90 | 56.1 | 18.59 | 42.80 | 3.65 | 1.20 | 1.62 | 32 | 6.21 | 2.54 |
| | 2.92 | 2.19 | 2.70 | 93.2 | 50.34 | 72.28 | 3.38 | 1.33 | 1.93 | 27 | 8.31 | 3.40 |
| 9.88 | 1.93 | 1.60 | 1.22 | 42.3 | 25.33 | 29.96 | 2.88 | 1.72 | 1.77 | 19 | 6.07 | 3.93 |

Run No. 516-531

CASE O-1 $D' = 4.75$ ft $\rho A/2 = 5.675$ $V = 8.89$ ft³  ($D = 1.3$ ft)

| T (sec) | H (ft) | U _{bmax} (ft/s) | U _{bmax} (ft/s ²) | F _{max} (lbs) | F _{m1} (lbs) | F _{m2} (lbs) | C _f | C _D | C _I | φ (°) | R _e (x10 ⁵) | K-C |
|---------|--------|--------------------------|--|------------------------|-----------------------|-----------------------|----------------|----------------|----------------|-------|------------------------------------|------|
| 1.98 | 1.83 | .31 | .80 | 13.5 | 5.09 | 11.52 | 25.44 | 9.00 | .84 | 96 | 1.37 | .13 |
| | 2.69 | .49 | 1.15 | 28.2 | 7.07 | 22.40 | 20.86 | 5.00 | 1.13 | 89 | 2.19 | .20 |
| 2.36 | 1.90 | .48 | 1.10 | 29.1 | 6.50 | 10.15 | 21.99 | 4.81 | 1.06 | 101 | 2.17 | .24 |
| | 2.93 | .97 | 1.90 | 50.7 | 15.54 | 39.95 | 9.57 | 2.80 | 1.22 | 71 | 4.33 | .48 |
| | 3.43 | 1.20 | 2.40 | 72.3 | 18.70 | 57.79 | 8.84 | 2.20 | 1.40 | 71 | 5.39 | .60 |
| 3.13 | 1.73 | .79 | 1.40 | 46.1 | 11.74 | 34.45 | 13.06 | 3.20 | 1.43 | 62 | 3.54 | .52 |
| | 3.51 | 1.63 | 3.00 | 120.2 | 33.53 | 89.72 | 7.95 | 2.14 | 1.74 | 62 | 7.32 | 1.08 |
| | 4.60 | 2.15 | 4.20 | 184.3 | 46.28 | 130.29 | 6.99 | 1.68 | 1.80 | 63 | 9.67 | 1.42 |
| 3.61 | 2.18 | 1.24 | 2.00 | 79.6 | 22.65 | 54.94 | 9.11 | 2.50 | 1.60 | 72 | 5.57 | .94 |
| | 3.25 | 1.70 | 3.15 | 145.0 | 34.40 | 96.84 | 8.85 | 2.02 | 1.79 | 72 | 7.63 | 1.29 |
| | 4.29 | 2.25 | 4.40 | 284.7 | 50.63 | 143.95 | 9.88 | 1.70 | 1.90 | 66 | 10.11 | 1.71 |
| 4.42 | 2.07 | 1.34 | 2.10 | 73.3 | 21.45 | 53.59 | 7.20 | 2.03 | 1.48 | 66 | 6.01 | 1.25 |
| | 4.30 | 2.39 | 3.60 | 309.3 | 63.87 | 104.30 | 9.56 | 1.90 | 1.68 | 62 | 10.11 | 1.71 |
| 6.25 | 2.21 | 1.50 | 2.00 | 78.4 | 26.48 | 62.95 | 6.12 | 2.00 | 1.83 | -- | 6.74 | 1.98 |
| | 2.97 | 1.89 | 2.70 | 135.1 | 48.24 | 96.78 | 6.64 | 2.29 | 2.08 | -- | 8.50 | 2.49 |
| 9.88 | 1.37 | 1.33 | 1.20 | 61.2 | 31.68 | 41.30 | 6.13 | 3.04 | 2.00 | -- | 5.95 | 2.74 |

Run No. 612-627

CASE P-1 $D' = 1.0 \text{ ft}$ $\rho A/2 = .533$ $\phi = 0$ ($D = 1.0 \text{ ft}$)


| T (sec) | H (ft) | U_{bmax} (ft/s) | F_{max} (lbs) | C_f | $R_e (x10^5)$ | K-C |
|---------|--------|-------------------|-----------------|-------|---------------|-------|
| 1.98 | 1.90 | .27 | .78 | 20.38 | .25 | .53 |
| | 2.60 | .50 | .83 | 6.40 | .47 | .98 |
| 2.36 | 1.93 | .46 | .89 | 8.01 | .43 | 1.09 |
| | 2.72 | .88 | 1.43 | 3.51 | .83 | 2.08 |
| | 3.60 | 1.23 | 1.88 | 2.35 | 1.16 | 2.91 |
| 3.13 | 1.80 | .81 | 1.21 | 3.51 | .77 | 2.54 |
| | 3.58 | 1.89 | 3.44 | 1.82 | 1.79 | 5.93 |
| | 4.67 | 2.56 | 4.78 | 1.39 | 2.42 | 8.01 |
| 3.61 | 2.27 | 1.06 | 1.51 | 2.56 | 1.00 | 3.83 |
| | 3.21 | 2.11 | 2.67 | 1.14 | 1.99 | 7.61 |
| | 4.93 | 2.69 | 5.15 | 1.35 | 2.54 | 9.71 |
| 4.42 | 2.03 | 1.31 | 1.22 | 1.36 | 1.23 | 5.77 |
| | 4.63 | 2.95 | 4.17 | .92 | 2.78 | 13.02 |
| 6.25 | 2.07 | 1.73 | 2.48 | 1.58 | 1.63 | 10.81 |
| | 2.91 | 2.21 | 3.42 | 1.33 | 2.08 | 13.79 |
| 9.88 | 1.95 | 1.60 | 1.66 | 1.23 | 1.51 | 15.81 |

Run No. 580-595

CASE P-2 $D' = .854 \text{ ft}$ $\rho A/2 = .659$ $V = .34 \text{ ft}^3$ $\phi = 0$ ($D = 1.0 \text{ ft}$)

| T (sec) | H (ft) | U_{bmax} (ft/s) | \dot{U}_{bmax} (ft/s ²) | F_{max} (lbs) | F_{m1} (lbs) | F_{m2} (lbs) | C_f | C_D | C_I | ϕ (°) | $R_e (x10^5)$ | K-C |
|---------|--------|-------------------|---------------------------------------|-----------------|----------------|----------------|-------|-------|-------|------------|---------------|-------|
| 1.98 | 2.01 | .38 | 1.15 | .72 | .53 | .60 | 7.56 | 5.79 | .78 | -- | .31 | .88 |
| | 2.73 | .33 | 1.40 | 1.01 | .94 | .89 | 3.87 | 3.59 | .95 | -- | .51 | 1.46 |
| 2.36 | 1.43 | .54 | 1.10 | .99 | .58 | .66 | 5.19 | 3.04 | .90 | 89 | .43 | 1.25 |
| | 2.75 | .82 | 1.80 | 1.41 | .80 | 1.30 | 3.15 | 1.81 | 1.08 | 89 | .66 | 2.27 |
| | 3.60 | 1.33 | 2.70 | 1.73 | .78 | 1.60 | 1.48 | .67 | 1.08 | 96 | 1.07 | 3.09 |
| 3.13 | 1.77 | .83 | 1.70 | 1.54 | .35 | 1.30 | 3.36 | .78 | 1.15 | -- | .67 | 3.06 |
| | 3.63 | 1.90 | 3.40 | 2.69 | .83 | 2.50 | 1.13 | .35 | 1.10 | -- | 1.53 | 6.96 |
| | 4.77 | 2.73 | 5.10 | 4.36 | 1.47 | 4.10 | .89 | .30 | 1.21 | 62 | 2.20 | 10.00 |
| 3.61 | 2.23 | 1.32 | 2.40 | 2.08 | .35 | 1.88 | 1.80 | .30 | 1.18 | 82 | 1.07 | 5.59 |
| | 3.36 | 2.08 | 3.60 | 4.05 | .75 | 3.56 | 1.43 | .26 | 1.48 | 70 | 1.68 | 8.78 |
| | 4.83 | 2.94 | 4.50 | 6.70 | 1.57 | 4.80 | 1.18 | .28 | 1.60 | 72 | 2.37 | 12.43 |
| 4.42 | 2.07 | 1.41 | 2.20 | 2.01 | .36 | 1.80 | 1.55 | .28 | 1.23 | 68 | 1.13 | 7.27 |
| | 4.67 | 2.77 | 4.10 | 6.35 | 1.80 | 4.76 | 1.26 | .36 | 1.74 | 56 | 2.20 | 14.35 |
| 6.25 | 2.20 | 1.80 | 1.70 | 2.67 | .83 | 1.98 | 1.26 | .39 | 1.75 | 36 | 1.45 | 13.15 |
| | 3.04 | 2.19 | 2.50 | 4.28 | 1.46 | 3.08 | 1.36 | .46 | 1.85 | 32 | 1.77 | 16.02 |
| 9.88 | 2.00 | 1.59 | 1.25 | 2.22 | .97 | 1.50 | 1.34 | .58 | 1.80 | 29 | 1.28 | 18.36 |

Run No. 596-611

CASE Q-1 $D' = 1.563 \text{ ft}$ $\rho A / 2 = 1.627$  (D=1.9ft)

| T (sec) | H (ft) | U_{bmax} (ft/s) | F_{max} (lbs) | C_f | $R_o (\times 10^5)$ | K-C |
|---------|--------|-------------------|-----------------|-------|---------------------|-------|
| 1.98 | 1.77 | .36 | 4.08 | 19.89 | .52 | .45 |
| | 2.67 | .58 | 6.41 | 11.91 | .85 | .73 |
| 2.36 | 1.89 | .60 | 6.56 | 11.17 | .89 | .91 |
| | 2.73 | .97 | 10.33 | 6.80 | 1.43 | 1.46 |
| | 4.04 | 1.37 | 13.07 | 4.26 | 2.03 | 2.08 |
| 3.13 | 1.83 | .90 | 13.44 | 10.22 | 1.33 | 1.80 |
| | 3.62 | 1.89 | 21.91 | 3.79 | 2.78 | 3.78 |
| | 4.92 | 2.69 | 33.84 | 2.88 | 3.97 | 5.39 |
| 3.61 | 2.23 | 1.41 | 11.49 | 3.54 | 2.09 | 3.26 |
| | 3.27 | 2.04 | 21.16 | 3.13 | 3.01 | 4.72 |
| | 4.91 | 2.80 | 32.84 | 2.58 | 4.12 | 6.46 |
| 4.42 | 2.00 | 1.50 | 9.06 | 2.46 | 2.22 | 4.25 |
| | 4.62 | 2.83 | 28.88 | 2.22 | 4.17 | 8.00 |
| 6.25 | 2.20 | 1.67 | 8.61 | 1.91 | 2.46 | 6.66 |
| | 2.93 | 2.42 | 17.72 | 1.87 | 3.57 | 9.68 |
| 9.88 | 2.07 | 1.64 | 7.39 | 1.70 | 2.41 | 10.34 |

Run No. 548-563

CASE Q-2 $D' = 1.479 \text{ ft}$ $\rho A / 2 = 2.449$ $V = 2.223 \text{ ft}^2$  (D=1.9ft)

| T (sec) | H (ft) | U_{bmax} (ft/s) | \dot{U}_{bmax} (ft/s ²) | F_{max} (lbs) | F_{m1} (lbs) | F_{m2} (lbs) | C_f | C_D | C_I | ϕ (°) | $R_o (\times 10^5)$ | K-C |
|---------|--------|-------------------|---------------------------------------|-----------------|----------------|----------------|-------|-------|-------|------------|---------------------|-------|
| 1.98 | 2.00 | .37 | .95 | 2.86 | .64 | 2.67 | 8.70 | 1.91 | .65 | 82 | .51 | .49 |
| | 2.63 | .61 | 1.20 | 4.10 | 1.06 | 3.74 | 4.56 | 1.16 | .76 | 75 | .85 | .81 |
| 2.36 | 1.92 | .58 | 1.15 | 4.67 | .85 | 3.79 | 5.77 | 1.03 | .77 | 95 | .80 | .92 |
| | 2.97 | .97 | 1.90 | 7.20 | 1.60 | 6.70 | 3.15 | .70 | .82 | 89 | 1.35 | 1.54 |
| | 3.81 | 1.33 | 2.80 | 10.18 | 2.26 | 9.50 | 2.34 | .52 | .79 | 95 | 1.86 | 2.13 |
| 3.13 | 1.73 | .79 | 1.55 | 6.09 | .86 | 5.36 | 3.94 | .57 | .80 | 71 | 1.11 | 1.68 |
| | 3.57 | 1.92 | 3.40 | 16.77 | 2.80 | 13.79 | 1.85 | .30 | .94 | 77 | 2.68 | 4.07 |
| | 4.90 | 2.60 | 4.30 | 28.35 | 7.50 | 20.35 | 1.77 | .46 | 1.10 | 62 | 3.63 | 5.50 |
| 3.61 | 2.22 | 1.36 | 2.29 | 9.96 | 1.64 | 8.84 | 2.20 | .36 | .90 | 66 | 1.90 | 3.31 |
| | 3.39 | 2.04 | 3.40 | 17.71 | 3.90 | 14.61 | 1.74 | .38 | 1.00 | 66 | 2.85 | 4.97 |
| | 4.80 | 2.96 | 4.70 | 34.38 | 9.42 | 24.18 | 1.60 | .43 | 1.20 | 65 | 4.13 | 7.22 |
| 4.42 | 2.10 | 1.47 | 2.05 | 9.18 | 1.65 | 7.95 | 1.74 | .31 | .90 | 59 | 2.05 | 4.39 |
| | 4.80 | 2.79 | 4.00 | 31.45 | 9.40 | 22.42 | 1.65 | .49 | 1.30 | 46 | 3.89 | 8.33 |
| 6.25 | 2.16 | 1.65 | 1.90 | 11.06 | 4.00 | 9.85 | 1.67 | .60 | 1.20 | 30 | 2.30 | 6.96 |
| | 2.95 | 2.23 | 2.74 | 21.57 | 8.94 | 16.54 | 1.77 | .73 | 1.40 | 20 | 3.12 | 9.44 |
| 9.88 | 2.15 | 1.64 | 1.30 | 9.17 | 4.63 | 7.84 | 1.40 | .70 | 1.40 | 18 | 2.23 | 10.92 |

Run No. 564-579

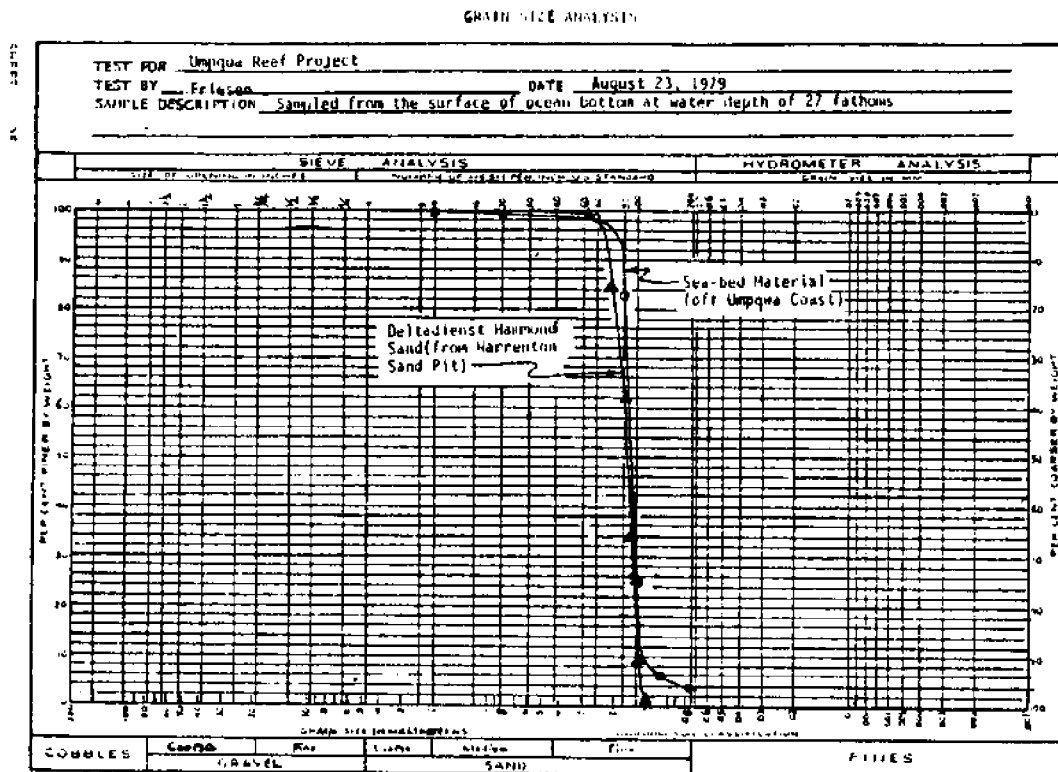
CASE R-1 $D' = 2.208 \text{ ft}$ $pA/2 = 1.753$ $V = 5.78 \text{ ft}^3 - \text{sec}^{-1}$ ($D = 1.9 \text{ ft}$)

| T (sec) | H (ft) | U_{bmax} (ft/s) | \dot{U}_{bmax} (ft/s ²) | F_{max} (lbs) | F_{m1} (lbs) | F_{m2} (lbs) | C_f | C_D | C_I | ϕ (°) | R_e ($\times 10^5$) | K-C |
|------------|-----------|----------------------|--|--------------------|-------------------|-------------------|-------|-------|-------|---------------|----------------------------|------|
| 1.98 | 1.95 | .29 | .95 | 12.28 | -- | 9.57 | 31.34 | -- | .90 | 79 | .60 | .26 |
| | 2.57 | .41 | 1.18 | 20.87 | 2.81 | 20.54 | 26.75 | 3.50 | 1.07 | 82 | .84 | .36 |
| 2.36 | 1.87 | .41 | 1.25 | 20.18 | 3.08 | 14.19 | 25.62 | 3.86 | 1.13 | 88 | .85 | .44 |
| | 2.69 | .85 | 1.90 | 39.63 | 7.67 | 27.51 | 11.64 | 2.24 | 1.30 | 71 | 1.75 | .90 |
| | 3.54 | 1.18 | 2.60 | 55.79 | 12.12 | 39.96 | 8.39 | 1.83 | 1.38 | 76 | 2.47 | 1.26 |
| 3.13 | 1.77 | .72 | 1.70 | 28.75 | 6.65 | 25.00 | 11.73 | 2.70 | 1.31 | 77 | 1.50 | 1.02 |
| | 3.38 | 1.90 | 3.20 | 88.65 | 23.70 | 54.57 | 5.17 | 1.37 | 1.53 | 66 | 3.96 | 2.69 |
| | 4.43 | 2.64 | 4.25 | 135.95 | 34.90 | 78.06 | 4.10 | 1.05 | 1.64 | 62 | 5.50 | 3.74 |
| 3.61 | 2.20 | 1.24 | 2.10 | 45.85 | 11.90 | 33.77 | 6.26 | 1.63 | 1.44 | 82 | 2.59 | 2.03 |
| | 3.15 | 2.02 | 3.00 | 77.26 | 21.90 | 54.64 | 3.99 | 1.13 | 1.63 | 78 | 4.21 | 3.30 |
| | 4.40 | 2.85 | 4.10 | 137.79 | 33.83 | 84.84 | 3.57 | .88 | 1.65 | 78 | 5.94 | 4.55 |
| 4.42 | 1.93 | 1.37 | 1.90 | 36.79 | 10.45 | 30.48 | 4.11 | 1.17 | 1.44 | 69 | 2.86 | 2.74 |
| | 4.23 | 2.34 | 4.00 | 93.80 | 53.09 | 85.16 | 3.61 | 2.04 | 1.90 | 46 | 4.87 | 4.68 |
| 6.25 | 2.20 | 1.57 | 1.65 | 38.90 | 20.10 | 32.97 | 3.33 | 1.71 | 1.76 | 30 | 3.27 | 4.44 |
| | 2.87 | 2.16 | 2.60 | 67.52 | 46.00 | 57.33 | 3.05 | 2.08 | 1.97 | 21 | 4.49 | 6.10 |
| 9.88 | 1.97 | 1.44 | 1.15 | 28.72 | 12.08 | 20.22 | 2.92 | 1.22 | 1.57 | 23 | 3.00 | 6.43 |

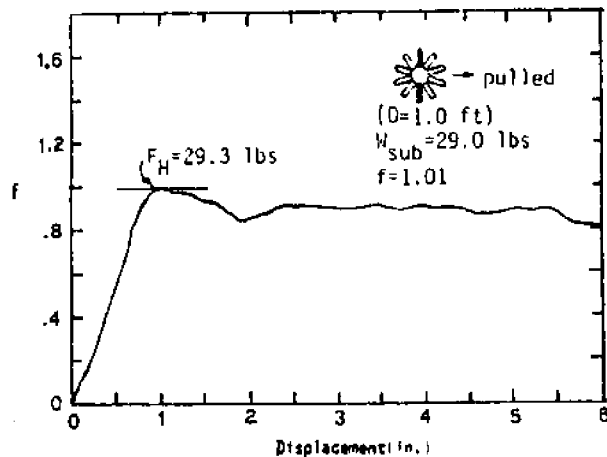
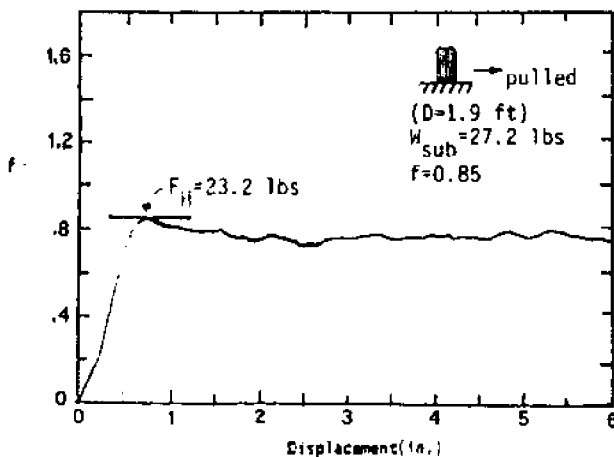
Run No. 676-691

APPENDIX B
Friction Tests

1. Grain Size Distribution of Warrenton Sands Compared with Sea-bed Materials at 27 Fathoms off Umpqua Coast

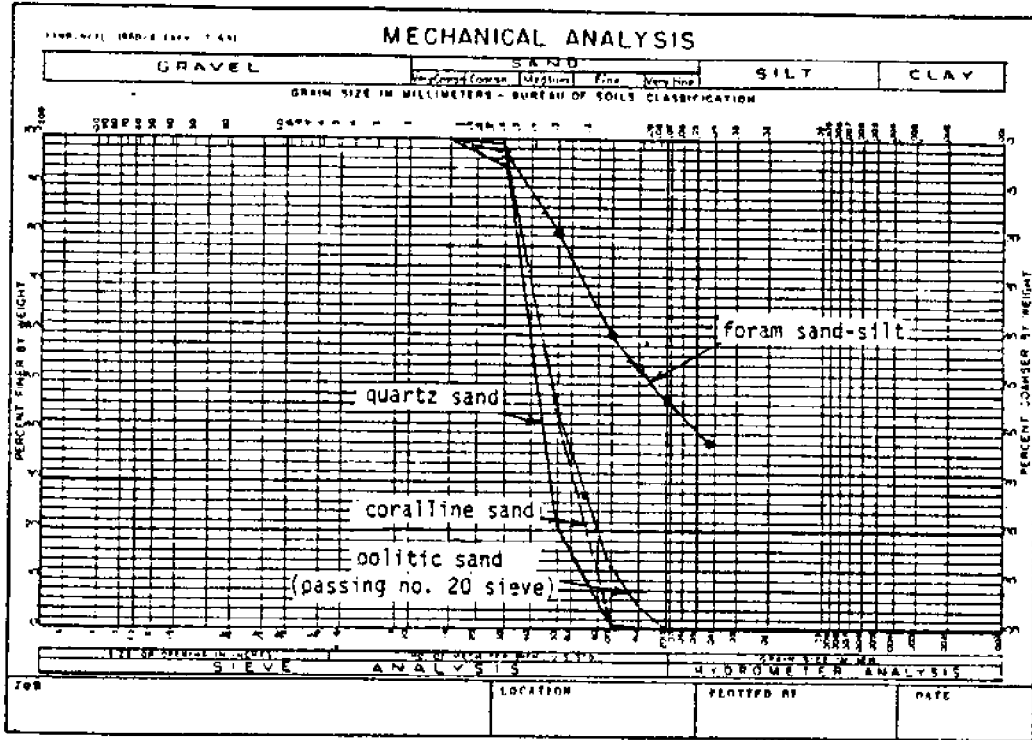


2. Sample Records of Bottom Resistance Test

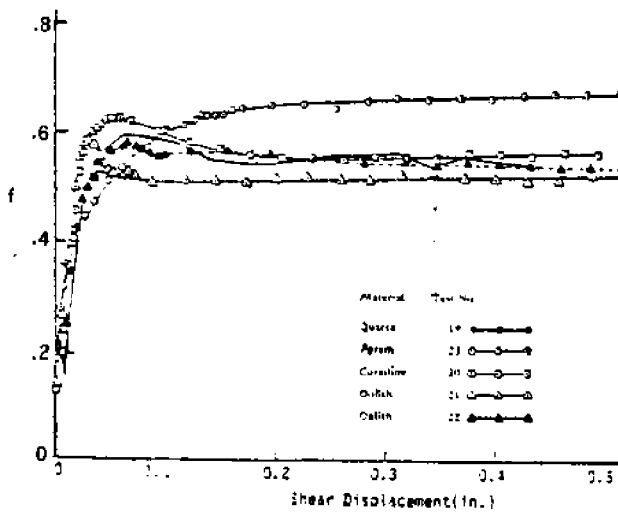


3. Friction Tests (Source: Civil Engineering Laboratory, TN no. N-1542, 1979)

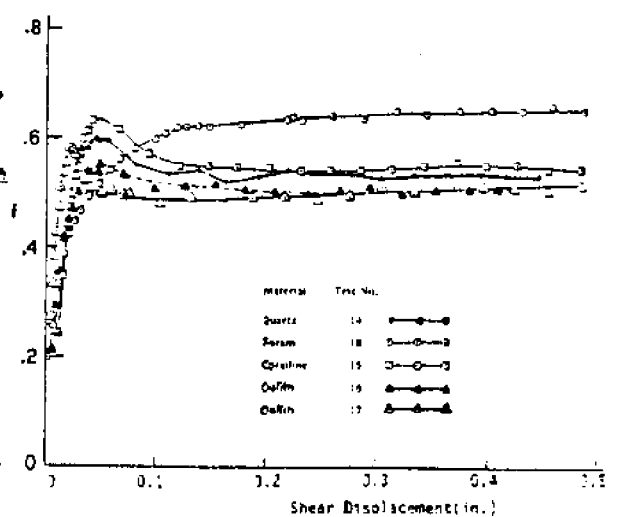
(a) Grain Size Distribution of Soil Materials Used



(b) Friction Tests of Soil Samples on Rough Steel or Smooth Concrete



(on smooth concrete)



(on rough steel)

